UNIVERSITY COLLEGE LONDON

Novel Pseudo Magneto-electric Dipole Antennas

by

Linyu Cai

A dissertation submitted for the degree of

Doctor of Philosophy

in the

Department of Electronic and Electrical Engineering

University College London

Supervised by Porf. Kenneth Tong

August 19, 2021

1

Declaration of Authorship

I, Linyu Cai, declare that this thesis titled, 'Novel pseudo magneto-electric dipole antennas' and the work presented in it are my own original work, and that all source materials used have been clearly identified and acknowledged, no part of the dissertation contains materials previously submitted to the examiners of this or other universities, or any materials previously submitted for any other examinations.

Abstract

By Linyu Cai

One of the major requirements for modern wireless communications is very high data transmission, so antennas with simple geometry, wide operation bandwidth and stable high gain features are in increasing demand. In this thesis, three novel pseudo magneto-electric (ME) dipole antennas operating in 5G Frequency Range 1 (FR1) sub-6GHz and Frequency Range 2 (FR2) millimeter-wave (mmW) band are introduced and analyzed. Comparing with conventional ME dipole antennas, which always require a vertical quarter-wave cavity to generate the magnetic dipole resonance, the pseudo-ME dipole designs proposed in this thesis do not rely on the cavity to provide the complementary magnetic dipole mode, therefore, they have extremely simple geometry. Meanwhile, it achieved wide bandwidth (50.30%) and high gain (average 8.74 dBi) the in-band gain variation is only $\pm$ 1dB. Based on the novel cavity-less Pseudo-ME dipole antenna geometry, a wide axial ratio bandwidth (54.1%) circularly polarized pseudo-ME dipole antenna is also designed to overcome the polarization misalignment problem in multipath-rich wireless environments, this antenna has two pairs of orthogonal electric dipoles and magnetic dipoles to achieve the wide axial ratio bandwidth performance. Finally, an aperture-coupled printed pseudo-ME dipole antenna is designed for operating in millimeter-wave band, it has 32.3% of impedance bandwidth and stable high gain 7.4 $\pm$ 0.8 dBi. Especially, there is none typical via-hole formed cavity in the geometry, so the fabrication of the mmW band antenna becomes simpler.

Impact statement

The Fifth Generation (5G) mobile technologies bring a rapid increase in mobile phone traffic. Wideband band antenna becomes an initial part of meeting the demand of higher data rate and wider bandwidth. At the same time, due to the extremely limited space and complex electromagnetic environment in terminal products (such as a mobile phone), it is challenging to implementing a small size antenna. Thus, modern antennas must have simple geometry, low-profile, wide bandwidth and high gain.

In this thesis, a non-cavity magneto-electric (ME) dipole antenna geometry has been presented. This geometry has great advantages of simple geometry, low-profile, sufficient wide bandwidth and stable high-gain. There is no vertical-cavity geometry to form the magnetic dipole when compared with the conventional ME dipole antenna. Therefore, the geometry of the non-cavity ME dipole antenna becomes simpler and reduce the fabrication difficulty and cost. In addition, the height of the antenna is only 0.15 λ_0, which is 40% less than the conventional 0.25 λ_0. The low-profile feature makes the antenna easier to be implemented in a limited space.

Moreover, the fabrication of the ME dipole antenna in the millimeter wave (mmW) frequency bands is challenging due to the vertical cavity geometry. In contrast, it is easier to implement the non-cavity ME-dipole antenna into the mmW band. Thus, an aperture-coupled millimeter wave bands ME dipole antenna has been designed and verified. This compact size antenna has the impedance bandwidth that covered the entire 5G FR2 band and achieved an average 7.1 dBi in-band gain. It is suitable to be implemented into 5G terminal devices.

Circularly polarized antennas are widely used in satellite communication systems, navigation systems and radar systems. A sub-6GHz wide axial ratio (AR) bandwidth circularly polarized ME dipole antenna has also been designed and verified. The proposed antenna has two orthogonal resonances with appropriate amplitudes and phase differences operating at relatively separated frequencies. Therefore, the AR bandwidth achieved 54.1% by feeding the proposed circularly polarized (CP) ME dipole antenna with a single coaxial cable. The wide AR bandwidth feature gives the antenna the ability to overcome polarization mismatch issue over a wide bandwidth. Implementing a circularly polarized antenna in the transmitter of MIMO systems improves the diversity gain and system throughput effectively.

Acknowledgements

I would like to express my sincere gratitude to my first supervisor Dr. Kin-Fai Tong for his consistent support, guidance, and motivation of my research since I started my MSc degree in UCL five years ago.

I would like to give my thanks to my parents for their unconditional support both financially and mentally.

I also want to thank for my friends, Fan Yang, Yikuan Li, Tongyang Xu who always give me their kind help whenever I need.

Signed: _____

Date: _____

Contents

List of figures

14

15

17

List of tables

Abbreviations

AiP	**A**ntenna-**i**n-**P**ackage
AoC	**A**ntenna-**o**n-**C**hip
AR	**A**xial **R**atio
AUT	**A**ntenna
BW	**B**andwidth
CP	**C**ircular **P**olarization
CST	**C**omputer **S**imulation **T**echnology
DC	**D**irect **C**urrent
EM	**E**lectro**m**agnetic
FDD	**F**requency **D**ivision **D**uplex
FNBW	**F**irst **N**ull **B**and **W**idth
FR1	**F**requency **R**ange 1
FR2	**F**requency **R**ange 2
GNSS	**G**lobal **N**avigation **S**atellite **S**ystem
GPS	**G**lobal **P**ositioning **S**ystem

HPBW	**H**alf-**P**ower **B**eamwidth
LTE	**L**ong-**T**erm **E**volution
LWA	**L**eaky-**W**ave **A**ntenna
ME	**M**agneto-electric
MIMO	**M**ultiple-**I**nput **M**ultiple-**O**utput
PCB	**P**rinted **C**ircuit **B**oard
RAN	**R**adio **A**ccess **N**etwork
RL	**R**eturn **L**oss
RSRP	**R**eference **S**ignal **R**eceive **P**ower
SINR	**S**ignal-to-**N**oise **R**atio
SIW	**S**ubstrate **I**ntegrated **W**aveguide
SMA	**S**ub**M**iniarure version **A**
SMK	**S**ub**M**iniarure version **K**
SNR	**S**ignal-to-**N**oise **R**atio
SWR	**S**tand **W**ave **R**atio
TDD	**T**ime **D**ivision **D**uplex
VSWR	**V**oltage **S**tand **W**ave **R**atio

Symbols

A	Amplitude	
Δ_1	beamwidth difference across the frequency	°
Δ_2	beamwidth difference across the plane	°
a_1	incident power in port 1	W
a_2	reflected power in port 2	W
b_1	incident poer in port 1	W
b_2	reflected power in port 2	W
D	Antenna Directivity	dBi
f_c	center frequency	Hz
f_{high}	upper frequency	Hz
f_{low}	lower frequency	Hz
G	Antenna gain	dBi
g	width of Gap	mm
H_{air}	height from the ground plane to radiating layer	mm
$H_{Substrate}$	height of the substrate	mm
L_{Ground}	side length of the ground plane	mm
L_{Open}	length of the transmission line at the open end	mm
L_{Patch}	length of patch	mm
$L_{aperture}$	length of the feeding aperture	mm

L_{Sub}	length of substate	mm
P_A	Supplied power	W(J/s)
P_i	incident power	W(J/s)
P_r	reflected power	W(J/s)
P_{ra}	radiated power	W(J/s)
R	the real part of the impedance	Ω
r	sphere radius	m
R_a	distance to antenna center	m
R_{Ring}	the radius of quarter-wave ring arc	mm
S_{11}	Reflection coefficient at port 1	dB
S_{12}	Transmission coefficient from port 2 to 1	dB
S_{21}	Transmission coefficient from port 1 to 2	dB
S_{22}	Reflection coefficient at port 2	dB
t	time	s
T_{sub1}	the thickness of substrate 1	mm
T_{sub2}	the thickness of substrate 2	mm
W_{Patch}	width of patch	mm
W_{Con}	width of short lead	mm
W_{Ring}	width of quarter-wave ring arc	mm
$W_{aperture}$	width of the feeding aperture	mm
W_{Sub}	width of substrate	mm
X	the imaginary part of the impedance	Ω

Z_0	characteristic impedance	Ω
Z_{11}	impedance	Ω
Z_L	Load impedance	Ω
Γ	reflection coefficient	rad
θ	elevation angle	rad
λ	wavelength	m
λ_0	free-space wavelength	m
λ_g	Guided wavelength	m
φ	azimuth angle	rad
ω	angular frequency	rad/s

1.Introduction

The rapid development of modern wireless technologies creates a solid foundation for a gigabit or higher interconnected world [1]–[3]. The high-speed data transmission will significantly improve our lives, in both leisure and work, in the future, bringing new industries and benefitting daily lives. For example, modern wireless technologies allow thousands of users to access the internet simultaneously, watching 4k or even 8k football games or movies from smart mobile devices [4][5]. In the Smart-City scenario, wireless technologies create connections between car-to-car and car-to-infrastructure, including massive real-time traffic information [6]. In the telemedicine scenario, it is also possible to achieve a network capacity of 1 Gbps for uplink and downlink to meet the needs of ultrasound imaging terminals for real-time transmission of dynamic high-definition images [4].

Among all the possibilities, one method to realize the significantly high data transmissions is increasing the spectrum utilization, i.e., space timing coding technology. Or increasing the spectrum bandwidth is more straightforward [3][4]. Therefore, as the very front-end of a wireless communication system, wideband and high gain antennas play a critical role to make data transmission possible. Wide communication bandwidth allows more data from different channels to be received at the same time, and high gain guarantees the stability of data transmission, increase the SNR, and strengthen the viability, especially the millimeter-wave (mm-wave) wireless communications [7]–[9].

According to the white books on 5th Generation wireless communication systems (5G) new antennas presented in [4], modern wireless technologies require the antennas support full-band beamforming. High-precision beamforming brings better Reference Signal Receive Power (RSRP) and the

signal-to-noise ratio (SNR) [2]. In the C-band/TDD 2.6 GHz frequency band, some 5G antennas already support high-precision beamforming. The Sub-3 GHz FDD frequency band may also be considered to support high-precision beamforming in the future [4]. Nowadays, the 4G services are still providing stable data service for users. Therefore, a collaborative design is a necessary attribute of 5G antennas. The coordination of radio access networks (RAN) and antennas in 5G networks will reach a new height. All frequency bands of the 5G network will support minimal site deployments. To support such a wide bandwidth, reconfigurable and tune-able structures are more desired due to adjacent channel interference and cross-talk in some applications, however, the geometry of the tunable device (i.e., tuning frequency or pattern by lumped elements, such as PIN diode, capacitor.) are usually complex [10][11]. Modern, and future wireless communications require antennas to have wide operating bandwidth and stable radiation patterns to support the full-band operation; also, simple geometry is necessary for easy fabrication and low-cost deployment.

In 1954, an antenna feed design combining the complementary electric dipole and magnetic dipole sources was presented [12]. The antenna feed has an identical radiation pattern in the E- and H-planes. Therefore, it can serve as a good feeding mechanism for parabolic reflector. Based on this idea, after decades of research, magneto electric (ME) dipole antennas have evolved and became more and more popular in modern wireless communications. Nowadays, magneto-electric dipole antennas are well known for the features of wide impedance bandwidth, stable high gain, similar E- and H-plane radiation patterns, and high front-to-back ratio. However, the geometries of the conventional ME dipole antennas reported in the literature are still complex. It is relatively difficult and expensive to manufacture these ME dipole antennas for mass production. Moreover, it is challenging to realize a pseudo-ME dipole in the mm-wave band.

In this thesis, three pseudo magneto-electric dipole antennas of simple geometry, wide bandwidth and high gain are proposed to solve the problems stated above. A cavity-less linearly polarized (LP) Pseudo-ME dipole antenna operating in the C-band has been first designed, analyzed, and experimentally validated. Based on the novel cavity-less Pseudo-ME dipole antenna concept, implementing Pseudo-ME dipole into mm-wave band becomes less complex; thus, an aperture coupled Pseudo-ME dipole in the 5G mm-wave band is then introduced. Finally, the design of a wide axial ratio bandwidth circularly polarized Pseudo-ME dipole antenna in the S-band based on the cavity-less concept is presented.

1.1   Aims

In the thesis, we aim to design antennas which have:

- Wide impedance bandwidth
- High gain
- Stable polarization
- Simple geometry
- Low fabrication cost

to support modern high-performance wireless communications.

It is essential for antennas to have wide impedance bandwidth to support the massive data transmission in modern wireless communications.

On the other hand, high gain is also a critical feature required. The high antenna gain guarantees stable and detectable signal strength at the predicted distance ranges and within the system dynamic range with reduction on noise and interference contributions. Moreover, the gain of a wideband antenna is required to be stable across the whole operating bandwidth for reliable transmission and

reception. A stable radiation pattern across the entire operating band is also essential. As the antennas are required to point in a specific direction, if the antenna radiating direction changes with the frequency, then re-alignments are needed for different frequencies or channels.

1.1.1 Research contributions

The main contributions of this research are:

A low-profile cavity-less pseudo magneto-electric (ME) dipole antenna is proposed. Conventionally, a ME dipole antenna has a quarter-wave cavity to facilitate the magnetic dipole mode for radiation simultaneously with electric dipole to achieve wide bandwidth and stable high gain. While in this thesis, a novel simple pseudo-ME dipole antenna without the quarter-wave cavity has been first demonstrated. This cavity-less design can achieve comparable 1. wide impedance bandwidth, 2. slightly higher gain, 3. and smaller in-band gain variation. Also, the overall thickness of the pseudo-ME dipole antenna becomes thinner and simpler for easy fabrication without the quarter-wave cavity. The height of the antenna is only $0.164\ \lambda_0$ (λ_0 is the free space wavelength), much less than the traditional $0.25\ \lambda_0$, making it possible to implement into limited space. It is worth mentioning that all Pseudo-ME dipole antenna designs presented in this thesis have applied the cavity-less concept.

Applying the cavity-less concept, a high gain and wide bandwidth pseudo-ME dipole antenna in the mm-wave band has been designed and verified. The proposed antenna was designed on two layers of PCB. Traditional cavity geometry in the mm-wave band consists of a series of via-holes for creating the magnetic dipole cavity, that increases the fabrication complexity. Benefit from the cavity-less geometry, that no via-hole in this design, which reduces the antenna fabrication difficulty in the mm-wave band. The proposed mm-wave

pseudo-ME dipole has achieved a wide 33.6% impedance bandwidth and a 7 dBi average gain.

A wide axial ratio (AR) bandwidth circularly polarized Pseudo-ME dipole antenna has also been presented. By feeding the proposed circularly polarized (CP) Pseudo-ME dipole antenna with a single coaxial cable, the AR bandwidth achieved is 54.1%. Traditional CP radiation is generated by two orthogonal resonances which have a 90° phase difference, and the two resonances have to operate in close frequencies, so the AR bandwidth is limited. The proposed antenna has two pairs of orthogonal resonances with appropriate amplitudes and phase differences operating at relatively separated frequencies, therefore, the AR bandwidth of the single-port CP Pseudo-ME dipole antenna increase dramatically. Furthermore, the antenna radiating layer is printed on a single dielectric layer PCB, making it easy to fabricate.

1.1.2 Thesis overview

This thesis has six chapters, and the thesis outline is listed as follows:

Chapter1 gives the main objectives of this research work and poses the contributions of the research.

Chapter2 reviews the relevant fundamental antenna background theory, including the essential antenna parameters, such as gain and bandwidth, and the basic radiating principle and performance of electric dipole antennas, magnetic dipole antennas, and magneto-electric dipole antennas. Also presents the evolution of the magneto-electric dipole antenna in the context of the original concept of combination of two complementary sources, the first magneto-electric dipole antenna with high gain and wide bandwidth. Moreover, linearly polarized, and circularly polarized Pseudo-ME dipole antennas reported in the literature will be discussed.

Chapter 3 presents a low-profile cavity-less pseudo-ME dipole antenna. It demonstrates that the cavity-less Pseudo-ME dipole has comparable performance without a quarter-wave cavity.

Chapter 4 discusses a new wide 3dB-axial ratio bandwidth circularly polarized pseudo-ME dipole antenna. The presented Pseudo-ME dipole antenna has two pairs of electric dipoles and magnetic dipoles resonances. Those two pairs of orthogonal resonances with proper amplitudes and phase differences provide the antenna with extensive 3dB-axial ratio bandwidth.

Chapter 5 presents an aperture-coupled pseudo-ME dipole antenna operating at a 5G millimeter-wave band. The simple geometry of the antenna makes it easy to fabricate and implemented into communication systems.

Chapter 6 concludes the proposed novel pseudo-ME dipole antennas and verified whether they fulfill the research targets. Corresponding future work will also be presented for further study.

2.Background Theory

2.1   Introduction

The essential antenna background knowledge for this research will be provided in this chapter. There will be a brief introduction of the electromagnetic wave in section 2.2 since the antenna is designed to transmit or receive it [13]. In section 2.3, the primary antenna parameters will be introduced. In sections 2.4 to 2.6, the essential information of the electric dipole antennas, the magnetic dipole antennas, and magneto-electric dipole antennas will be highlighted. Section 2.7 reviews several LP and CP magneto-electric dipoles antennas.

2.2   Electromagnetic wave

James Clerk Maxwell derived a waveform of the electric and magnetic equations. The equation describes the electric field (E-field) that interferes with the magnetic field (H-field) and vice versa [14][15]. These oscillating magnetic and electric fields form electromagnetic waves (EM waves). EM waves carry energy in the form of oscillating and orthogonal electric and magnetic fields. A medium is not necessary for propagation, so it can travel (radiate) in free space or vacuum.
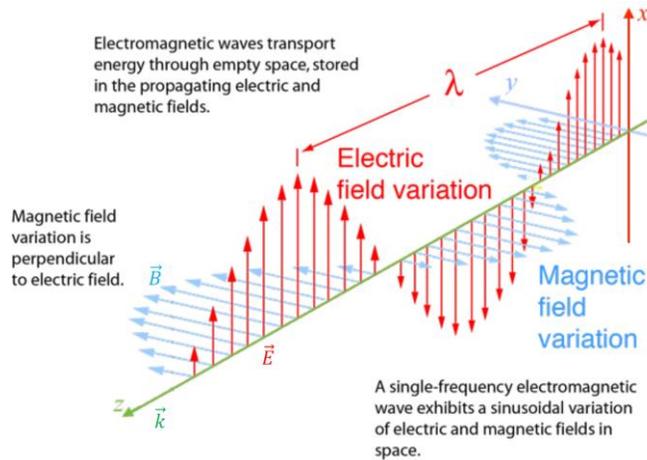
Fig. 2.1: Electromagnetic waves [1]

Fig. 2.1 shows the electric and magnetic fields are orthogonal, and they are propagating along the z-axis. The electric field ($\vec{E}$) and magnetic field ($\vec{B}$) can be determined by Eq. 2.1 and Eq. 2.2 [16], respectively. Where A represents the amplitude and ϕ_x *and* ϕ_y represent the phases.

$$\vec{E} = A \sin\left(\omega t + \phi_x\right)\hat{x}$$

Eq. 2.1

$$\vec{B} = A \sin\left(\omega t + \phi_y\right)\hat{y}$$

Eq. 2.2

2.3   Antenna Parameters

There are serval parameters to define the performance of antennas. In this section, the antenna parameters used in this thesis will be explained. Firstly, the parameters related to defining the operating frequency of the antenna will be explained, including the impedance, VSWR, S_{11}, efficiency, and bandwidth. Secondly, the antenna radiating performance parameters will be introduced. They are directivity, gain, radiation patterns, and field regions.

2.3.1   Impedance

The input impedance of the antenna, Z_L, can be calculated by dividing the voltage and the current at the input port of the antenna [16]. It is a complex quantity and presented by Eq. 2.3, where R represents the real part of the

34

impedance, and *X* represents the imaginary part of the impedance. It is one of the most fundamental parameters since the reflection coefficient, efficiency, and gain are related to the input impedance.

$$Z_L = R + jX$$

<div align="right">Eq. 2.3</div>

For example, an antenna has an impedance of 50 Ω. Since there is no imaginary part in the impedance, that means the voltage and the current are in-phase. Likewise, assuming a complex number gives the impedance, i.e., $Z_L = 50 + j50$ Ω. The magnitude of the impedance could be derived by Eq. 2.4, equal to 70.71Ω.

$$Magnitude = \sqrt{R^2 + X^2}$$

<div align="right">Eq. 2.4</div>

The phase will be derived by Eq. 2.5 and equal to 45° in this case. This means the phase of the voltage is 45° advanced to that of current.

$$Phase = tan^{-1}\left(\frac{X}{R}\right)$$

<div align="right">Eq. 2.5</div>

2.3.2 Reflection coefficient

Another essential parameter to characterize antenna performance is the reflection coefficient (Γ). It tells how much energy is reflected from the antenna due to the impedance mismatch. Moreover, there are several ways to describe this, such as return loss (RL), scattering parameters (S-parameter), and voltage standing wave ratio (VSWR). Also, an antenna operating frequency is related to

the reflection coefficient to display how much impedance mismatch across the frequency band.

The relation between reflection coefficient and antenna impedance is explained in Eq. 2.6. Z_0 is the characteristic impedance of the transmission line. When Z_0 and Z_L are mismatched, reflection will present, energy will be reflected rather than transmitting to the antenna. So, it is imperative to do the impedance match to avoid loss; in other words, keep the load impedance Z_L of the antenna as close as possible to the characteristic impedance Z_0 is required. Generally, the characteristic impedance of most antennas or a transmission line is 50 Ω.

$$\Gamma = \frac{Z_L - Z_0}{Z_L + Z_0}$$

Eq. 2.6

2.3.3 Return loss

Return loss (RL) describes how much power loss in the signal returned in a transmission line or antennas. It is usually presented as a ratio in decibels (dB) and can be calculated by Eq. 2.7.

$$RL(dB) = 10log_{10}\frac{P_i}{P_r}$$

Eq. 2.7

where *RL* (dB) is the return loss in dB, P_i is the incident power, and P_r is the reflected power. Generally, the larger value of return loss represents the lower level of impedance mismatch in the network.

2.3.4 VSWR

An alternative way to express the reflection of power at discontinuities is the voltage standing wave ratio (VSWR), which could be calculated from Eq. 2.8. VSWR is always a value between 1 and infinity. When VSWR equals to 1, it means the impedance matching is perfect. While the more extensive the VSWR is, the worse the impedance matching is.

$$VSWR = \frac{(1 + |\Gamma|)}{(1 - |\Gamma|)}$$

Eq. 2.8

2.3.5 S-parameters

Another parameter to evaluate the amount of power transmitted to a two-port network is the scattering parameters (S-parameters). Eq. 2.9 describes the 2-port network showed in Fig. 2.2, where a_1 and b_1 represent the input/output power at port 1, and a_2 and b_2 represent the input/output power at port 2. V_1 and V_2 represent the voltage at port 1 and port 2 and I_1 and I_2 represent the current at port 1 and port 2.
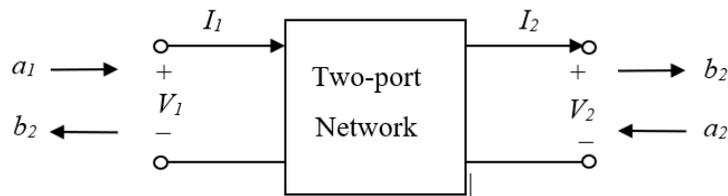
Fig. 2.2: Two-port network inputs and outputs

$$\begin{bmatrix} b_1 \\ b_2 \end{bmatrix} = \begin{bmatrix} S_{11} & S_{12} \\ S_{21} & S_{22} \end{bmatrix} \cdot \begin{bmatrix} a_1 \\ a_2 \end{bmatrix}$$

Eq. 2.9

Therefore, the reflection coefficient could also be calculated by S-parameters, as shown in Eq. 2.10. Generally, for a one-port antenna, S_{11} represents the ratio between the reflected and incident power.

$$S_{11} = \left.\frac{b_1}{a_1}\right|_{a_2=0} \qquad \text{Eq. 2.10}$$

Moreover, S_{11} will be the parameter to describe the reflection in this thesis. The operating bandwidth will be determined by the expression, $10\log(|S_{11}|) \leq -10$ dB, which means 90% of the input power has been delivered into the antenna. The reflection coefficient is a measure to show how much power is fed into an antenna. A low reflection coefficient only means the impedance of the antenna is well-matched with the system characteristic impedance in the frequency band. However, it does not mean the power will be radiated out from the antenna. Other parameters, such as the gain, efficiency, and radiation patterns, must be considered together to define how much signal will be radiated.

2.3.6 Fractional bandwidth

Antennas are usually designed to operate at a specific range of frequency. Generally, the frequency band with $S_{11} \leq -10$ dB is considered as the antenna operating frequency. Alternatively, VSWR ≤ 2 is another commonly used indicator that could be used to consider the operating bandwidth. Depending on applications, the bandwidth requirement is different. Narrow bandwidth antennas receive a less interfering signal from the undesired frequency, so the signal-to-noise ratio in the operating band remains high. A wide bandwidth antenna could support more channels; broadcast and television applications usually require a wideband antenna. The bandwidth of an antenna, *BW*, is usually expressed as a relative value to the center frequency, as shown in Eq. 2.11 f_{high} and f_{low} represent the high and low frequency points where S_{11} equal to -10 dB and f_c is the center frequency between f_{high} and f_{low}. For example, a

standard microstrip patch antenna is usually considered a narrowband antenna, and its bandwidth is usually less than 5% [17]. However, pseudo Magneto-electric dipole antenna has a wider bandwidth, larger than 40% generally.

$$BW = \frac{f_{high} - f_{low}}{f_c} \times 100\%$$

<div align="right">Eq. 2.11</div>

2.3.7 Efficiency

In antenna theory, antenna efficiency usually means "radiation efficiency". Eq. 2.12 defines radiation efficiency as the ratio between the gain and directivity. It can also be derived by dividing the total radiated power to power fed into the antenna in the transmission case. θ and ϕ are the elevation angle and azimuth angle in the spherical coordinate system.

In addition to the radiation efficiency, there is another quantity called "total efficiency". The total efficiency can be derived by dividing the total radiated power from the antenna to the power transmitted to the antenna terminal. Due to the impedance mismatch, the total efficiency is always smaller than or equal to the radiation efficiency.

$$radiation\ efficiency = \frac{power\ gain\ in\ all\ direction\ (\theta, \phi)}{directivity\ in\ all\ direction\ (\theta, \phi)}$$

<div align="right">Eq. 2.12</div>

2.3.8 Directivity

The antenna's directivity is a ratio between the averaged radiation power intensity at a particular direction and the total power radiated by the antenna

multiplied by a factor of 4π (4π represents the surface area of a sphere). Eq. 2.13 defines the directivity of an antenna. On the other hand, directivity could also be expressed by the relation of the antenna under test (AUT) and an isotropic radiator, as shown in Eq. 2.14, where P_{ra} is the total radiated power. The unit of directivity is dBi, which is the radiated/received power in dB compared with an isotropic radiator (i for isotropic). In some cases, dBd is also used, which means the power in dB compared with a dipole antenna (d for dipole).

$$D(\theta, \varphi) = \frac{4\pi(\ power\ radiated\ per\ unit\ solid\ angle\ in\ direction\ \theta, \phi)}{total\ power\ radiated\ by\ the\ antenna} \qquad \text{Eq. 2.13}$$

$$D(\theta, \varphi) = \frac{power\ density(\theta, \phi)}{\frac{P_{ra}}{4\pi r^2}} \qquad \text{Eq. 2.14}$$

One thing worth mentioning is, although an isotropic radiator does not exist in practice, it radiates equally in all directions so that the directivity of it is defined as 1 or 0 dBi.

2.3.9 Gain

Accordingly, the gain could be defined similarly as directivity. In a lossless antenna (no conduction or dielectric losses), the gain equals to the directivity.

$$G(\theta, \varphi) = \frac{4\pi(\text{ power radiated per unit solid angle in direction } \theta, \phi)}{\text{total power accepted from the source}}$$

Eq. 2.15

It can also be defined as the ratio based on the radiation intensity in a specific direction to the power supplied to the input port of the antenna (P_A).

$$G(\theta, \varphi) = \frac{\text{power density}(\theta, \phi)}{\dfrac{P_A}{4\pi r^2}}$$

Eq. 2.16

2.3.10 Radiation pattern

The radiation pattern shows the electromagnetic fields angular distribution of an antenna. It is a three-dimensional plot and is usually represented as a function in a spherical coordinate system (*r, θ, φ*).

In practice, the radiation pattern is usually illustrated in the principal planes. For example, in chapters 4 and 6, the radiation patterns of proposed antennas will be represented as a function of elevation angle θ with the azimuth angle ϕ equals 0° (in xz-plane) or 90° (in yz-plane), which is also the H-plane and E-plane of the proposed antennas respectively. In chapter 5, the radiation patterns of ϕ equals 45° and 135° will also be discussed.

The E-field and H-field radiated from different parts of the antenna will interfere with each other. There will be zero radiation at some specific angles due to the

field from different parts are out of phase. Likewise, the radiation will be strengthened at some angles because the field arrives in the far-field in phase. These different features of a radiation pattern are defined as nulls and lobes, and they can be further classified into the first null points, main lobe, side lobes, and back lobes [16].
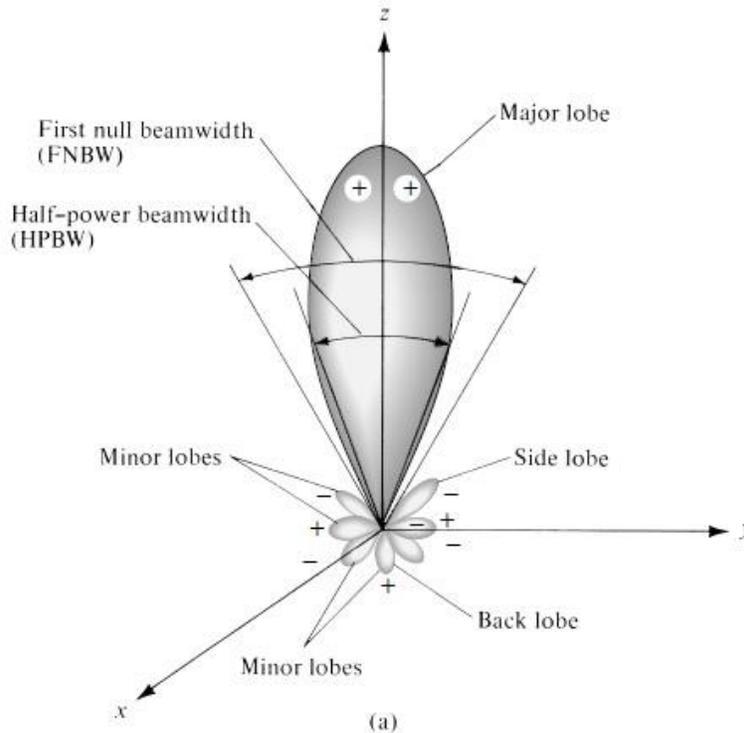
Fig. 2.3: Radiation pattern in three-dimension [16]

Fig. 2.3 shows a general radiation pattern of an antenna. The main lobe indicates the main radiation direction in the positive z-direction. In contrast, the back lobe is the beam radiating in the negative z-direction, which is approximately 180° opposite to the main lobe. The rest of the beams are called side lobes. A passive antenna does not generate extra power but may concentrate the power in the desired direction, which means the power radiated in the side lobes and the back lobes are diverted from that in the main lobe. In general, the back or side lobes should be minimized as they radiate at the undesired directions.

42

The antenna radiation pattern is usually presented in a 2D cut of a specific plane in a polar coordinate system or cartesian coordinates system. Fig. 2.4 depicts the radiation pattern in the cartesian coordinate system. The half-power beamwidth (HPBW) of the antenna is defined by the beamwidth between the two half-power points [16]. The power strength radiates in the direction outside the half-power beamwidth is always more than 3 dB lower than the maximum value in the antenna main lobe, so it is also called 3-dB beamwidth. First-null beamwidth (FNBW) could also describe the radiation pattern, which is the angular separation between the first two null points.
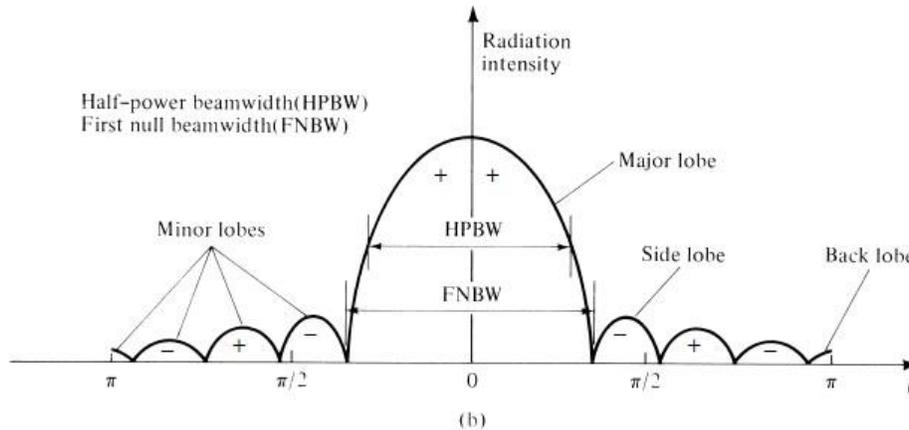
Fig. 2.4: Linear plot of radiation pattern [2]

Isotropic, omnidirectional, and directional are three types of common antenna radiation patterns. An isotropic radiator is an ideal radiation pattern that does not exist in the real world. It is usually used as a reference to define the directivity of an antenna. An omnidirectional patterns antenna could be applied for the broadcasting antenna. It is defined as *"an essential non-directional pattern in the given plane and a directional pattern in any orthogonal plane"* [16] to provide the communications system reliability transmit or receive the signal to/from unknown directions. A highly directional antenna could be used for point-to-point transmission since such patterns receive or transmit signals more efficiently in a specific direction. For example, microstrip patch antennas have

43

a directional pattern, so they are useful for cases when the locations of the transmitters/receivers are known.

2.3.11 Polarization

Another critical parameter that needs to be considered when designing or describing an antenna is polarization. Four types of polarizations will be discussed in this section: linear polarization, circular polarization, elliptical polarization, and dual polarization.

Linear polarization means the electric field or magnetic field stays at a single fixed plane when propagating. Generally, the linearly polarized antenna could be suitable for line-of-sight communications. Depending on the communication environment, the polarization of the wave does sometimes change when propagating from the transmitting antenna to the receiving antenna.

(a) Rotation of wave

(b) Polarization ellipse
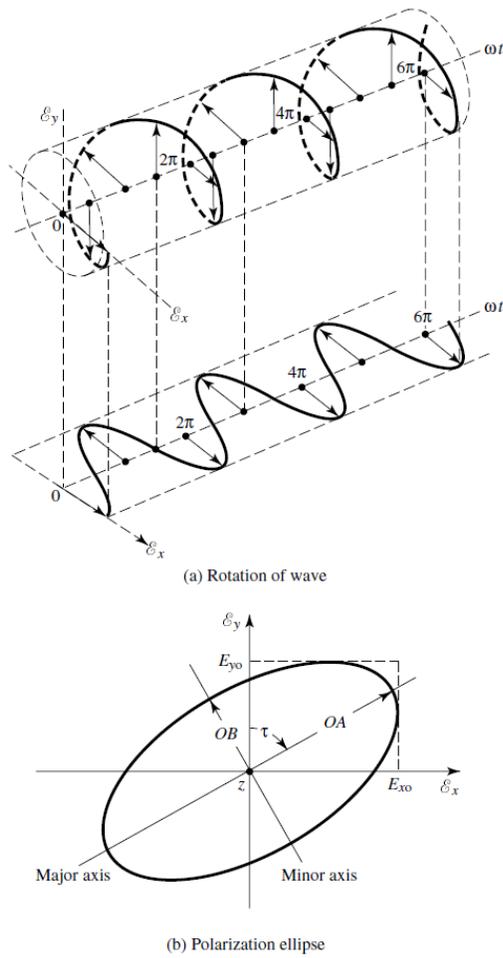
Fig. 2.5: (a) The electric field of circular polarization. (b). Elliptical polarization [16]

2.3.12 Field regions

There are three regions around the antenna: reactive near-field, radiating near-field, and far-field [16]. The field regions of the antenna as shown in Fig. 2.6.

45
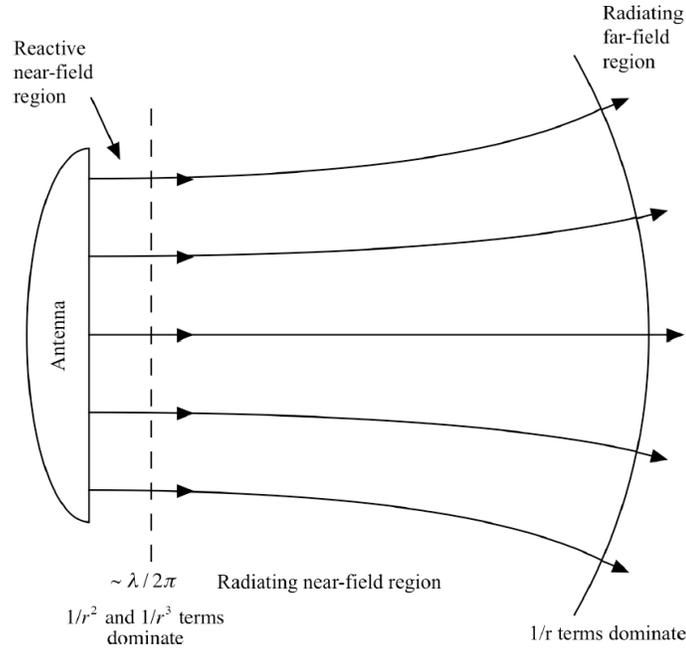
Fig. 2.6: The field regions of antenna

2.3.12.1   Reactive near-field

In the reactive near-field, the power is stored instead of propagating [14], [16]. In most cases, the regions belonging to the reactive near-field can be determined by Eq. 2.17. R_a is the distance from the antenna, D is the major (maximum linear) dimension of the antenna, λ is the wavelength.

$$R_a < 0.62 \sqrt{\frac{D^3}{\lambda}}$$

Eq. 2.17

2.3.12.2   Radiating Near-field (Fresnel Region)

Radiating near-field is also known as the Fresnel Region. In this region, the EM fields start to transit from reactive to a radiating field in this region. However, since they have not entirely transited, the shape of the radiation pattern still

varies with distance. Eq. 2.18 expresses the radiating near-field boundaries at distance R related to the major dimensions and wavelength.

$$0.62\sqrt{\frac{D^3}{\lambda}} \leq R_a \leq \frac{2D^2}{\lambda}$$

<div align="right">Eq. 2.18</div>

Since the reactive near-field does not radiate, and the radiation pattern of the antenna in the radiating near-field keeps transforming, it is usually to place the receiving antenna outside of these regions.

2.3.12.3   Far-field

In the far-field region, the electric field and the magnetic field are orthogonal, so the EM wave propagates as a "plane wave". The signal strength only decreases with R^2. Eq. 2.19 represents the far-field region:

$$R_a > \frac{2D^2}{\lambda}$$

<div align="right">Eq. 2.19</div>

2.4   Electric dipole

This thesis aims to present novel designs of high gain, wideband and simple structure pseudo magneto-electric dipole antennas. These Pseudo-ME dipole antenna features result from the cooperation of the electric dipole mode and magnetic dipole mode. In the next two sections, the basic features of an electric dipole and a magnetic dipole, including their radiation mechanism will be discussed. That would be helpful to understand the performance of pseudo-ME dipole antennas in later chapters.

2.4.1   Half-wavelength electric dipole

An electric dipole is one of the simplest forms of antennas. It is cost-effective and easy to fabricate, so it is widely used in many applications [19].
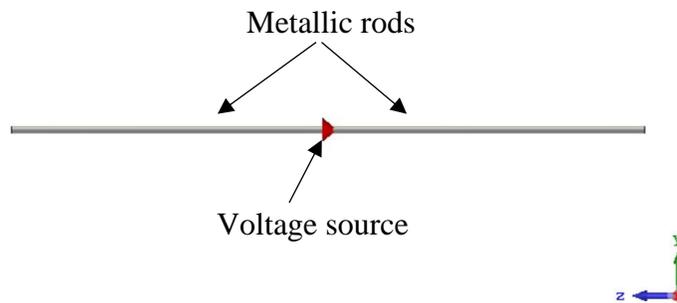
Fig. 2.7: The geometry of a half-wavelength dipole

The half-wavelength dipole is one of the most commonly used dipoles [16]. Fig. 2.7 shows a traditional common half-wavelength dipole antenna. It only consists of two metallic rods and a voltage source connecting the two metallic rods. Due to the rapid development of printed circuit techniques, dipoles could also be printed as two metal strips on the substrate [20]. Furthermore, the traditional dipole usually has narrow bandwidth due to the small volume [16]; it could be

made of thick wires or wider strips for wider operating bandwidth [20][21][22]. The impedance of a half wave-length dipole is $73 + j42.5 \, \Omega$, for the purpose of good impedance matching, the length of a half-wavelength dipole is usually around $0.48 \, \lambda_0$ (λ_0 is the free-space wavelength) of the operating frequency to achieve a $70 \, \Omega$ impedance [16].

When a voltage source is added in the gap between the two metallic rods; the two open ends of the half-wave-dipole antenna could be considered as open-circuit transmission lines. The current should be 0 A at the open ends, so if the total length of the antenna is about $\lambda_0/2$, the current will add in-phase and has the maximum magnitude at the dipole center. Fig 2.8 shows the current distribution on the dipole, the current is flowing in the negative z-direction, and the most substantial current is distributed at the center of the dipole.
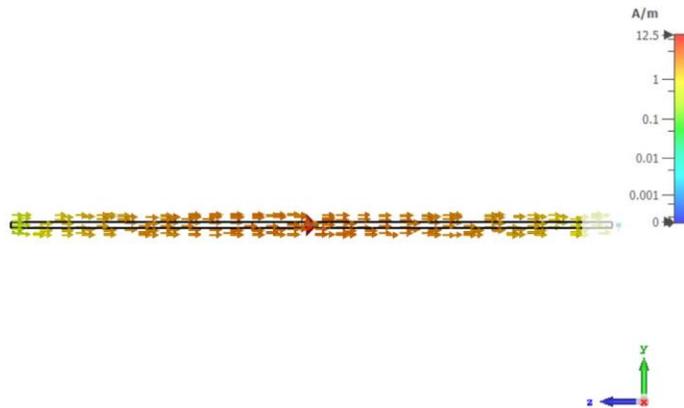
Fig. 2.8: The current distribution along a half-wave dipole at phase equals 90°

Since the current is flowing along the z-axis, there is a positive and negative charge building up in this direction, as shown in Fig. 2.9. From Fig. 2.9, the E-field has the most substantial distribution at the two ends of the dipole. It travels from the left arm to the right arm in a half period, the other way back in the next half period.
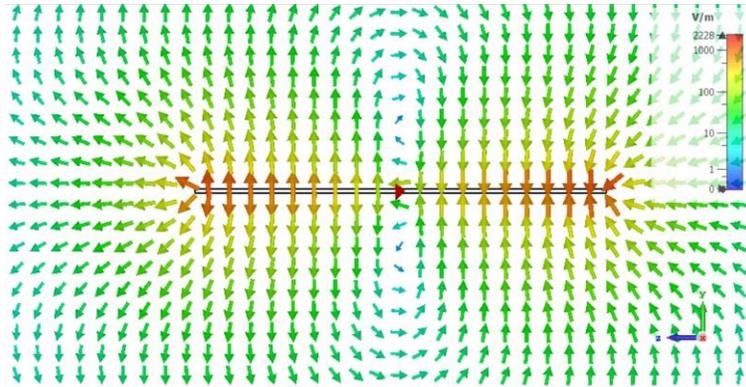
Fig. 2.9: The electric field of electric dipole when phase equal to 0°

Fig. 2.10 shows the radiation pattern of the half-wavelength dipole, the E-plane has an " inverted-8" shape, and the H-plane has an "o" shape, omni-directional [16].
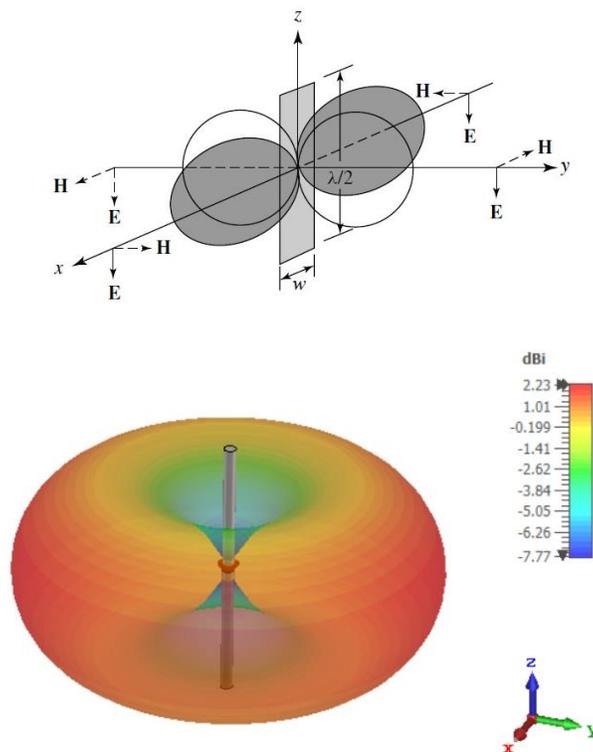
Fig. 2.10: The Radiation pattern of a half-wave dipole in three dimensions

50

2.4.2 Wideband electric dipole

As mentioned before, an electric dipole antenna is usually made of two pieces of cylindrical rods (or metallic strips). The rod radius or the strip width is much less than its length, so the impedance bandwidth of an electric dipole antenna is usually narrow due to the small volumes [16]. The operating bandwidth of the dipole can be widening by increasing the radius of the rod or the strip width, since more fundamental resonance can be generated. Those antennas are known as wideband dipoles.
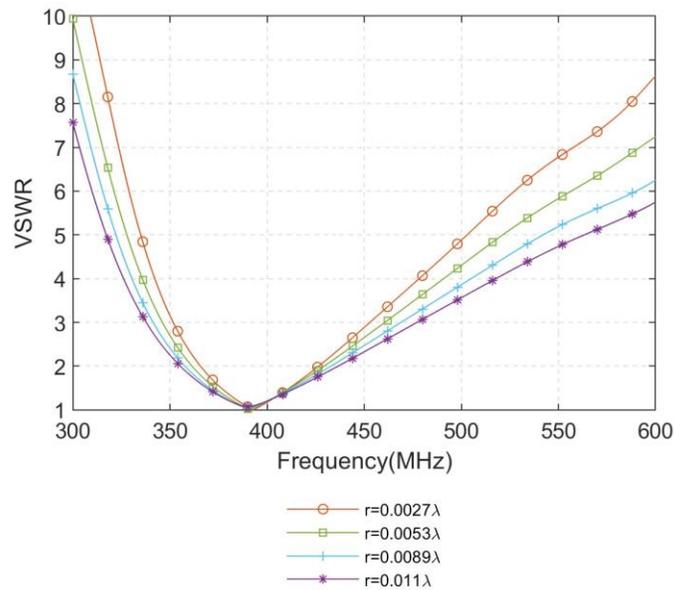
Fig. 2.11: VSWR of a half-wave dipole with different radius

Fig. 2.11 presents the VSWR of a half-wave dipole with different radii. It can be observed that the operating bandwidth (VSWR ≤ 2) are generally around 20% of the dipole increased with thicker rods.

2.5   Magnetic dipole

Magnetic dipoles are another type of primary antennas which have been widely used. Compared with electric dipoles, magnetic dipoles have a 3 dBi gain, while the realized gain of an electric dipole is 2.15 dBi [23].

A magnetic dipole antenna could be realized as a slot antenna. It has a simple structure. Generally, Fig. 2.12 shows a simple rectangular slot antenna, the length of the slot is around 0.5 λ_0, and the width of the slot is usually much less than the length. When exciting the aperture with an appropriate field, the aperture will generate an omni-directional radiation pattern with linear polarization in the y-axis.
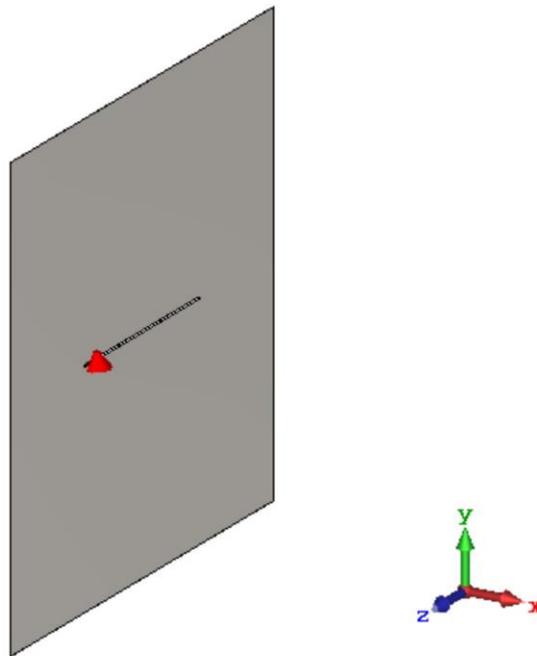
Fig. 2.12: The radiation pattern of a half-wave dipole in three dimensions

In Fig. 2.12, a voltage source is added across the shorted end of the slot antenna. The voltage source generates the electric potential difference between the slots. Assuming the slot has the length of $\lambda_0/2$ of the operating frequency, then the two

ends of the slot could be considered as short-circuited. From Fig. 2.13, it can be observed that the electric field has the most substantial distribution in the center of the slot, and it becomes weaker when close to the ends of the slot.
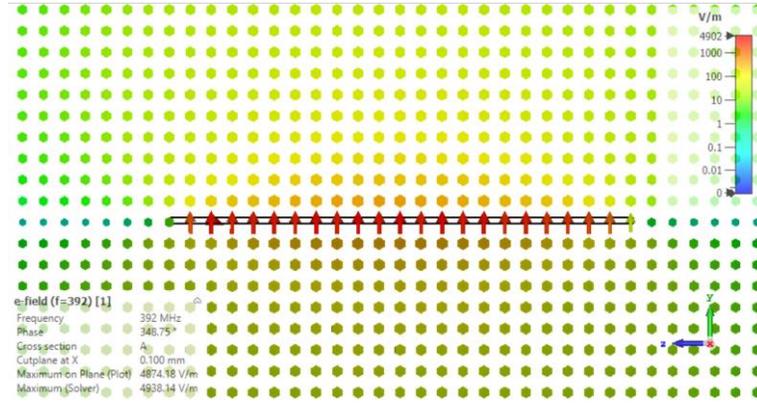
Fig. 2.13: The electric field along with the slot when phase equal to 0°

The long edge of the slot could be considered as two short-circuited transmission lines, so the current has the most substantial distribution at both ends and the weakest distribution in the middle of the slot as shown in Fig. 2.14.
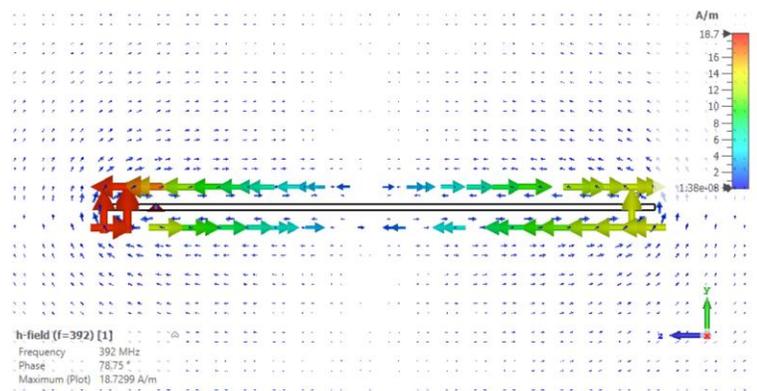
Fig. 2.14: The current distribution along with the slot

The current has almost zero magnitudes in the middle of the slot antenna. Theoretically, the impedance is infinite in the middle of the slot antenna, while the voltage has zero magnitudes at the ends of the slot, then the impedance is 0 Ω. Generally, matching a slot antenna with a 50 Ω transmission line, the practical feeding point is not located at the center but between the ends and the center of the slot. It worth to mention that the feeding locations for Pseudo-ME dipole antenna presented in chapter 4 to 6 in in the center of the open slot.

Fig. 2.15 shows the radiation pattern of a magnetic dipole antenna (rectangular slot antenna), the E-plane has an "o" shape omni-directional pattern, and the H-plane has an " inverted-8" shape [16].
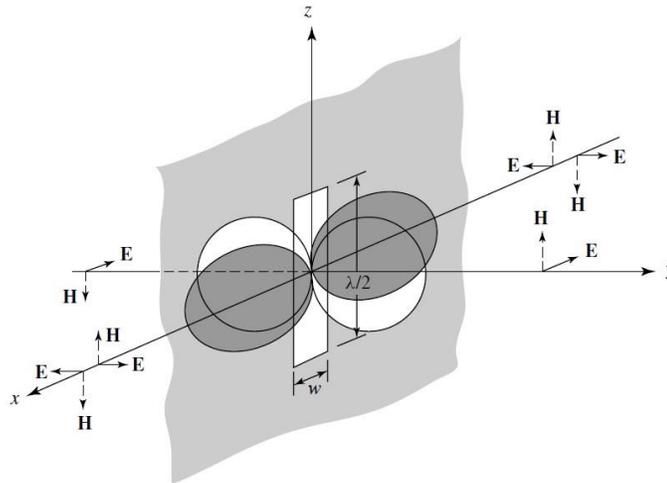
Fig. 2.15: Radiation fields of a magnetic dipole

2.6   Magneto-electric dipole antenna

In sections 2.4 and 2.5, the basic radiating principle of an electric dipole antenna and a magnetic dipole antenna has been introduced. The radiation pattern of the slot antenna is identical in shape to that of a half-wave dipole except for the E- and H-fields are interchanged [16]. Therefore, if locating an electric dipole and magnetic dipole in a perpendicular position, the electric field of both antennas will add up. Chlavin made this discovery in 1954 [12], then Wong and Luk explained the detailed operating principle and presented the pseudo Magneto-electric dipole antenna in 2008 [24].

(a)
E-plane pattern of
dipole

(b)
E-plane pattern of
slot

(c)
Combined pattern
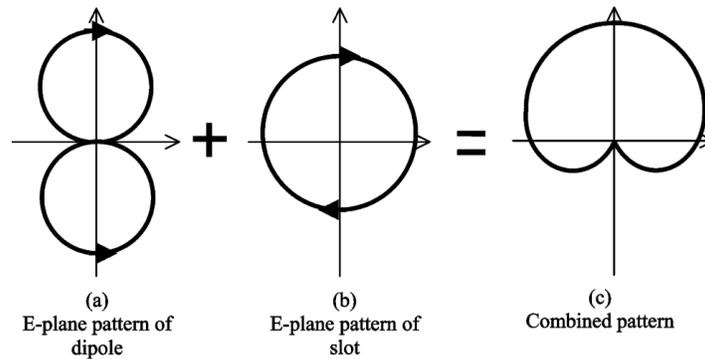
Fig. 2.16: E-plane radiation pattern of combined electric dipole and magnetic dipole [24]

Fig. 2.16 shows the combination of the radiation patterns of a pair of complementary sources. the collocated electric dipole and magnetic dipole operating at the same frequency. The radiating power will be added in the broadside direction while the total power is suppressed in the backside [24]. As a result, this combination makes the antenna has similar 'cardio' shape radiation patterns in E- and H-plane. Moreover, if the operating frequency of two complementary sources has a slight difference, wide operating bandwidth and stable high gain could be obtained.

In the next chapter, the detailed literature review of magneto-electric dipole antenna will be presented.

2.7   Literature Review

Magneto-electric (ME) dipole antennas are well-known for the advantages of high gain and wide bandwidth. These features are resulted when the electric dipole mode and the magnetic dipole mode operating at slightly different frequencies. Furthermore, the ground plane reflecting the backward radiation will provide higher antenna gain and a higher front-to-back ratio. In this chapter, the origin design, the evolution of ME dipole antennas, and various state-of-the-art designs of ME dipole antennas will be discussed.

In 1954, Chlavin [12] presented the original conception of combining an electric dipole and magnetic dipole. By exciting these two complementary sources simultaneously, Chlavin produced an antenna feed with equal radiation patterns in E- and H-plane [12]. In 2008, Wong and Luk [24] introduced a wideband unidirectional antenna composed of a shorted bowtie patch antenna and electric dipole, which has a 60% impedance bandwidth. It consists of a horizontal planar dipole (electric dipole) and a vertical quarter-wave slot cavity (magnetic dipole). The two complementary dipoles radiate at the adjacent frequency bands to provide the wide impedance bandwidth, stable and high gain, and similar radiation patterns in both E- and H-planes across the operating frequency band. Since antennas with the low-profile feature are in high demand, Ge [19] presented a low-profile ME dipole with folded-cavity geometry. It has an impedance bandwidth of 45.6% and a stable high gain in the operating frequency band; most importantly, the height of the Pseudo-ME dipole is reduced to 0.169 λ_0. It makes it possible to be implemented into limited space.

Given the features mentioned above, a series of ME dipole designs has been reported after. A microstrip line fed ME dipole, which stacks an electric dipole on top of a shorted bowtie patch is reported [25]. It has 60% impedance bandwidth (VSWR ≤ 2). A beamwidth reconfigurable ME dipole fed by a Γ-shaped probe has been presented [24]. The reported antenna supports dynamic

beamwidth reconfigurability in H-plane by controlling the pin diodes conduction state, which connects the strip and the grating reflector [26]. To reduce the antenna's profile, a microstrip line fed pseudo Magneto-electric dipole antenna, consisting of a horizontal planar dipole and a vertically oriented folded shorted slot cavity pair is reported [26][19]. Dual-band ME dipole antennas have been designed to support multi-band applications [27][21][28]. By implementing different feeding methods, ME dipoles with different polarization have also been reported, such as dual-polarization [29][30][31][32][33] or circular polarization [34][35][36][37].

2.7.1 Linear polarization ME dipole antennas

2.7.1.1   An antenna feed with equal E- & H-planes

Fig. 2.17 (a) shows the combination of two complementary-sources suggested by Chlavin [12]. Fig. 2.17 (b) shows the physical antenna feed of an electric dipole, and an open-end waveguide is combined with equal amplitude. When the two sources are located at the same position or very close together, a symmetrical radiation pattern in the E- and the H- plane will be obtained. So, it achieves a circular beam cross-section which can be used to optimize the efficiency of illumination of a circular aperture, for example, a circular parabolic dish antenna. Furthermore, the combination of back radiation will become zero, theoretically resulting in a 'cardio' shape radiation pattern. This feed has been used to illuminate a 20-inch parabolic dish antenna with the result that the E- and H-planes have equal beamwidth, and the side lobes are 30 dB down from the main lobe.
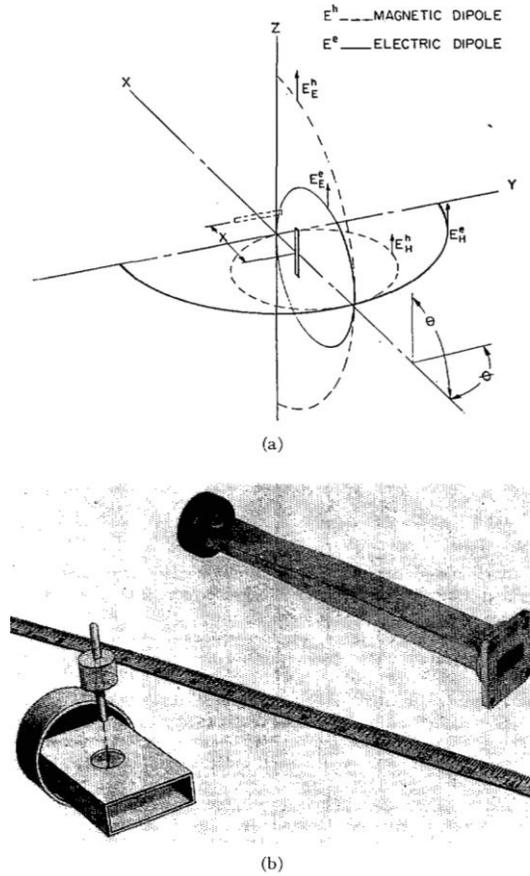
Fig. 2.17: (a). Electric and magnetic field distribution for two complementary dipoles (b). Test feed [12]

2.7.1.2   Wideband shorted bowtie patch antenna with dipole

Slot antennas are widely used for wireless communications since they can achieve wide impedance bandwidth [38]–[42]. A directional radiation pattern can be produced by adding a ground plate as a reflector underneath the radiating slot [24]. Inspired by the previous two complementary sources design, in 2008 Wong and Luk presented an antenna that consists of bowtie patches and an electric dipole with a directional radiation pattern [24]. In Fig. 2.18, two symmetrical triangle shape patches formed a bowtie antenna; the bowtie antenna could be considering a slot antenna with an open-end. Furthermore, a dipole consists of two parametric strips is introduced. This combination gives the

antenna an excellent front-to-back ratio and similar radiation patterns in E- and H-planes. The impedance bandwidth of the antenna is 63%. The maximum gain achieved is 7 dBi and a moderate 2 dB gain variation in the frequency band.
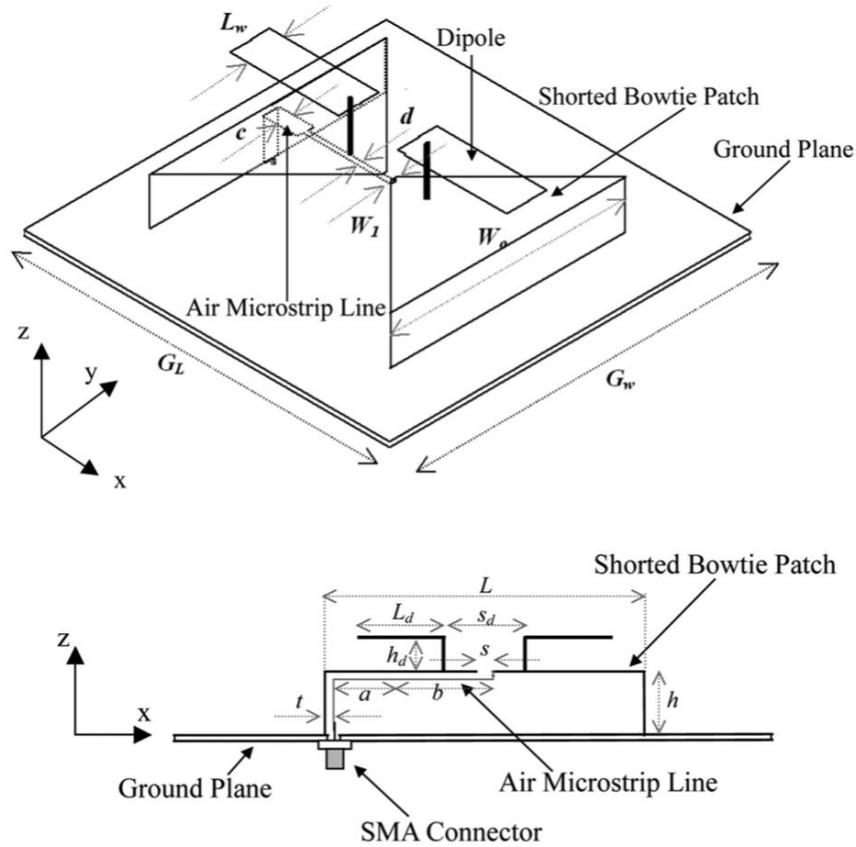
Antenna Parameters (mm)							
G_L	G_w	h	L	s	W_0	W_1	h_d
115	115	15	76.4	3	75	1.6	15
$(0.77\lambda_L)$	$(0.77\lambda_L)$	$(0.10\lambda_L)$	$(0.52\lambda_L)$	$(0.02\lambda_L)$	$(0.51\lambda_L)$	$(0.01\lambda_L)$	$(0.10\lambda_L)$

Antenna Parameters (mm)			Feed mechanism Parameters (mm)				
L_d	L_w	S_d	a	b	c	d	t
35	13	18.6	11	27.7	4.9	1.6	1
$(0.23\lambda_L)$	$(0.074\lambda_L)$	$(0.11\lambda_L)$					

λ_L is corresponded to the lowest operating frequency.

Fig. 2.18: 3D and side view of the bowtie patch antenna with dipole [24]

2.7.1.3   A low-profile ME dipole antenna

After 2010, modern wireless communications, such as 3G technology, Wi-Fi, and LTE, introduced new requirements into antenna front-end designs. Due to the great demand for higher data transmission speed and miniaturization of mobile devices. The antennas are required to have (i). high gain to compensate for the free space pass loss. (ii). wide bandwidth, so it can be used to cover more channels in the required band. (iii). low-profile features so that they can integrated easily into various device structures [19][33][43].

A low-profile wideband unidirectional antenna is shown in Fig. 2.19. The ME dipole comprises a pair of horizontal patches; the two horizontal patches work as a wideband electric dipole [44]. A pair of vertical folded short patches compose a quarter-wave cavity; such cavity provides a magnetic dipole mode antenna. A DC grounded coaxial cable is used to feed the ME dipole antenna. Like the previous design introduced in section 2.7.1.2, a rectangular cavity ground plane is used as a reflector to provide high gain and reduce the back-lobe radiation. Although the height of the antenna is less than 0.25 λ_0, benefit from the vertical oriented folded short patches, the height of this antenna is only 0.169 λ_0, and this low-profile antenna also obtained wide impedance bandwidth of 45.6% of VSWR $\leq$ 1.5.

Generally, the ground plane reflector should be set at a quarter wavelength (wavelength at the center frequency of interest) away from the radiation layer to achieve a relatively equal reflection at both low and high-frequency bands. The ground plane provides roughly 3 dB more gain to the antenna.
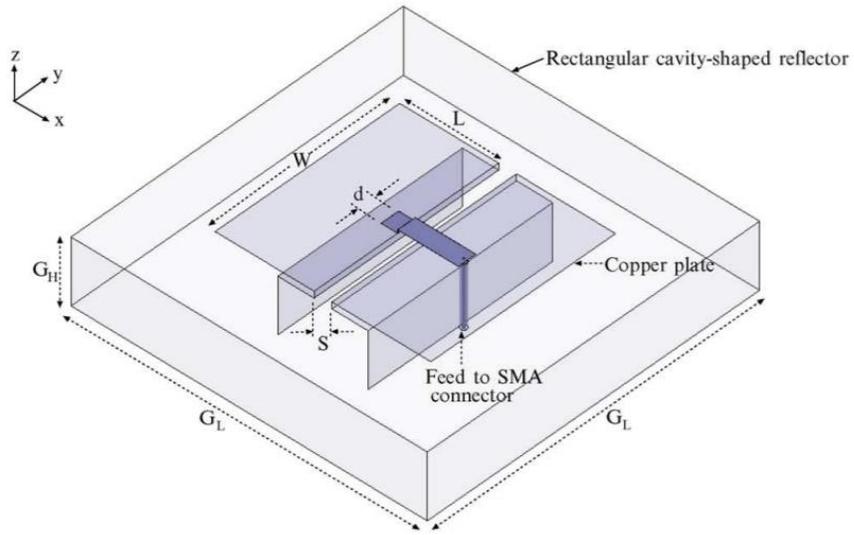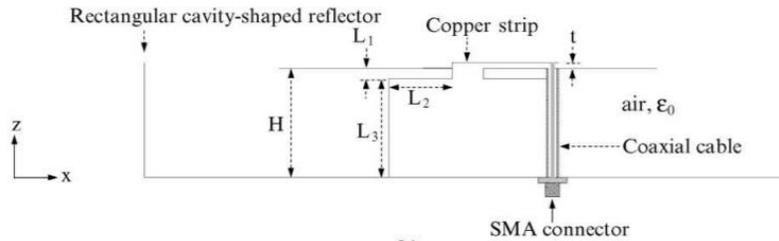
Parameters	W	L	L_1	L_2	L_3	H
Values/mm	60	30	1.8	11	17.2	19
	(0.518λ)	(0.259λ)	(0.016λ)	(0.095λ)	(0.148λ)	(0.164λ)
Parameters	S	d	t	G_L	G_H	
Values/mm	5.4	5.7	1	112	20	
	(0.047λ)	(0.049λ)	(0.009λ)	(0.967λ)	(0.173λ)	

λ *is the free-space wavelength at the center frequency*

Fig. 2.19: Geometry of the low-profile E dipole (a) 3D view (b). side view [44]

2.7.1.4   60 GHz Plated Through Hole Printed ME Dipole Antenna

62
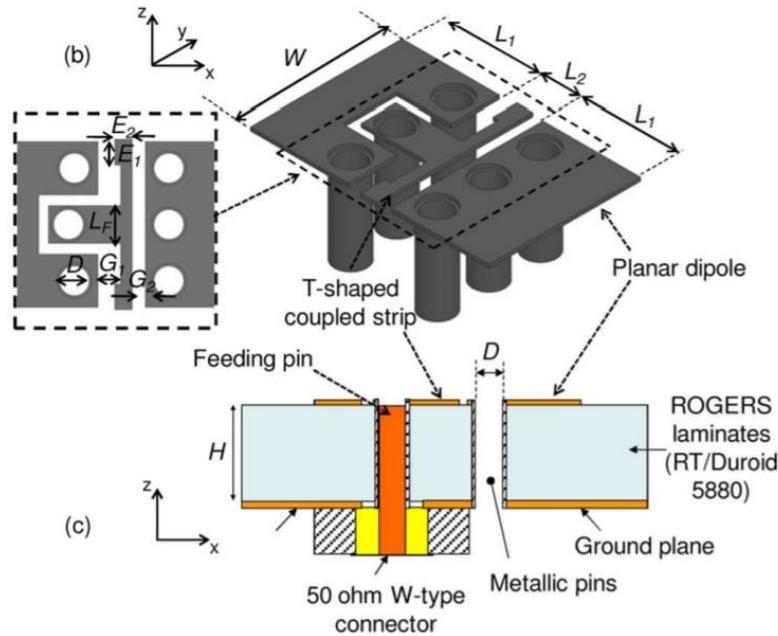
Fig. 2.20: 3-D view and side view of the 60-GHz printed ME dipole antenna [45]

In 2012. Kung Bo Ng published a 60 GHz ME dipole antenna designed by a plated through hole printed technique with the use of a microwave substrate (Rogers 5880, $\varepsilon_r = 2.2$, thickness H = 0.787 mm) [45]. Fig. 2.20 shows 3-D view and side view of the 60-GHz printed ME dipole antenna. It is excited by a T-shaped coupled strip feed, a GSG transmission line structure is formed since the feeding pin is in parallel with two shorting pins on its two sides. A W-type connector (from Anritsu: W1-103F) is located underneath the ground plane. This printed ME dipole antenna has 33% impedance band width of $S_{11} < $ -15 dB from 50 to 70 GHz and an average 7.5 dBi gain.

2.7.1.5   Comparison

The two complementary source antenna feed origin design, the first designed ME dipole antenna, and a low-profile pseudo-ME dipole antenna have been introduced in the previous sections. Some more designs of linear polarization ME dipole antenna designed have been published. Especially, our previous work of a pseudo-ME dipole antenna has achieved a comparable wide bandwidth and

a higher average gain and smaller in band gain variation. The antenna specifications have been listed in Table 2.1 for comparison.

Table 2.1: Comparison with state-of-art ME dipole antennas

	Center Frequency (GHz)	Bandwidth (VSWR≤2	Gain(dBi)	Height (λ_0)	Quarter-wave Cavity	No. of Feed Points
[19]	2.4	52.60%	6.7 ± 2.2	0.169 λ_0	Yes	1
[46]	1.48	92.00%	5.2 ± 2.5	0.250 λ_0	Yes	2
[30]	1.44	68.00%	6.3 ± 3.3	0.240 λ_0	Yes	2
[45]	61.25	44.90%		0.230 λ_0	YES	1
[47] Work in Chapter 4	2.34	41.00%	8.8 ± 0.9	0.164 λ_0	None	1

2.7.2 Circularly polarized magneto-electric dipole antennas

Circularly polarized antennas have been widely used in satellite communications [35][48]. It does not require polarization alignments between satellite and ground station antennas, which provide the communications systems more stability. However, for a single feed circularly polarized antenna, the axial ratio bandwidth is usually narrow, typically less than 10% [49][50]. Due to the wideband feature of ME dipole, a few antenna designs based on the ME dipole antenna have obtained wider impedance bandwidth and AR bandwidth [35], [51]–[53]. A dielectric-based mm-wave band ME dipole antenna achieves a wide impedance bandwidth of 56.7% for VSWR $\leq$ 2 and 41% of 3-dB AR bandwidth; however, with a gain variation of ± 2.6 dB in the operating frequency band [54]. An aperture coupled CP ME dipole antenna array fed by a low-loss gap waveguide also achieved 14.5% of AR bandwidth [36]. In this section, two highlighted CP ME dipole antennas would be introduced.

2.7.2.1   Crossed dipole loaded with ME dipole.

In 2015, Xuat and Park proposed a circularly polarized antenna with a 27% of 3-dB axial ratio bandwidth and a comprehensive 3-dB AR beamwidth of 165° [35]. The antenna combined a crossed dipole with an ME dipole antenna, as shown in Fig. 2.21. The circularly polarized radiation is achieved by exciting the pair of crossed dipole antennas which double quarter-wavelength rings feeding the two crossed dipoles with equal amplitude and 90° phase difference. Moreover, a four-patch ME dipole antenna is coupled-fed by a pair of crossed-dipoles, the crossed dipole provides the two fundamental resonances, within the introduce of the ME dipole, extra resonance has been generated. Therefore, the impedance bandwidth has been increased to 59.8%, and axial ratio bandwidth has also increased to 26.5%.
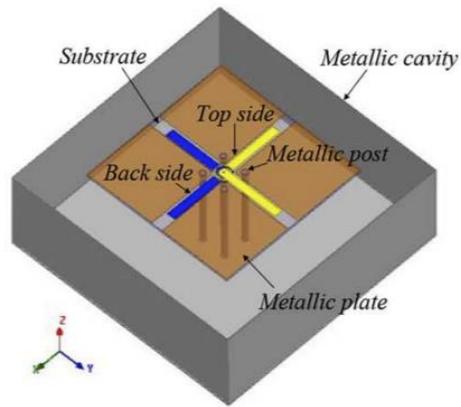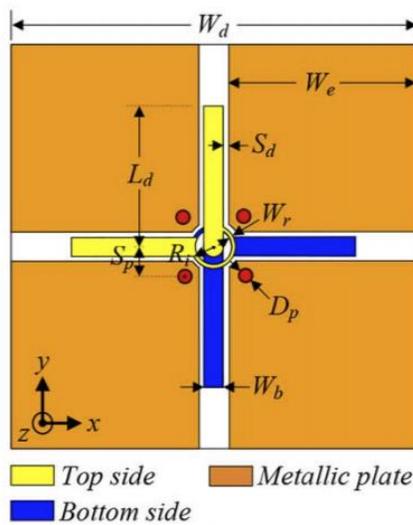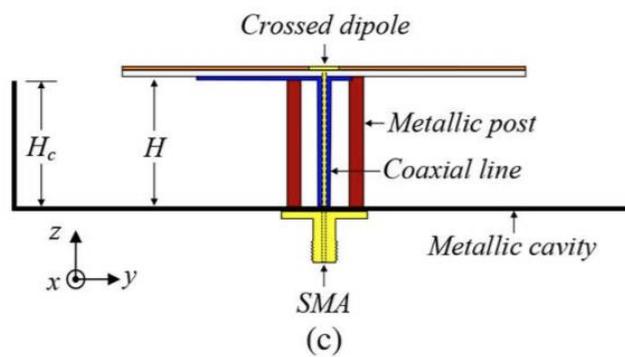
Fig. 2.21: The geometry of the crossed dipole loaded with Pseudo-ME dipole [35]

Generally, a CP antenna usually has two resonances operate at close frequencies. In this study, the presence of ME dipole geometry provides the antenna with another two resonances at closed frequency so that yield an extra AR center point. Therefore, either the impedance bandwidth or the AR bandwidth extends. In addition, A metallic cavity is used as a reflector in the bottom of the antenna.

2.7.2.2   A 60-GHz Aperture-Coupled Pseudo-ME dipole Antenna Array

Recently, investigation of 60 GHz antenna technology has attracted significant attention [55][56]. High-gain characteristics become critical to antennas operating at 60 GHz, since it is necessary to compensate for the high oxygen absorption in the propagation medium and channel [57][58]. On the other hand, circularly polarized wave can provide more promising channel performance, especially in the presence of obstacles and reflectors.
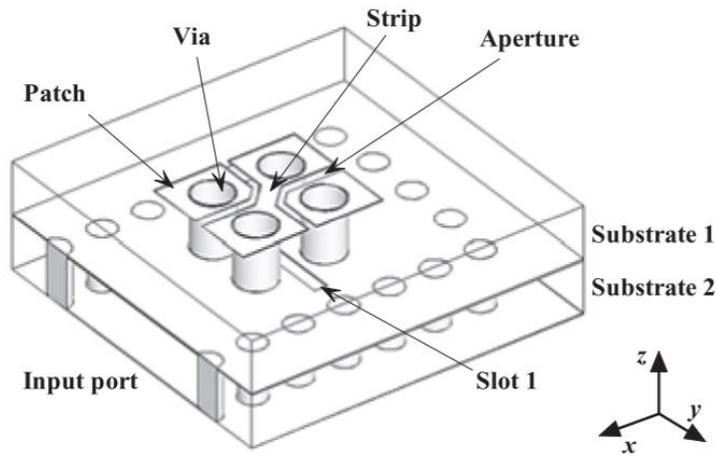
(a)
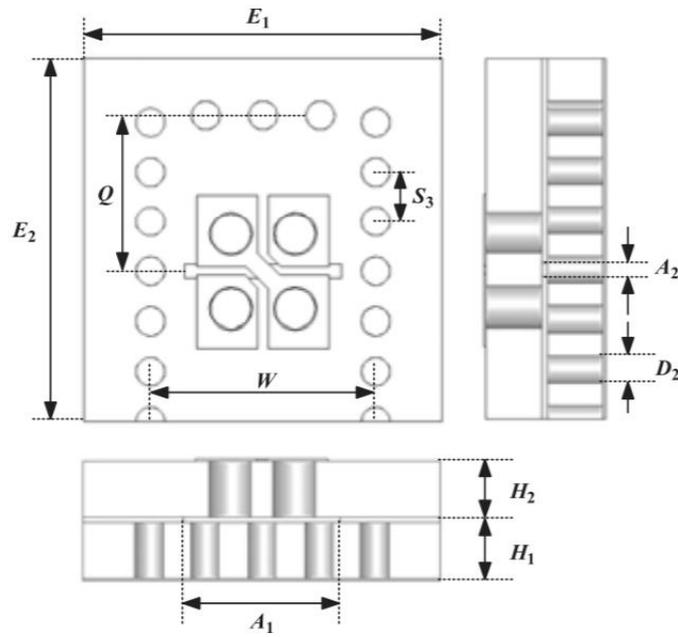
(b)

Fig. 2.22: Geometry of the SIW-fed CP aperture coupled Pseudo-ME dipole [34]

Li and Luk have presented a SIW-fed aperture-coupled ME dipole antenna that operates at 60 GHz band with circular polarization [34]. The impedance bandwidth of the antenna is 28%, and the AR bandwidth is 28.8%. The gain is 7.7 ± 1.4 dBi over the frequency band. The geometry of the antenna is shown in Fig. 2.22. The antenna is fed by an aperture located on the top layer of a substrate integrated waveguide (SIW) in Substrate 2. The radiating structures are implemented in the top substrate, consisting of vertical metallic pins and four horizontal patches. The two pair horizontal patches form two electric dipoles, while slots between the patches realize the magnetic dipoles. The feeding slot between the radiating and feeding layers excited the electric dipole vertical and the magnetic dipole simultaneously. To generate the CP radiation, or in other words, activate the parallel electric dipole, and the vertical magnetic dipole with a 90° phase difference, an additional metallic strip is added to connect two

68

patches at the diagonal direction. Thus, the input power from the slot could be coupled to excite the orthogonal ME dipole.

2.7.2.3   A comparison of reported CP Pseudo-ME dipole antennas

Table 2.2: Comparison of reported CP Pseudo-ME dipole antennas

	F_{cen} (GHz)	BW ($S_{11}{\leq}10dB$)	3-dB AR BW	Gain (dBi)	footprint (λ_o^2)	Height (λ_o)	Quarter-wave Cavity	No. of Feed Points
[34]	60.5	28.8%	25.9%	7.7 ± 1.4	1 x 1	0.31	None	1
[35]	1.1	59.7%	26.8%	8 ± 0.5	0.64 x 0.64	0.17	Yes	1
[59]	1.3	57.0%	51.8%	9.6 ± 0.4	π x 0.7^2	0.2	None	2
[60]	2.5	57.6%	39%	9.4 ± 1.4	π x 0.52^2	0.26	Yes	2
[61]	2.6	50.2 %	27%	6.2 ± 0.6	0.48 x 0.48	0.26	None	1
Antenna in Chapter 5	4	70.4%	54.1%	8.7 ± 0.9	1 x 1	0.22	None	1

Two designs of circularly polarized Pseudo-ME dipole antennas have been highlighted in sections 2.7.2.1 and 2.7.2.2. There are more CP ME dipole antennas can be found in the literature; Table 2.2 provides a detailed comparison among these antennas in impedance bandwidth, AR bandwidth, gain, feeding method, footprint, height, and cavity.

2.7.3 Concluding remarks

Pseudo-ME dipole antennas have been developed after decades of research. Generally, since the antenna has wide bandwidth and high-gain features, it is widely used for many modern wireless applications. Furthermore, as the antenna's geometry is not complicated, it could play a useful role in mm-wave

applications. It could also be loaded with other antennas to achieve better performance.

However, the reported Pseudo-ME dipole antenna geometry is still complicated, especially the Pseudo-ME dipole antennas for circular polarization, which makes it challenging to fabricate. Moreover, the vertical-cavity geometry of Pseudo-ME dipole antenna makes it difficult to implement into the mm-wave band. In the next chapter, a novel Pseudo-ME dipole without the quarter-wave cavity will be presented and analyzed.

3. A Simple-geometry Low-profile Cavity-less Pseudo Magneto-electric dipole Antenna

3.1 Introduction

Chapter 2.7 has introduced the operating principle of the magneto-electric dipole antennas and other previous designs. To our best knowledge, all the magneto-electric dipole antennas reported so far have the same feature: a vertical quarter-wave slot cavity created by a pair of conductor walls is utilized to generate the magnetic dipole mode. The fabrication of such vertical walls in the millimeter-wave frequency bands may be challenging. However, our recent study reveals that even without the quarter-wave vertical slot cavity, it is still possible to generate the magnetic dipole mode by directly activating the slot formed by the gap between the two horizontal rectangular patches with a coaxial cable.

In this chapter, a simple coaxial-fed pseudo magneto-electric dipole antenna is designed and experimentally evaluated. The pseudo magneto-electric dipole antenna presented in this chapter achieves a considerable bandwidth by utilizing the single combined electric and magnetic modes to provide more stable and higher gain across the passband. The simulations were performed by using CST Microwave Studio [18]. Prototype antennas have also been fabricated to verify the antenna performances.

3.2 Antenna geometry

Fig. 3.1 shows the geometry of the proposed antenna, and Table 3.1 gives the detailed physical and electrical dimensions. The antenna consists of two

horizontal rectangular patches; a coaxial cable serves as the feedline and a square ground plane.

The first attempt aims to design the pseudo-ME dipole antenna operating at S-band (center frequency at 2.5 GHz) to verify the feasibility. A polystyrene foam board with a thickness of 1.5 mm is used to support the two horizontal patches. The dielectric constant of the polystyrene foam board is 1.004 [62], which is very close to that of air. Thus, the effect on the antenna performance from the foam could be neglected.

Since the two horizontal patches on the radiating layer form a half-wavelength electric dipole, the length of each patch is 30 mm (0.25 λ_0) so that the electric dipole operates at around 2.5 GHz. Due to the existence of the ground plane, the fringing field of the electric dipole extends the electric length of it, so it operates lower than 2.5 GHz, this issue will be further discussed in the parametric study.

A narrow gap separates the two horizontal patches. Such gap forms an open-ended slot antenna geometry and operates as the magnetic dipole. The gap between the two patches (Gap) is 2 mm. The magnetic dipole should operate at a close frequency to the electric dipole to ensure the Pseudo-ME dipole has high gain and wide bandwidth. Thus, the patch width is set at 60 mm so that the magnetic dipole could also operate at a similar frequency. The size of each patch is 30 mm × 60 mm (L_{Patch} × W_{Patch}).

A semi-rigid coaxial cable (RG402, 50 Ω, Ø 3.58 mm) positioned at the center of the ground plane, is utilized to excite the pseudo magneto-electric dipole antenna. The length of the semi-rigid cable was first set as the quarter-wavelength of 2.5 GHz (30 mm) so that the ground plane could provide gain improvement in the operating band. In the meantime, the antenna with a low-profile feature has the advantage in limited space. Therefore, after performing

the parametric study of the antenna, it has been found out that the length of semi-rigid cable can be reduced to 21 mm (0.164 λ_0) and remains a high gain performance.

As shown in Fig. 3.1, on the top end of the semi-rigid cable, the inner and outer conductors are connected to the middle of the edges of the two horizontal patches, respectively. The bottom end is connected to a SMA connector under the ground plane. It is worth mentioning that the semi-rigid cable outer conductor is also connected to the ground plane. With such a connection, the geometry of the proposed antenna is no longer balanced. Furthermore, the ground plane play an important role of isolating the unexpected radiation from the coaxial cable, and the measured results show that the affection the radiation from the cable is minimum since they matched well with the simulated results well. Therefore, like the other Pseudo-ME dipole antennas reported in the literature, a balun is not necessary.

The square aluminum ground plane on the bottom of the antenna is also utilized to reflect the negative z-directed radiation to provide a unidirectional radiation pattern and a higher front-to-back ratio. The size of the ground plane is set up to 120 mm^2 (λ_0^2) to ensure maximum reflection.

Table 3.1: Dimensions of the cavity-less Pseudo-ME dipole antenna

Parameter	L_{Patch}	W_{Patch}	Gap
Value (mm)	30 (0.234 λ_0)	60 (0.468 λ_0)	2 (0.008 λ_0)
Parameter	H_{Air}	h	L_{Ground}
Value (mm)	21 (0.164 λ_0)	1.5 (0.011 λ_0)	120 (1 λ_0)
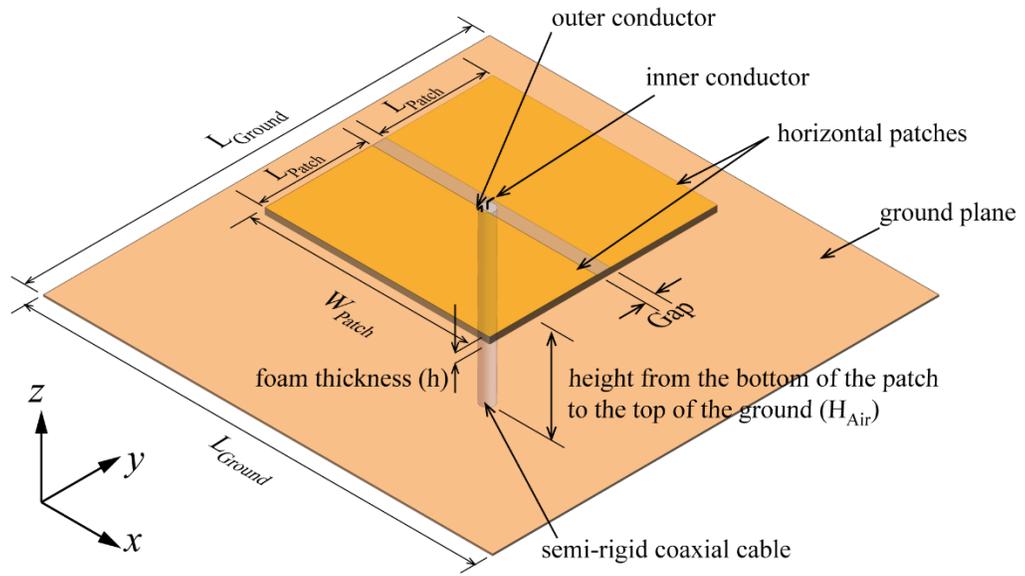
Fig. 3.1: The geometry of the cavity-less Pseudo-ME dipole antenna.

3.3   Operation principle

Magneto-electric dipole antennas usually have the features of high gain and wide bandwidth. Such advantages come from the condition that the electric dipole and the magnetic dipole are excited simultaneously with the same signal amplitude and phase. Besides, the ground plane on the bottom side of patches creates a strong reflection, which helps the antenna to achieve even higher gain and reduce the back-lobe level.

In Fig. 3.2 and Fig. 3.3, the electric field, and the magnetic field distributions of the proposed antenna at the center frequency at a different time of a cycle have been presented, with T being the period of one cycle. For the electric dipole mode, at time t = 0 and T/2, the electric field on the horizontal patches' travels in the positive and negative y-direction relatively. Therefore, the electric dipole is mainly excited at those moments. While t = T/4 and 3T/4, the magnetic field flows in positive and negative x-direction, respectively, and it has the most substantial distribution along the long edges of the gap. At these moments, the magnetic dipole is excited.
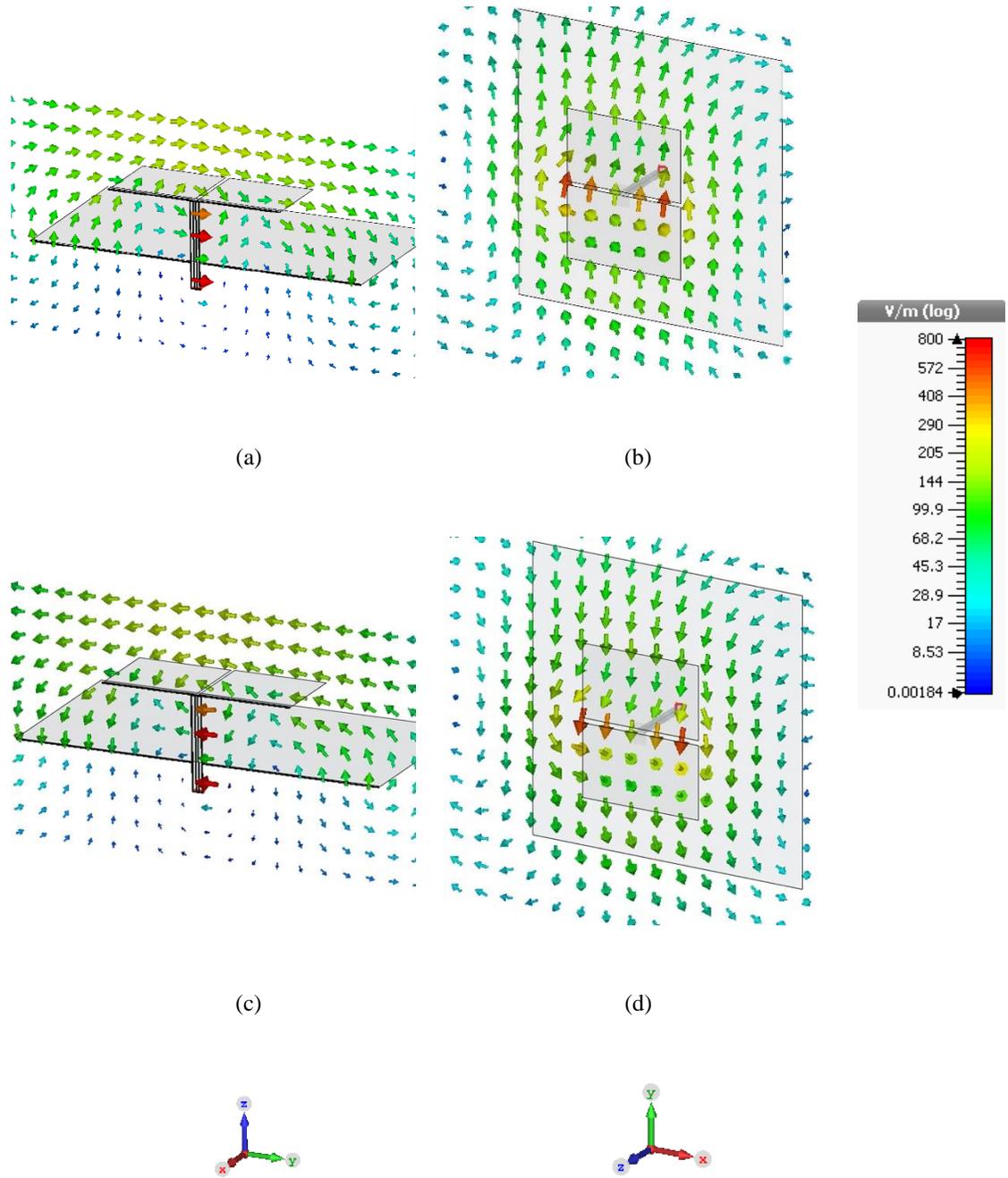
Fig. 3.2: E-field of electric dipole mode. yz plane cut (a). t = 0; (b). t = T/2; xy plane cut (c). t

= T/2; (d). t = T/2

(a)   (b)

(c)   (d)
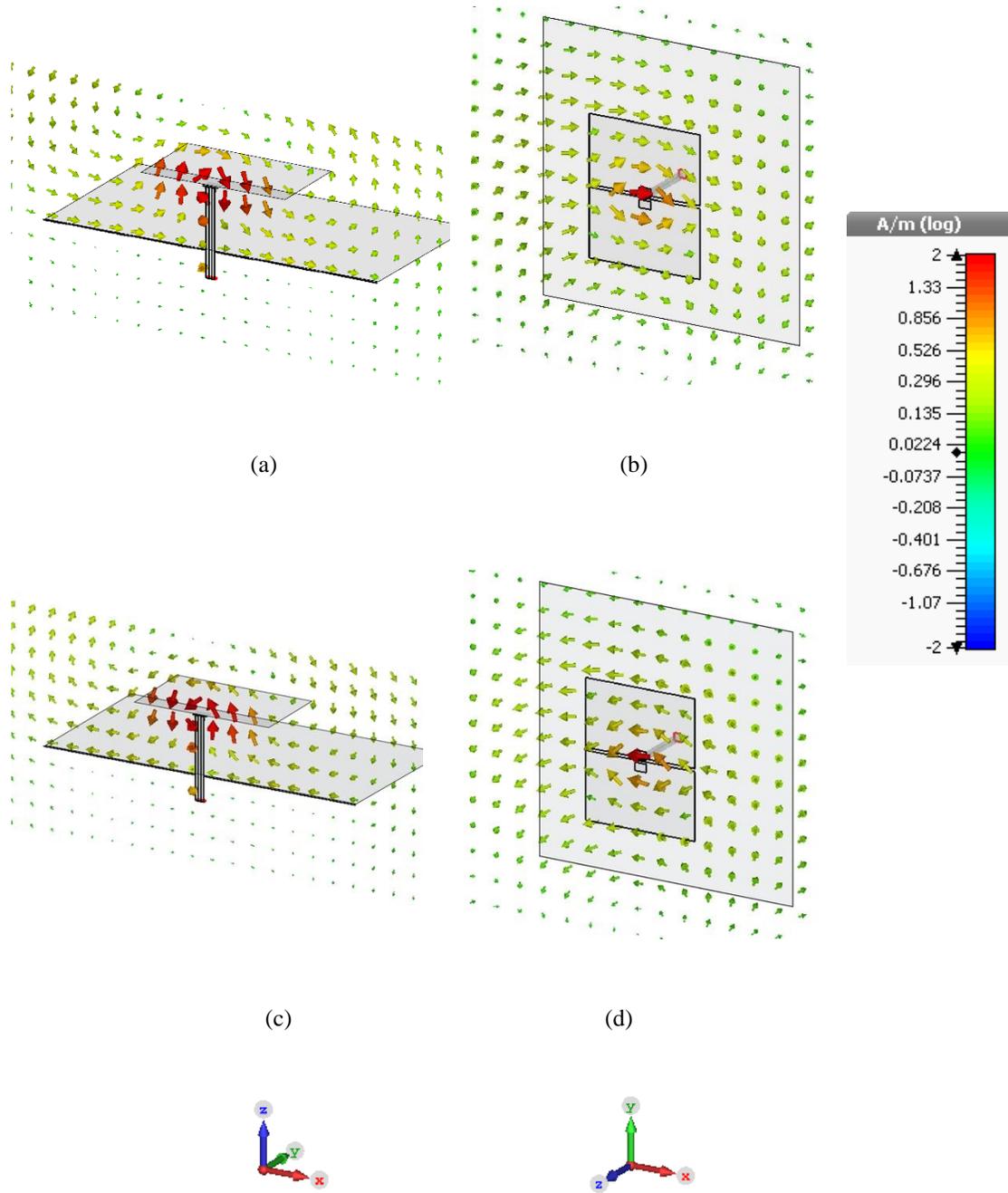
Fig. 3.3: H-field of magnetic dipole mode. xz plane cut. (a) t = T/4; (b) t = T/4; xy plane cut (c)

t = 3T/4; (d) t = 3T/4

3.4   Parametric study

A parametric study is presented in this section to investigate the influence of each parameter. Firstly, since the two horizontal patches on the radiating layer provide the two fundamental resonances (electric dipole mode and magnetic dipole mode), the length of the two patches (L_{Patch}) and the open-ended slot length between patches (W_{Patch}) will be studied. Secondly, the ground plane is employed as the reflector of the antenna. It gives the proposed antenna a unidirectional radiation pattern and increases the front-to-back ratio as well. The separation (H_{Air}) between the ground plane and radiating layer and the square ground plane (L_{Ground}) will be analyzed. The rest of the parameters remains the same values in Table 3.1 when each parameter is studied.

3.4.1 L_{Patch}

The two horizontal patches on the radiating layer produce the two fundamental resonances of the proposed antenna. Although the electric dipole and magnetic dipole have almost the same physical size, the electric dipole effective length has been elongated by the fringing field (as explained in section 3.4.2.). Therefore, the electric dipole mode operates at a relatively lower frequency. Fig. 3.4 shows the influence of L_{Patch} on Z_{11}. The first and second resonant modes have been significantly affected by tuning the patch length, which means the electric dipole mode mainly dominates the low-frequency band resonance.

Fig. 3.5 shows the influence on gain and the S_{11} of the proposed antenna against different L_{Patch}. (The dotted line is for S_{11} and the sloid line are for gain, and the following S_{11} and gain plot followed the same rule.) By tuning L_{Patch} longer, the operating band shifts to a low-frequency band since the first and second modes have been affected. Simultaneously, the gain at the low-frequency band is slightly increased and extended while the high-frequency band decreased slightly. These observations further evidence the electric dipole mode dominates antenna performance in the low frequency band.

1st mode   3rd mode

2nd mode
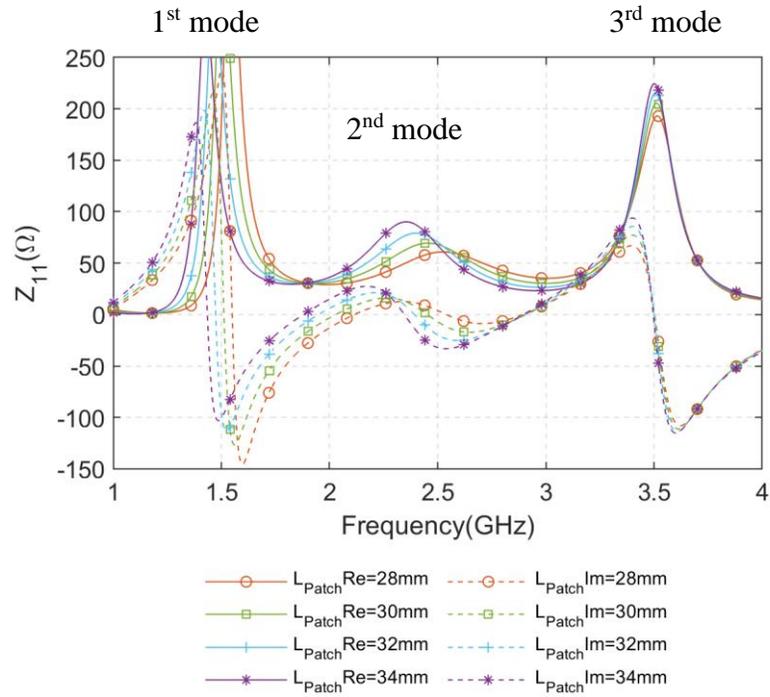
Fig. 3.4: Z_{11} of the cavity-less Pseudo-ME dipole antenna at different patch length (L_{Patch})
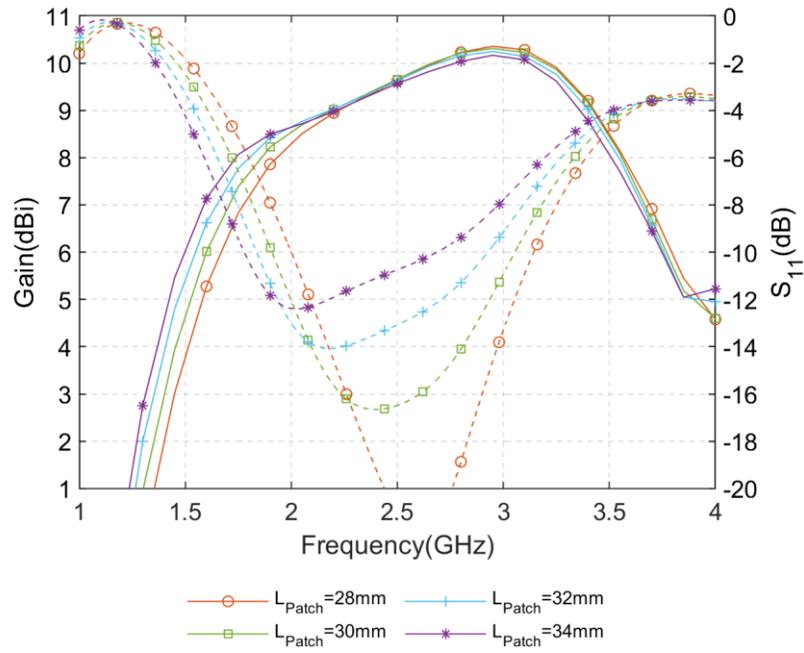
Fig. 3.5: Gain and S_{11} of the cavity-less Pseudo-ME dipole antenna at different patch length

(L_{Patch})

3.4.2 W_{Patch}

Fig. 3.6 shows the influence of W_{Patch} on Z_{11}. The second and the third modes of antenna have been noticeably affected by tuning the patch width, which means the magnetic dipole mode mainly dominates the high-frequency band resonance. By extending the length of W_{Patch}, the second and the third modes move to a lower frequency.

Fig. 3.7 depicts how the gain and the S_{11} of the proposed antenna change with different W_{Patch}. With shorter W_{Patch}, the low end of S_{11} and gain remain the same, while the high end of S_{11} extends, and the gain also has a significant increase at high frequency. As discussed in 3.4.1, the second resonant mode is also controlled by L_{Patch}, which means primary operating mode of the proposed antenna (the second mode), is composed of both electric and magnetic dipole modes.
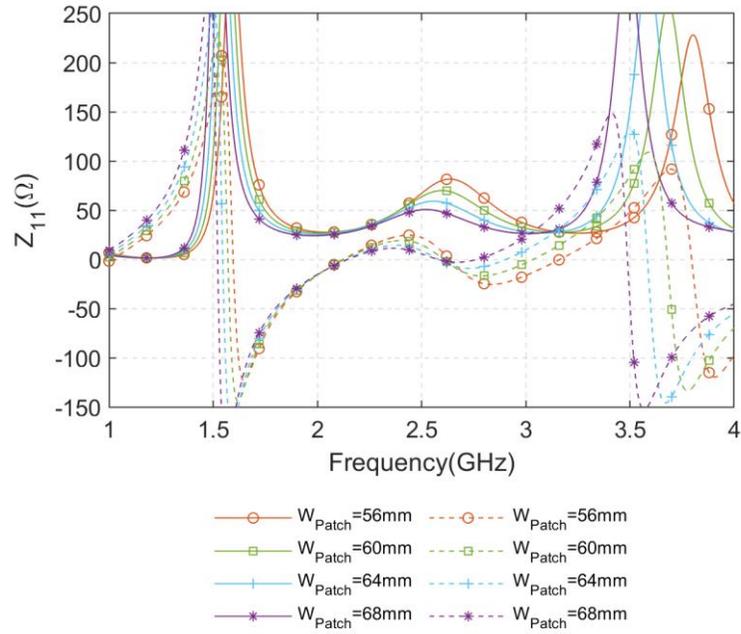
Fig. 3.6: Z_{11} of the cavity-less Pseudo-ME dipole antenna at different patch width (W_{Patch})
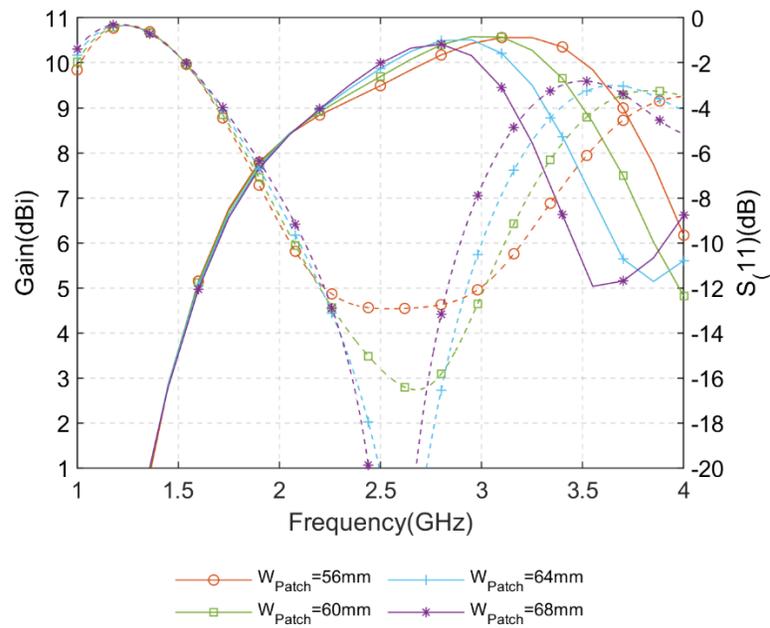
Fig. 3.7: Gain and S_{11} of the cavity-less Pseudo-ME dipole antenna at different patch width

(W_{Patch})

3.4.3 H_{Air}

In the next two sections, the influence of the ground plane on the antenna will be studied. The ground plane is roughly set at a quarter wavelength away from the radiating layer, providing the proposed antenna with a unidirectional radiation pattern and reducing the back lobe strength.

H_{Air} represents the separation between the radiating layer and the ground plane. Fig. 3.8 gives the influence of H_{Air} on Z_{11} of the proposed antenna. As explained before, the ground plane is employed as a reflector so that the signal strength has the maximum enhancement at the height of $0.25\ \lambda_0$ theoretically. Therefore, the three antenna modes show the corresponding reaction by tuning H_{Air}: when tunning H_{Air} shorter, all antenna resonances shift to a higher frequency band. From Fig. 3.9, it can be found that the impedance bandwidth remains wide but shift to a higher frequency with shorter H_{Air}. Likewise, the gain in the high-frequency band (Frequency roughly higher than 2.5 GHz) enhanced with shorter H_{Air}.
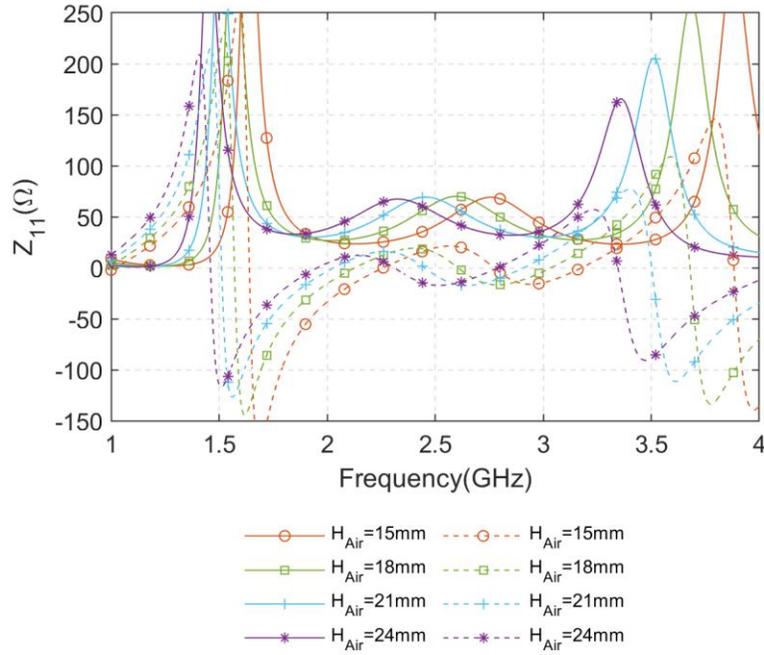
Fig. 3.8: Z_{11} of the cavity-less Pseudo-ME dipole antenna at a different height (H_{Air})

Generally, a quarter-wavelength separation from the ground plane gives the most balanced gain enhancement in the whole operating band, so usually, 0.25 λ_0 is a reasonable distance to set the separation for wide bandwidth and a balanced high gain. However, the low-profile feature becomes more attractive since it allows the antenna to be implemented into limited space, although the bandwidth might be sacrificed. To study how low-profile could the antenna be while the bandwidth is still maintained in an acceptable range, Table 3.2 shows the bandwidth and the in-band gain variation of the proposed antenna with different H_{Air} as a reference. Even at the height value of 18 mm (0.15 λ_0), the bandwidth still more than 40%. Therefore, depending on the applications, the cavity-less Pseudo-ME dipole height can be reduced to lower than 0.25 λ_0 for obtaining the low-profile feature.
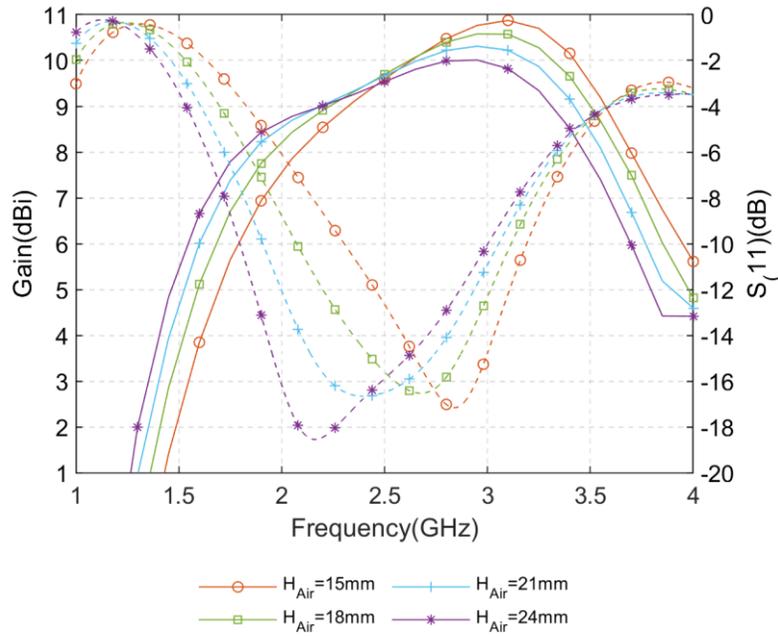
Fig. 3.9: Gain and S_{11} of the cavity-less Pseudo-ME dipole antenna at a different height (H_{Air})

Table 3.2: Impedance bandwidth with the different height (H_{Air})

H_{Air} (mm)	15	18	21	24
Bandwidth	34.2%	41.8%	47.5%	51.0%
Gain Variation (dB)	1.0	1.0	1.0	1.0

The plane also affects field distributions. Unlike a conventional electric dipole, in which the electric field always oscillates between the two arms, in the proposed antenna, the electric field also oscillates between the two far edges of two horizontal patches and the ground plane, as shown in Fig. 3.2 (a) and (c). This fringing field affects the operating frequency indirectly. Thus, in Fig. 4.11, all the three modes of the antenna are sensitive to the changing H_{Air}. It can also be observed that the impedance bandwidth of the proposed antenna will increase with increase H_{Air}, but the maximum gain will be reduced and suffered from more variation with the bandwidth.

3.4.4 L_{Ground}

The ground plane reflects the wave in the back-lobe direction to the main bore-sight direction. Although an infinite ground plane can increase the radiation element gain of a dipole antenna, theoretically 3 dB more gain will be achieved if the antenna is omnidirectional, it is not feasible to achieve so. To achieve the best balance between the ground plane size and the increased gain, the ground plane size needs to be sufficiently bigger than the radiating elements. Otherwise, the gain will be reduced by 1.5 dB if the ground plane is smaller than 0.5 λ_0^2 than the infinite ground plane case [63]. In Fig. 3.11, the simulated S_{11} and gain with different ground plane sizes have been depicted. The ground plane sizes have been set up as 50 mm (0.42 λ_0), 90 mm (0.75 λ_0), 130 mm (1.09 λ_0), and 170 mm (1.42 λ_0). It can be noticed that neither S_{11} nor gain shows the right consistency until L_{Ground} is more than 90 mm. However, when L_{Ground} is less than or equal to 50 mm (roughly smaller than 0.4 λ_0), the ground plane cannot perform as a good reflector in the low-frequency band. Since the wavelength is longer, the electric field of the electric dipole will travel to the bottom side of the ground plane rather than the top side. Thus, the gain decreases. And in Fig. 3.10, The main resonant mode of the antenna shifted and caused the influence on the bandwidth and gain when L_{Ground} is less than 50 mm. In these cases, the proposed Pseudo-ME dipole antenna operates more like a conventional wideband dipole.
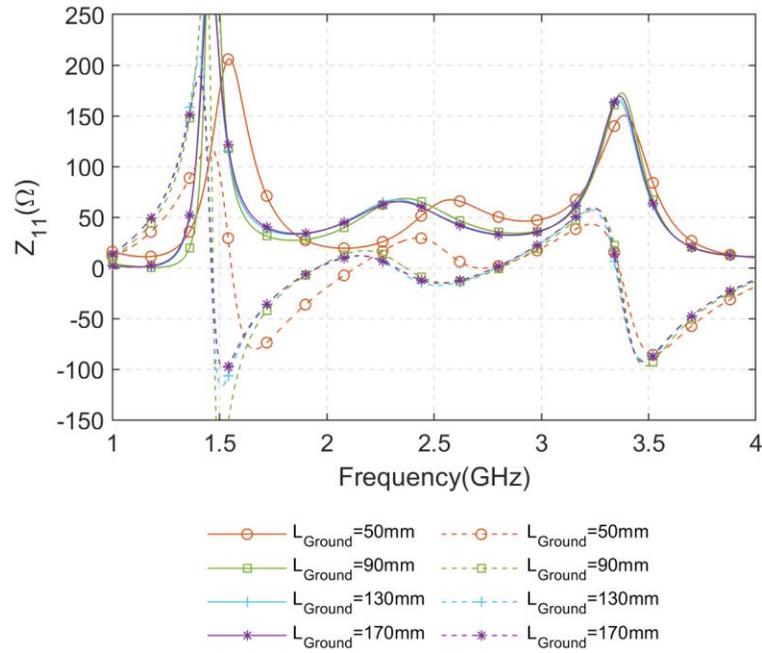
Fig. 3.10: Z_{11} of the cavity-less Pseudo-ME dipole antenna at the different ground size (L_{Ground})
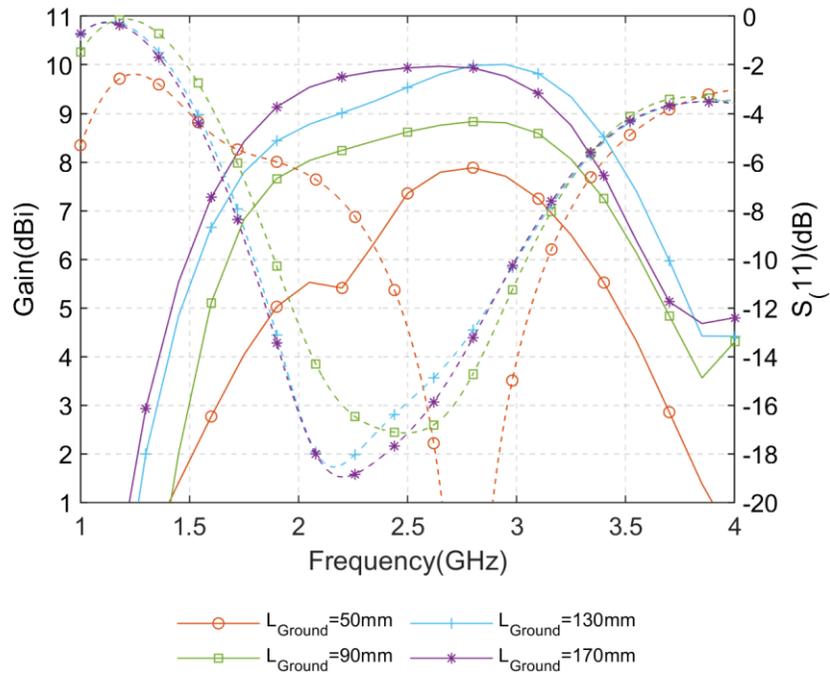
Fig. 3.11: Gain and S_{11} of the cavity-less Pseudo-ME dipole with different ground size (L_{Ground})

Fig. 3.12 and Fig. 3.13 shows the radiation patterns at E- and H-plane of the proposed antenna with different L_{Ground} to further understand why the gain decreases with an insufficient ground plane size. The back lobe of the antenna increased significantly with a smaller ground plane. When L_{Ground} equal to 50 mm, the front-to-back ratio decreased to 3 dB. When the L_{Ground} is larger than 130 mm (1.09 λ_0), both planes generally have the front-to-back ratio larger than 18 dB. The increased back lobe proves that the ground plane cannot operate as a perfect reflector when the size is less than λ_0.
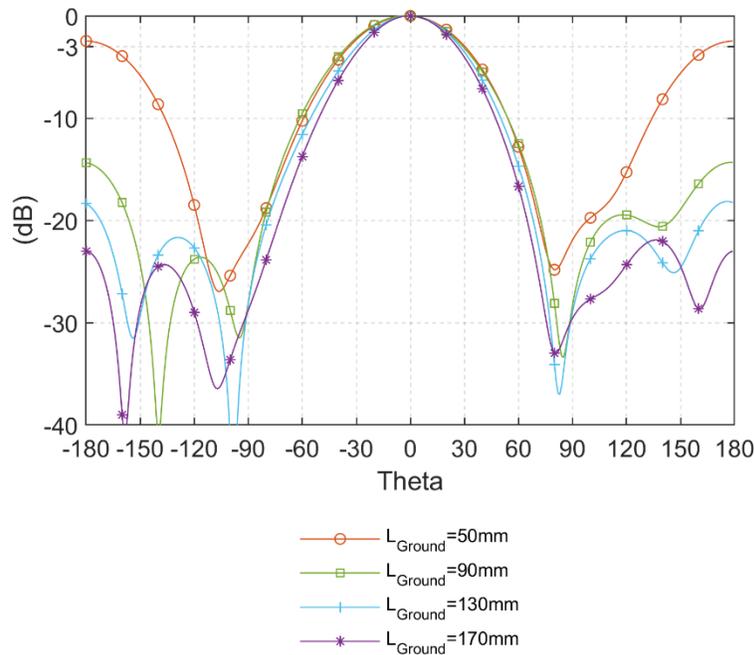
Fig. 3.12: E plane Radiation patterns of cavity-less Pseudo-ME dipole antenna with the different ground size (L_{Ground})
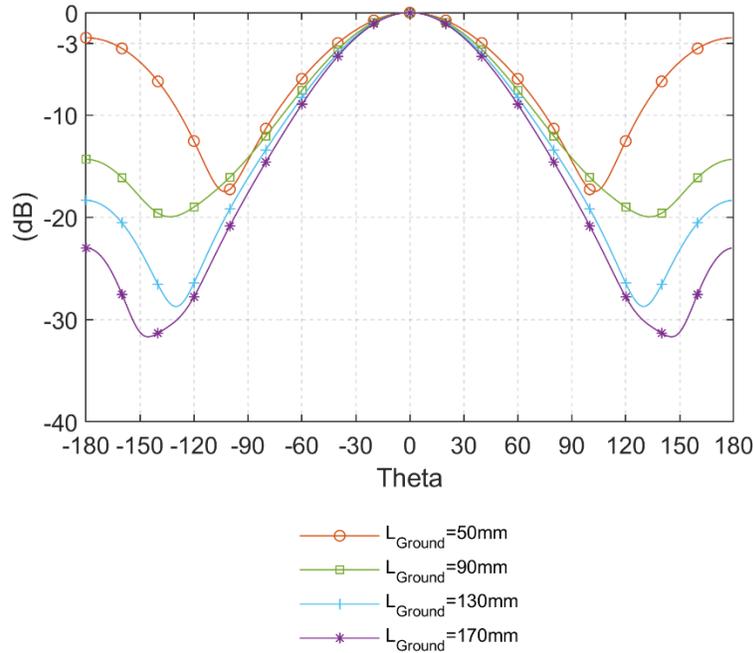
Fig. 3.13: H plane radiation patterns of cavity-less Pseudo-ME dipole antenna with the

different ground size (L_{Ground})

3.4.5 Parametric study summary

Parameters that determine the primary performance of the antenna have been studied in the last four sections. To design the cavity-less Pseudo-ME dipole antenna at the required frequency and obtain reasonable gain and impedance bandwidth: Firstly, L_{Patch} and W_{Patch} should be set up to around 0.25 λ_0 and 0.5 λ_0 respectively, so that the electric dipole and the magnetic dipole could operate at the close frequency band. Due to the fringing field effect, the electric dipole will operate at a lower frequency than the magnetic dipole. Secondly, a ground plane with a size of at least λ_0^2 needs to be put 0.25 λ_0 away from the radiating patches for a 3 dB gain enhancement. Based on the applications, the height of

the antenna could be reduced to 0.15 λ_0 and still obtain a wide impedance bandwidth of around 40%.

Based on the parametric study done so far, a series of figures of impedance bandwidth ($S_{11} \leq$ -10dB) and average gain (the average of the maximum and minimum gain in-band) related to each parameter is shown in Fig. 3.14. These data could be used as a reference for designing the cavity-less pseudo-ME dipole antenna in S-band or similar frequency bands.
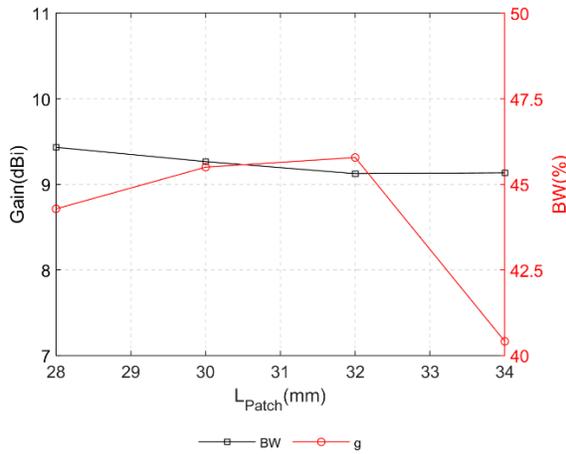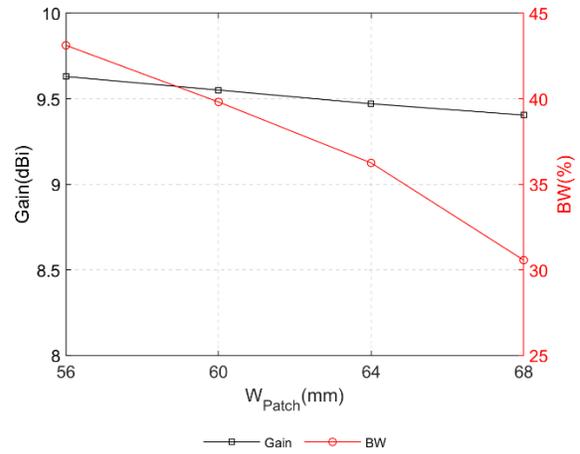
(a)   (b)
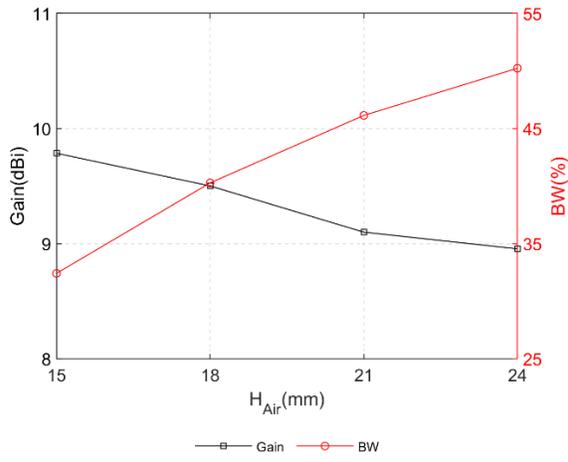
(c)
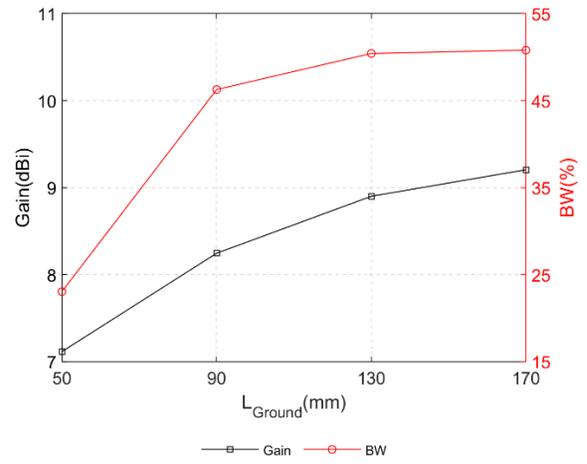
(d)

Fig. 3.14: Average gain and impedance bandwidth with different (a). L_Patch. (b). W_Patch. (c). H_Air

(d). L_Ground.

3.5   Simulation and experimental results

A prototype antenna, as shown in Fig. 3.15, has been fabricated to verify the performances of the proposed design. A semi-rigid cable is used to realize the coaxial cable modeled in the simulation. The two horizontal patches are made of thin adhesive copper foil. The measured S_{11} was obtained using a vector network analyzer (model number: R&S®ZN-Z229), and the antenna gain, and radiation patterns were measured in the UCL anechoic chamber. It worth mentioning that the measured results of the antenna proposed in chapters 5 and 6 are obtained in the same condition.

Fig. 3.15: The photography of fabricated cavity-less Pseudo-ME dipole prototype

The simulated results of the antenna show a comparable wide impedance bandwidth of 52.96% ($S_{11} \leq$ -10 dB) from 1.86 GHz to 3.2 GHz, and a stable and higher realized gain from 8.20 to 10.01 dBi ($\pm$ 0.91 dB variation), center at 2.37 GHz as depicted in Fig. 3.16. The maximum gain has increased by around 9.4% when compared with that of the highest reported. Simultaneously, the gain variation in the proposed antenna passband is much lower than that of those Pseudo-ME dipole antennas reported in the literature. The radiation mechanism and the effects of the antenna critical parameters are also explained with the assistance of the parametric study presented.

3.5.1 S_{11}, realized gain and efficiency.

The measured S_{11} and the realized gain results are shown in Fig. 3.16. It can be observed that the discrepancy between the measured and simulated results is minimum. The measured impedance bandwidth ($S_{11} \leq$ -10 dB) is 50.30% from 1.86 GHz to 3.11 GHz (2.66% narrower than the simulated result). The prototype antenna has a stable measured gain of 8.74 ± 1 dBi (average gain is 6.59% higher than the simulated result), across the operating frequency band. Due to the antenna effective aperture become relatively larger at higher frequency, the maximum measured gain achieved is 9.74 dBi at 2.80 GHz. Fig. 3.17 shows the radiation and total efficiency of the proposed antenna, which are higher than 99% and 89% respectively in the operating band.
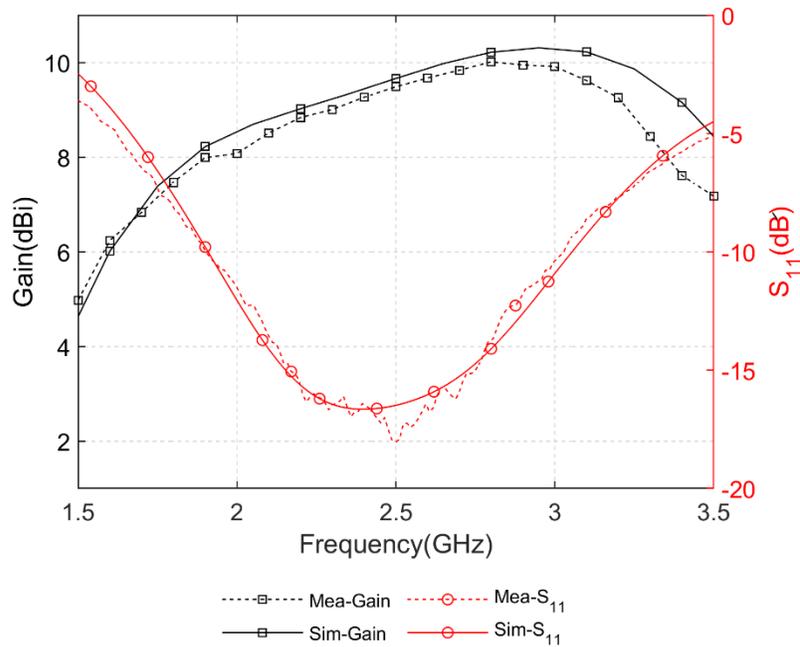
Fig. 3.16: Simulated and measured gain and S_{11} of cavity-less ME dipole
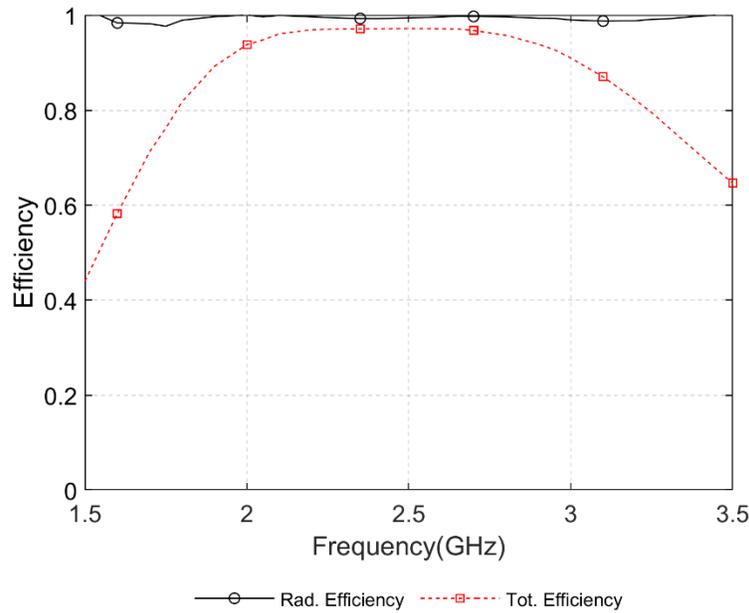
Fig. 3.17: Simulated radiation and total efficiency of the proposed cavity-less ME dipole

3.5.2 Radiation Patterns

The simulated radiation pattern in 3D has been shown in Fig. 3.18, which depicted the proposed pseudo-ME dipole antenna has high gain and similar pattern in E- and H-plane. The simulated and measured 2D radiation patterns at different frequency points have been presented in Fig. 3.19. The main E-plane is in the y-direction, and H-plane is in the x-direction. The antenna is linearly polarized with about -18 dB cross-polarization level. It should be mentioned that the simulated results of the cross-polarization are not shown in the figures for clarity since they are deficient (less than -80 dBi). The low cross-polarization in the simulations can be explained by the assumptions of the perfectly symmetrical structure and precise excitation point in the simulation model. The ideally symmetrical excitation of the wide electric dipole and magnetic dipole will not excite any cross-polarization. However, it is very difficult to achieve in the fabrication, mainly when soldering the coaxial cable to the excitation points on the two horizontal patches' sides in the practical case. The electric dipole and

93

magnetic dipole are orthogonally located, so the polarization effects are minimal. The measured and simulated co-polarization radiation patterns match well, particularly in the main beam (-45°< θ < 45°). Within the operating bandwidth from 1.8 GHz to 2.8 GHz, the antenna has stable unidirectional radiation patterns in both E- and H- planes.
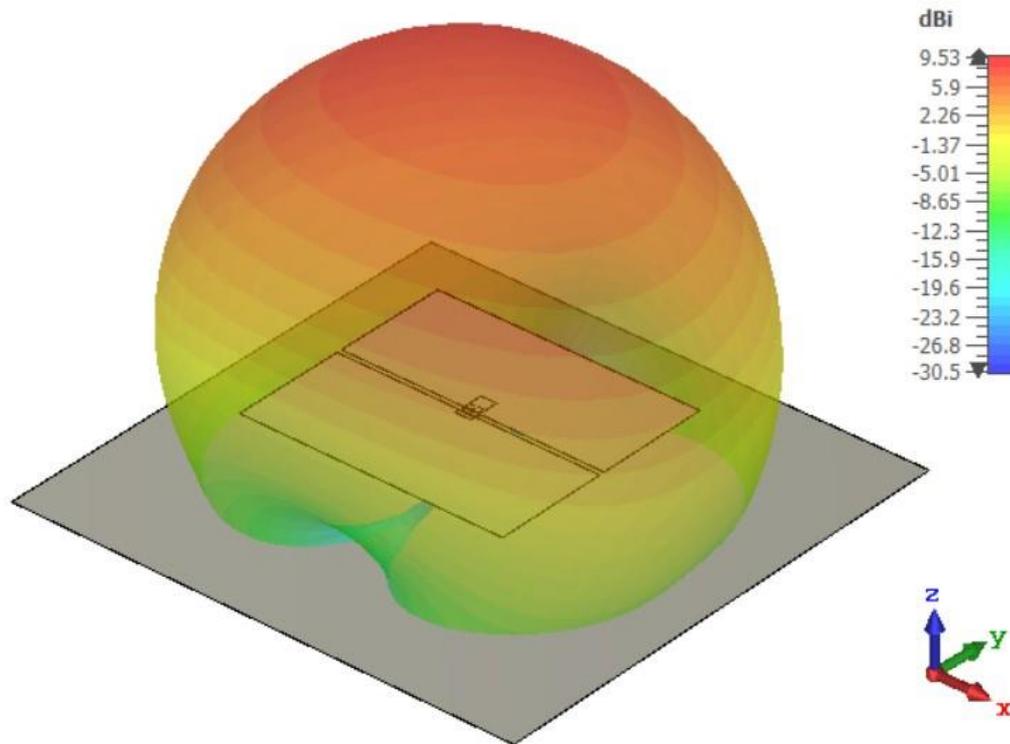
Fig. 3.18: Simulated radiation patterns of the proposed antenna in 3D

94

(a)   (b)

(c)   (d)

(e)   (f)
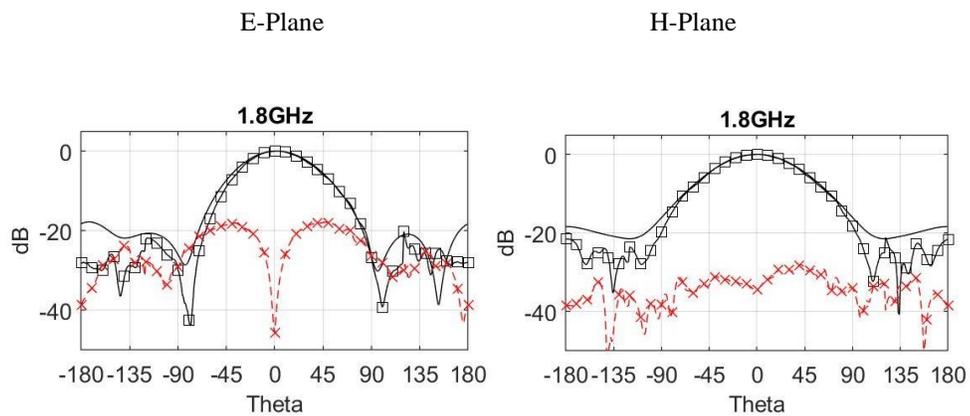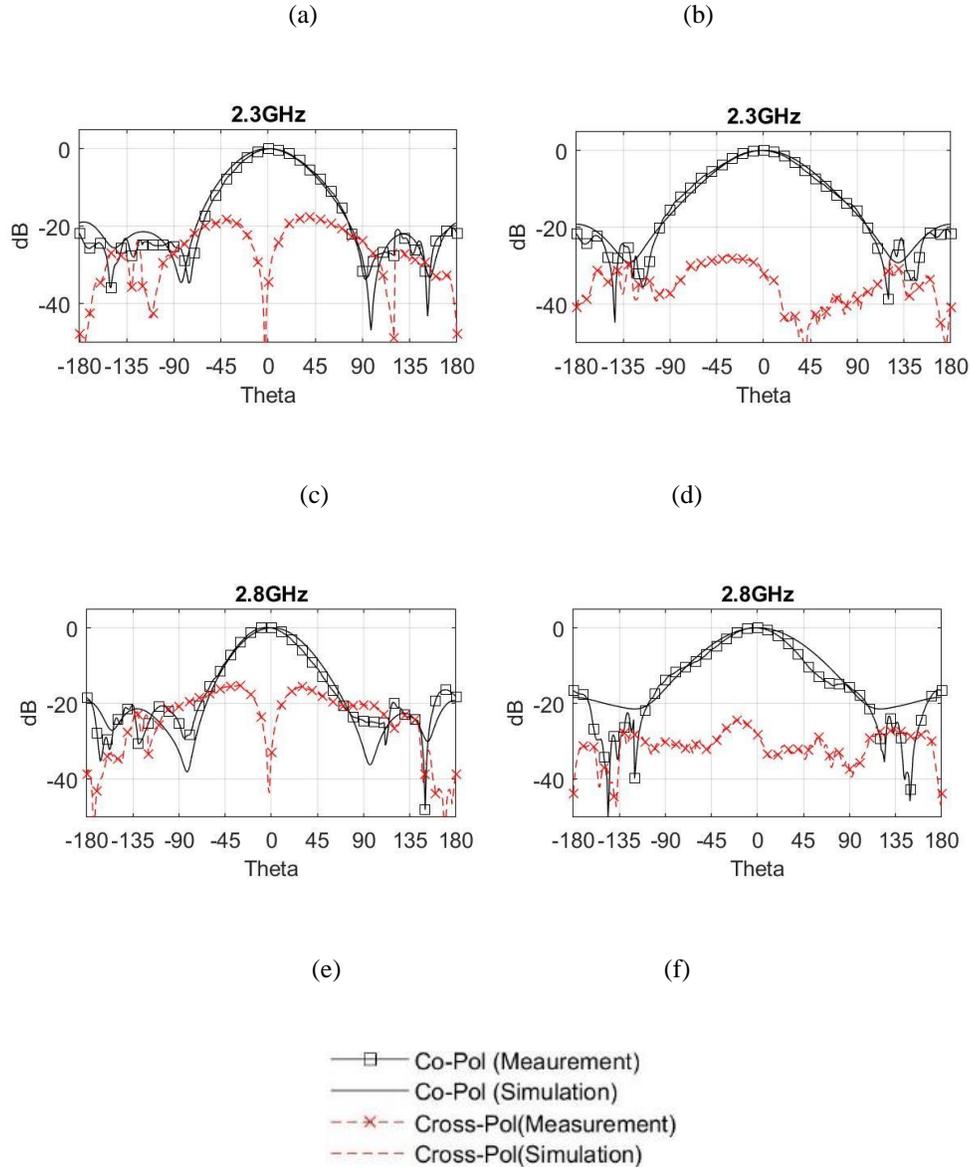
Fig. 3.19: Simulated and measured radiation patterns at (a) 1.8 GHz E-plane (b) 1.8 GHz H-plane, (c) 2.3 GHz E-plane, (d) 2.3 GHz H-plane, (e) 2.8 GHz E-plane, (f) 2.8 GHz H-plane

Table 3.3 summarizes the 3-dB beamwidth and front-to-back ratios at different frequency points. Δ_1 represents the 3-dB beamwidth difference across frequency at each plane, and Δ_2 represents the 3-dB beamwidth difference between E- and H-planes. Δ_1 for the two planes has a similar value of 10.3° and 12°, which means the proposed antenna has stable radiating performance at different frequencies. The proposed antenna also has very similar E-plane and H-plane radiation

95

patterns, as Δ_2 is always lower than 11°. Besides, the 3-dB beamwidth in the E-plane is always smaller than that of the H-plane. The observation can explain that the fringing field has elongated the sufficient length of the electric dipole and created a larger radiation aperture, as shown in Fig. 4.3 (a) and (c). Therefore, the directivity in the E-plane is higher.

Table 3.3: 3-dB beamwidth and the front-to-back ratio of the cavity-less Pseudo-ME dipole antenna

3-dB beamwidth (°)	1.8 GHz	2.3 GHz	2.8 GHz	$|\Delta_1|$
E-plane	61.8	56.8	51.5	10.3
H-plane	72.2	67.8	60.2	12
$|\Delta_2|$	10.4	11.0	8.7	
Front-to-back	18.4	19.1	19.2	

3.6   Concluding remarks

In this chapter, a cavity-less pseudo magneto-electric dipole antenna has been designed and its feasibility has been proven. The measured results demonstrate that the cavity-less magneto-electric antenna has a comparable performance than the conventional cavity base ME antenna. It has a bandwidth of 50.30% and a stable realized gain from 9.1 ± 0.91 dBi. Especially, low-profile feature could be achieved by adjusting the height of the antenna.

The cavity-less pseudo-ME dipole makes the geometry simpler, reduces the complexity and the cost of fabrication. This concept will be implemented in the next two chapters to design a circularly polarized antenna (chapter 4) and a millimeter-wave band antenna (chapter 5).

4. Crossed-dipole Feed Circularly Polarized Pseudo Magneto-electric dipole Antenna

4.1 Introduction

Antennas with circular polarization (CP) radiation features have several advantages over linearly polarized (LP) antennas. CP antennas have improved immunity to: (i). Polarization miss-match losses [64][65]. Radio signals are absorbed or reflected depending on the material they contact. If the polarization of the reflected incoming signal does not lie in a specific plane, the signal strength of LP antenna received will be weakened or even lost. While CP antennas can receive the signal from any plane perpendicular to the propagation direction almost equally. (ii). Multipath interference. Multipath means the receiving antenna received the signal from two or more paths at nearly the same time. CP antennas provide a guarantee for the stability of wireless connection systems and deal with various communication problems. Due to these features, circularly polarized antennas are commonly used in the scenario in which signals come from an uncertain direction, such as global navigation satellite systems (GNSS) and satellite communications [35][48][66].

Circular polarization is generated by two closely separated orthogonal resonances with equal magnitude and 90° phase difference. To provide a wideband dual-feed for achieving CP radiation, Wilkinson power divider [48][59][67], microstrip line to double slot line transmission [60], or T-junction power divider [68][69] are the most common feeding methods. However, these complex geometries increase the difficulty of fabrication and can introduce further losses into the system. Moreover, the usable impedance and AR

bandwidth of a single feed are usually narrow. Typically, the values are lower than 10% [70][71].

In chapter 4, a simple geometry wide bandwidth cavity-less pseudo-ME dipole antenna has been designed and verified. This single-fed antenna has a wide bandwidth, which inspired us to develop this geometry with CP characteristics. In this chapter, a novel cavity-less crossed-dipole fed pseudo magneto-electric dipole antenna with circular polarization will be presented. The 4-patch Pseudo-ME dipole is fed by a crossed-dipole feeding network. It has two pairs of electric dipole modes and magnetic dipole modes that cooperate to generate wideband CP radiation. The proposed single-fed CP pseudo-ME dipole antenna has a wide impedance bandwidth ($S_{11} < $ -10dB) of 70.4% from 2.46 to 5.10 GHz, a stable high gain of 8.7 ± 0.9 dBi in the operating band and achieves a maximum gain of 9.6 dBi at 3.27 GHz. Most importantly, by implementing the two pairs of orthogonal resonances, this antenna has two CP center points, the CP radiation bandwidth for AR $\leq$ 3 dB is 43.5% from 2.87 GHz to 5.0 GHz.

4.2   Antenna Geometry

Fig. 4.1 shows the geometry of the proposed antenna. Like the cavity-less LP Pseudo-ME dipole antenna discussed in chapter 4, the CP ME antenna also consists of mainly three parts. i. The radiating layer on the top of the antenna. It has four square horizontal patches A, B, C, D printed on the substrate (Rogers RT5880LZ, ε_r = 2.0, tan δ = 0.0021 @ 10 GHz)). Patches A, B are on the top side, while patches C, D are on the other side of the radiating layer. ii. A semi-rigid coaxial cable with a crossed-dipole feeding network geometry relays the input port signal to the four patches with proper magnitude and phase differences. iii. A square metallic ground plane at the bottom of the antenna. It also serves as a reflector to the backward radiation to provide a unidirectional radiation pattern and higher front-to-back ratio.
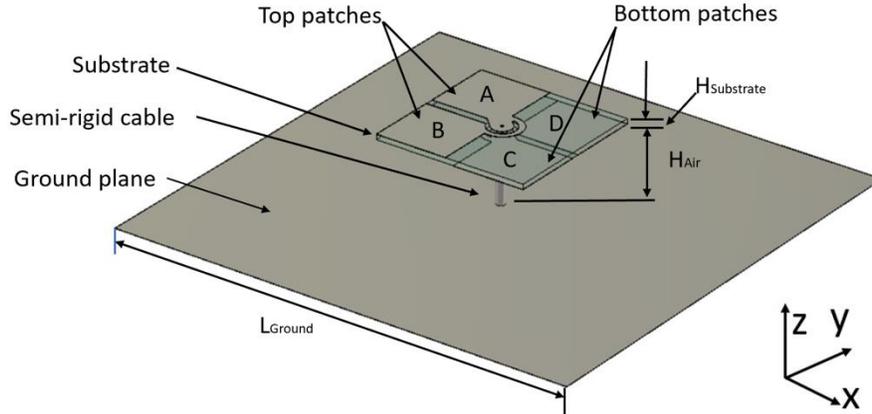
Fig. 4.1: The geometry of the crossed-dipole feed circularly polarized ME dipole

Fig. 4.2 (a) and (b) show the metallic patterns of radiating elements on the top and bottom sides in detail. A, B, C, D are four square patches and have the same dimensions of side length L_{Patch}. Patches A and B are connected to the inner conductor of the semi-rigid coaxial cable, and Patches C and D are connected to the outer conductor. The four patches form two electric and two magnetic dipoles, which provide four fundamental resonances. A crossed-dipole feeding network with two short and two long leads (the long lead is also called quarter-wave ring in this thesis) is located at the center of the substrate. Moreover, the length of two long leads of the crossed dipole is roughly 0.25 λ_g, which introduces the 90° phase difference between patches A and B, and patches C and D, for CP radiation.
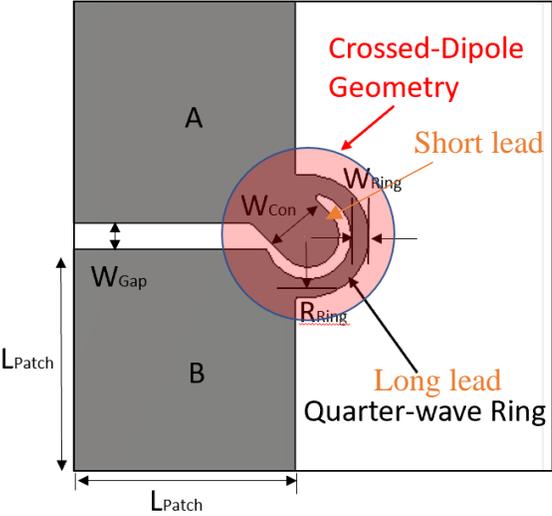
(a). Topside of the radiating layer
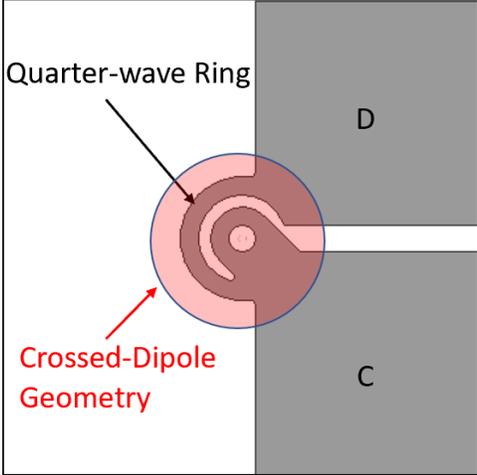
(b). The bottom side of the radiating layer

Fig. 4.2: (a). Patches A and B are connected to the outer conductor of the semi-rigid cable (b). Patches C and D are connected to the outer conductor of the semi-rigid cable

Table 4.1 provides detailed dimensions of the proposed CP Pseudo-ME dipole antenna. The substrate chosen for the radiating layer is Rogers 5880LZ with a thickness of 1.27 mm. Since the four horizontal patches are operating as half-wave electric dipoles and magnetic dipoles, each square patch has a length (L_{Patch})

which was first set to around a quarter wavelength. Although the radiating elements look like as rhombic patches rather than square patches in the operation, the simulation shows that it is closer to a quarter wavelength, not $\sqrt{2}$ of the quarter wavelength. The final optimized value is 18.5mm (0.233 λ_g), and the separation W_{Gap} between each patch is 2.1 (0.026 λ_g).

The crossed-dipole geometry aims to create the 90° phase difference between the orthogonal resonances. Thus, the long lead (quarter-wave ring) of the crossed dipole should have the length around a quarter wavelength, the final optimized radius of the long lead R_{Ring} is 5.2mm (0.064 λ_g), so the length of the long lead L_{Ring} can be calculated based on R_{Ring}, which is roughly 18.5mm (0.23 λ_g).

Moreover, the crossed-dipole geometry also plays a critical role in dividing equal power to four patches to achieve circular polarization. The width of the long lead W_{Ring} and the short lead W_{Con} is set as 1.5mm (0.019 λ_g) and 5.2mm (0.065 λ_g) to achieve the best impedance matching and equal magnitude of four resonances.

Finally, like the previous LP Pseudo-ME dipole in chapter 4, the ground plane should be set 0.25 λ_g away from the radiating layer to obtain the best gain enhancement. The final value of H_{Air} is 17.7mm (0.223 λ_g). Furthermore, the length of the sides of the flat ground plane reflector should be set at λ_0 to provide a balanced gain enhancement in the whole operating band, L_{Ground} is set as 120mm (1.070λ_0 or 1.513 λ_g).

Table 4.1: Dimensions of the proposed CP Pseudo-ME dipole antenna

$H_{Substrate}$	H_{Air}	L_{Patch}	W_{Gap}	R_{Ring}
1.27 (0.016 λ_g)	17.7 (0.223 λ_g)	18.5 (0.233 λ_g)	2.1 (0.026 λ_g)	5.2 (0.064 λ_g)
L_{Ring}	W_{Ring}	W_{Con}	L_{Ground}	
18.5 (0.23 λ_g)	1.5 (0.019 λ_g)	5.2 (0.065 λ_g)	120 (1.5 λ_g)	

4.3   Operation Principle

Conventionally, circular polarization is generated from a pair of orthogonal resonance, and they need to have equal magnitude and 90° phase difference. The two resonances usually operate at slightly different frequencies to obtain wider axial ratio bandwidth. The center of the two operating frequencies is called AR center frequency in the thesis, and the axial ratio should have the minimum value at the AR center frequency.

Benefit from the 4-patch pseudo-ME dipole geometry, the proposed antenna has two pairs of 45° angularly separated electric dipoles and magnetic dipoles as shown in Fig. 4.3. The two electric dipoles operate at the lower frequency band. In contrast, the two magnetic dipoles operate at a higher frequency band. That results in two AR center frequency points (electric dipoles contribute to the lower AR center point; magnetic dipoles contribute to the higher AR center point). An impressive AR bandwidth for a single-fed CP antenna is obtained.

Fig. 4.3 shows two pairs of rhombic electric dipoles located on the radiating layer orthogonal diagonals. Patches A and C are operated as the two arms of the Electric Dipole 1, and they are fed by the two short leads of the crossed-dipole feeding network. While Patches B and D are employed as the two arms of the Electric Dipole 2, and the two long leads feed them. Due to the quarter

wavelength arc geometry, the signal traveled to Electric Dipole 2 is 90° delayed. Thus, the low-frequency band CP could be generated.

The two straight open slots, formed by the gaps between the patches, are radiating as magnetic dipole antennas on the radiating layer. As shown in Fig. 5.3, Magnetic Dipole 1 located in the x-axis is orthogonal to Magnetic Dipole 2 in the y-axis. Benefit from the crossed-dipole feeding network as well; a 90° phase difference is achieved between the two magnetic dipoles. So, CP at the high-frequency band could be generated.

From Fig. 4.3, the length of the electric dipoles is longer than that of magnetic dipoles since they radiated on the diagonal. Therefore, circular polarization result from electric dipoles happens at a lower frequency. The magnetic dipoles dominate the circular polarization in a high-frequency band. By combining the resonances, wideband characteristics in impedance bandwidth and 3-dB AR bandwidth are achieved.
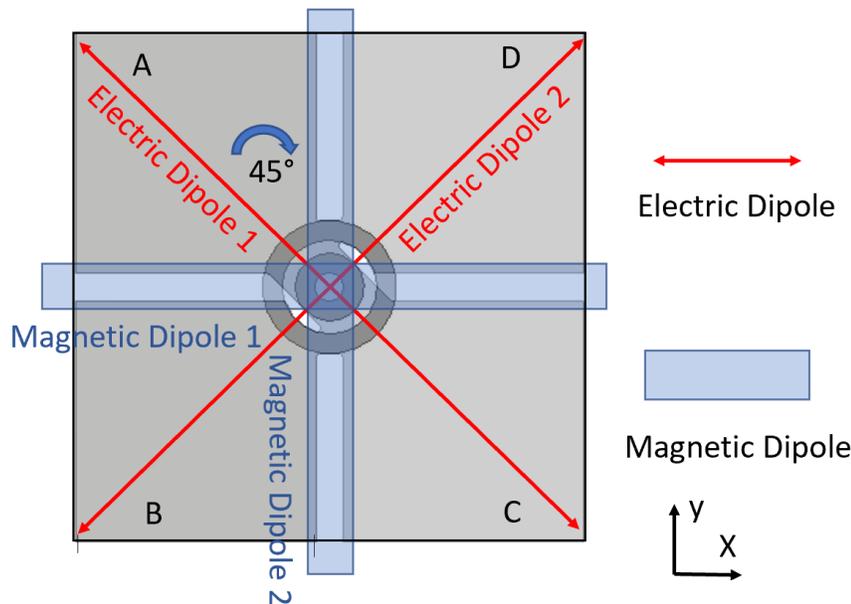
Fig. 4.3: The four fundamental mode of the crossed-dipole feed CP pseudo-ME dipole antenna

4.3.1 Electric dipole mode

To better understand how the circular polarization is generated. Fig. 4.4 illustrates the electric fields at a different time (t) in one period of oscillation (T) of the proposed CP antenna at the low-frequency band CP center point (3.5 GHz). When time t equals 1/8T and 5/8T, the electric field has the most vital distribution on the Patches B and D along the diagonal. At this moment, Electric Dipole 2 is mainly excited. When time equals 3/8T and 7/8T, the electric field has the most substantial distribution on the Patches A and C along the other diagonal direction, so Electric Dipole 1 is excited.
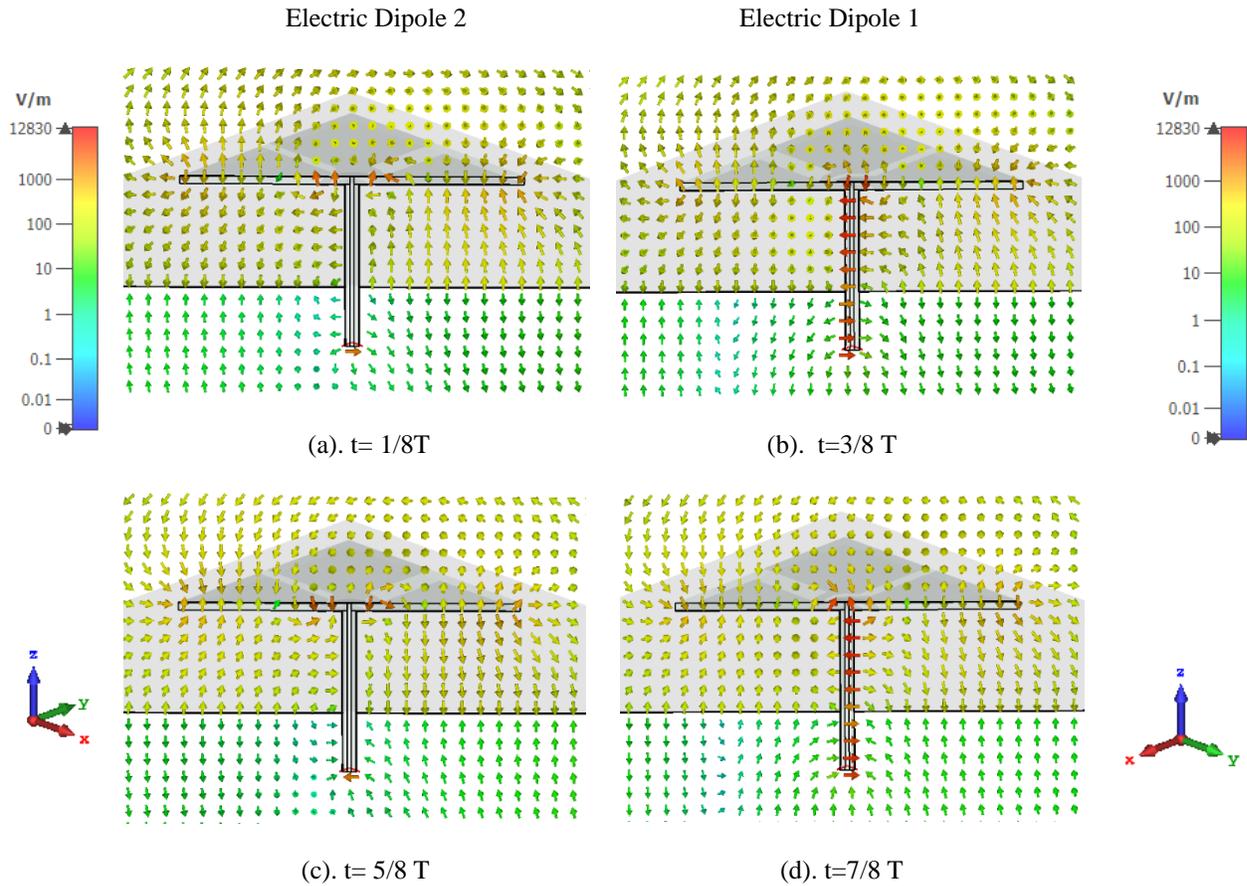
Fig. 4.4: The electric field of the two electric dipoles at different times.

4.3.2 Magnetic dipole mode

When the electric dipoles radiate, the open-slots between patches also radiate with proper magnitude and phase to generate the circular polarization in the high frequency band. Fig. 4.5 depicts the electric field at a different time (t) in the period of oscillation (T) of the proposed CP antenna at the high-frequency band CP center point (4.1 GHz). When time equals 0 and 1/2T, the electric field has the most substantial distribution along with the slot in the x-axis, which means Magnetic Dipole 1 is excited. When time equals 1/4T and 3/4T, the electric field has the most substantial distribution on the slot in the y-axis. Thus, Magnetic Dipole 2 is excited.

Magnetic Dipole 1   Magnetic Dipole 2

(a). t = 0   (b). t = 1/4T
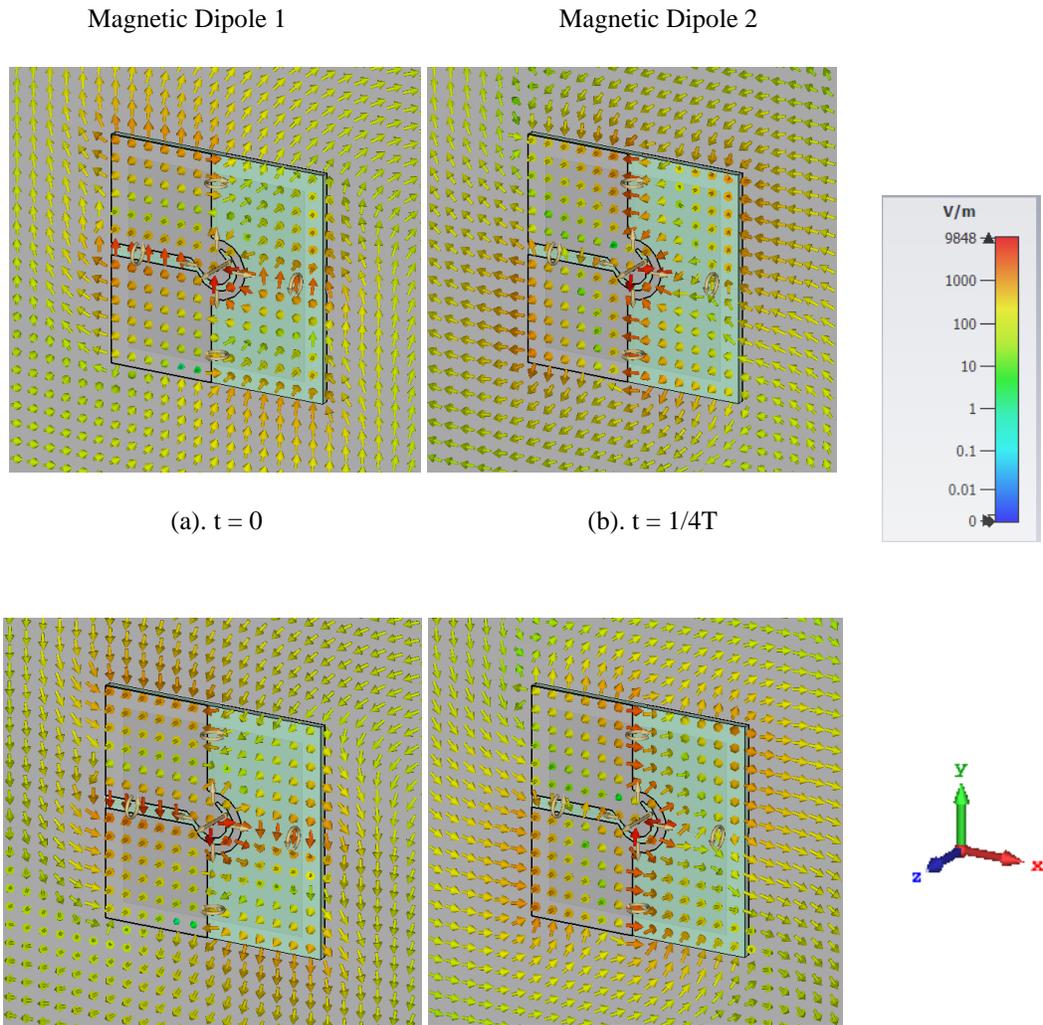
(c). t = 1/2T   (d). t = 3/4T

Fig. 4.5: The electric field of the two magnetic dipoles at different time.

4.3.3 Radiation principle summery

In sections 5.3.1 and 5.3.2, the electric field distribution of the electric dipoles and the magnetic dipoles have been analyzed, respectively. To sum up the radiating principle stated so far, Fig. 4.6 illustrate the main E-field and H-field distribution at different times. It demonstrates that the proposed CP Pseudo-ME dipole antenna has two pairs of electric dipole modes and magnetic dipole modes with a right-hand circular polarization.
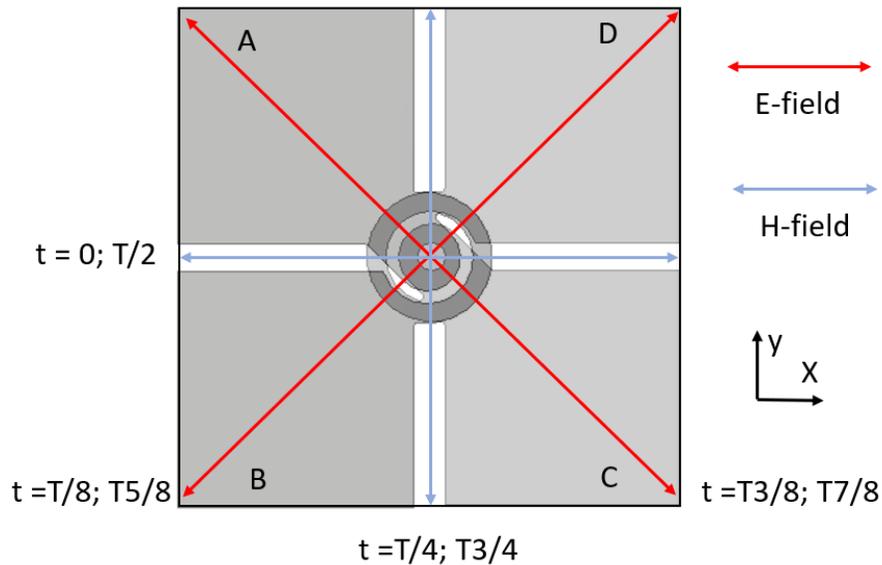
Fig. 4.6: The rotation of fields at different times.

In the meantime, to better understand the rotation of the electromagnetic wave from the proposed antenna, Fig. 4.7 and Fig. 4.8 plot the z-axis component distribution of E-field and H-field at different times. These two groups of figures demonstrate the CP Pseudo-ME dipole with right-hand polarization intuitively.

E-field distribution

t=T/8   t=3/8 T

t=5/8 T   t=7/8 T
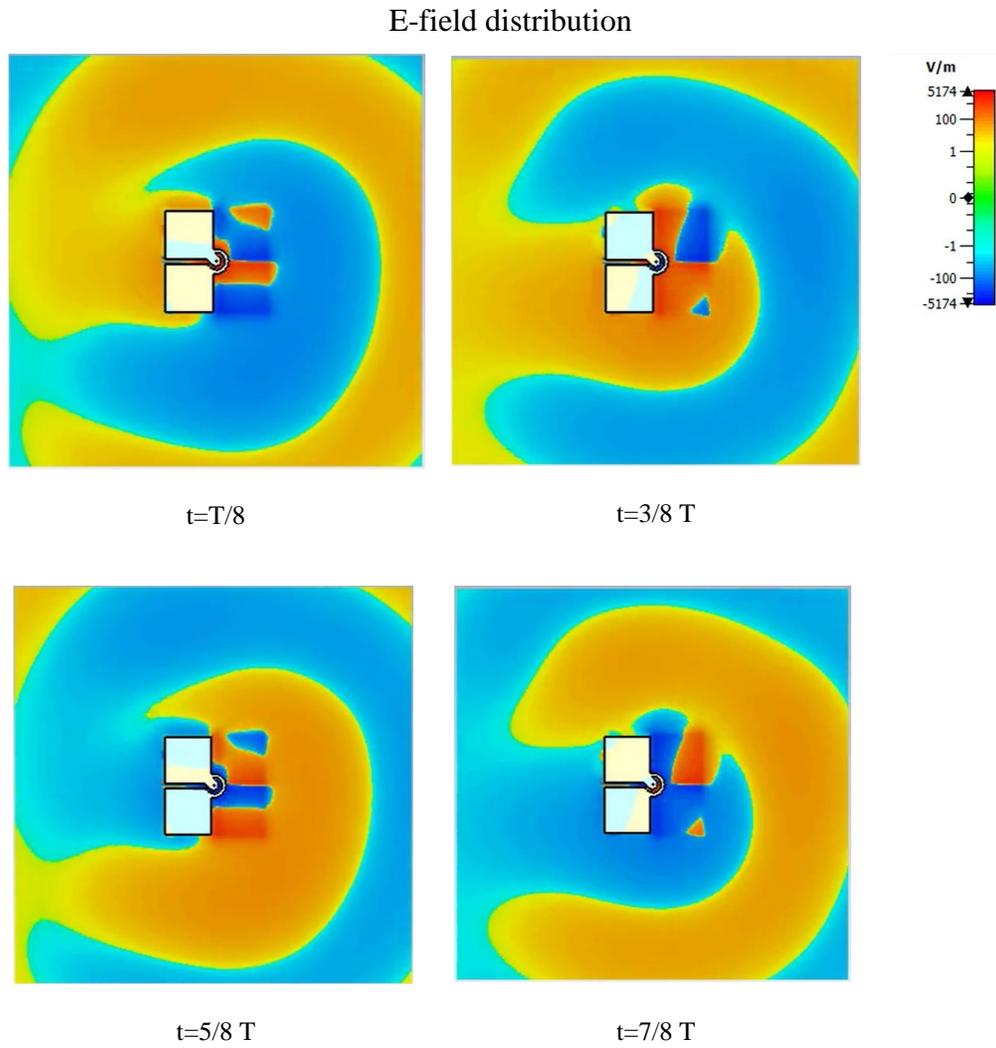
Fig. 4.7: E-field z-axis components distribution at different time

H-field distribution

t=0

t=T/4

t=T/2

t=3/4 T
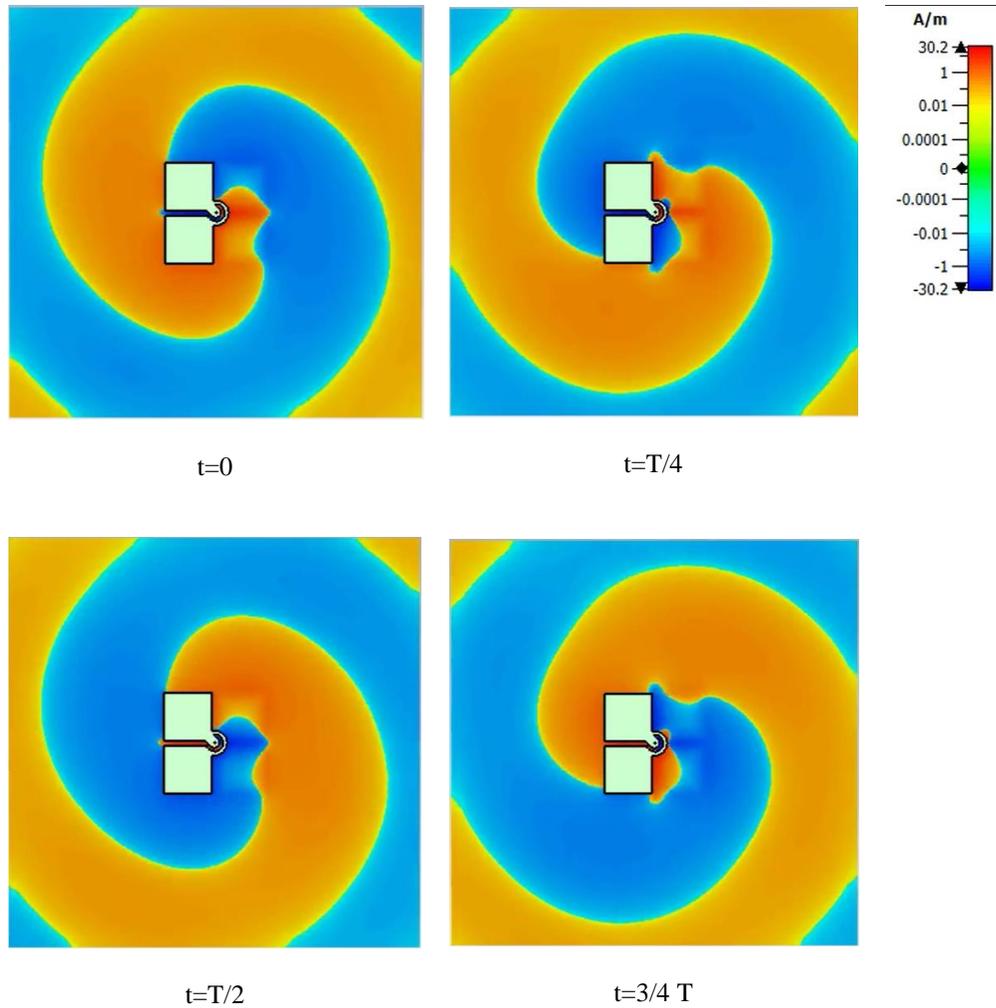
Fig. 4.8: H-field z-axis components distribution at different time

The left-hand polarization could be achieved by applying the crossed dipole feeding network in the opposite direction, the pattern of the radiation elements is shown in Fig. 4.9. Feeding Patch B and D by the short lead of the crossed dipole and feeding the Patch A and C by the long lead, then the left-hand polarization will be achieved.
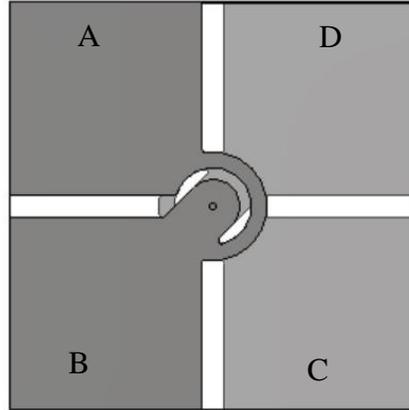
Fig. 4.9: Top view of left-hand polarization CP Pseudo-ME dipole antenna
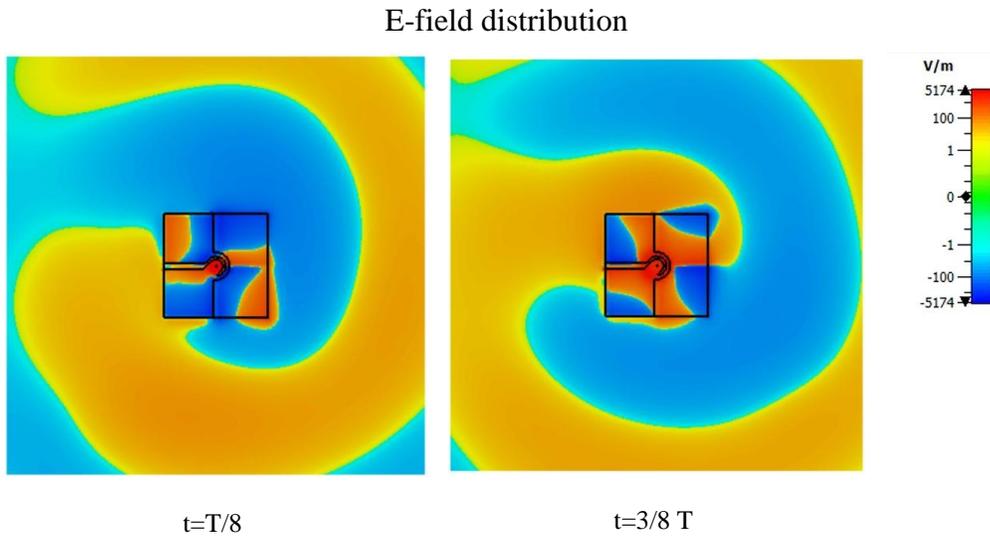
E-field distribution

t=T/8   t=3/8 T

t=5/8 T   t=7/8 T
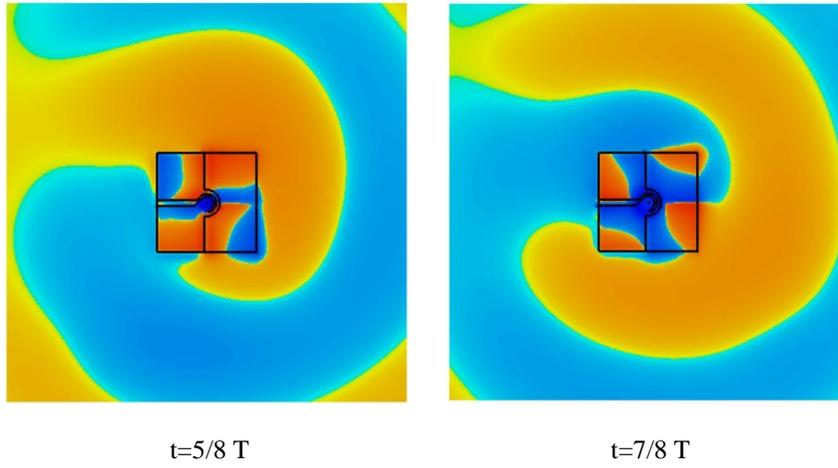
Fig. 4.10: E-field z-axis components distribution at different time

H-field distribution

t=0   t=T/4
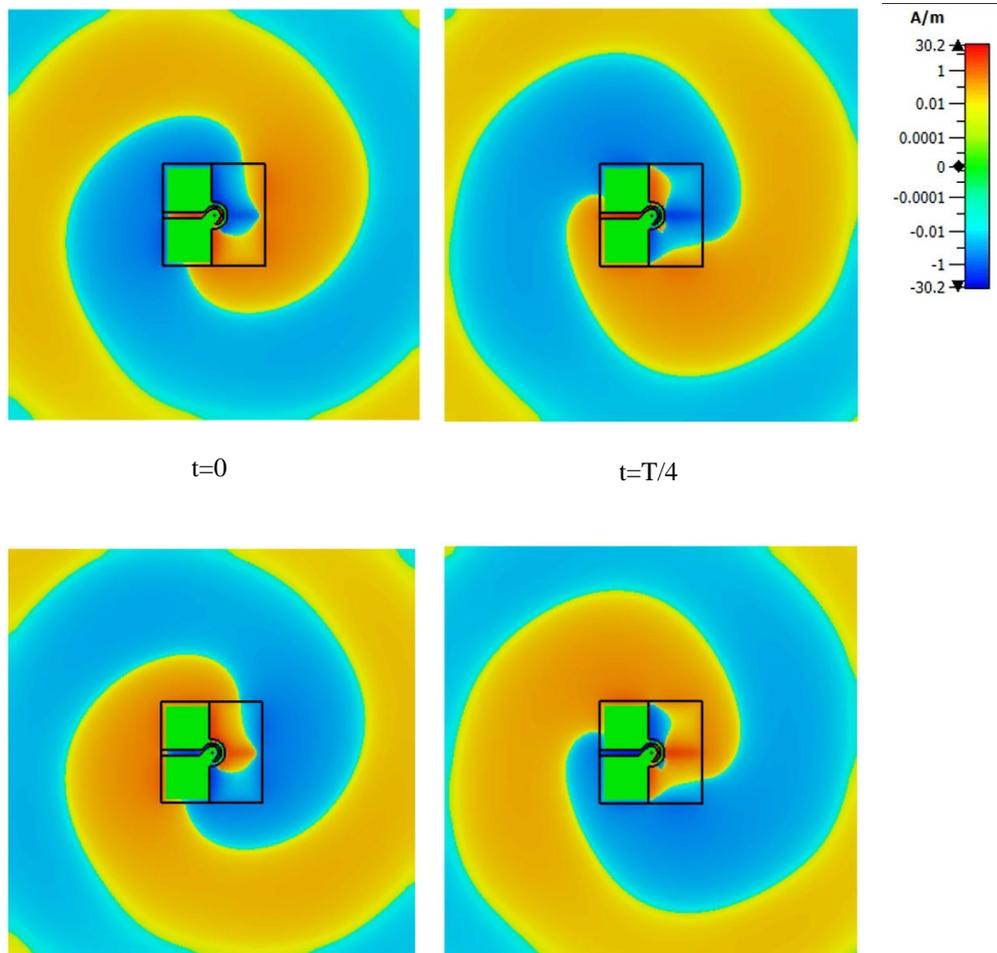
t=T/2   t=3/4 T

Fig. 4.11: H-field z-axis components distribution at different time

4.4 Parametric Study

A series of parametric studies will be discussed in this section to understand further the proposed circularly polarized pseudo-ME dipole antenna operation principle. Firstly, the four horizontal patches on the radiating layer play a key role in generating the fundamental resonances, providing a stable and high gain across the operating frequency. So, the length of each patch (L_{Patch}) is studied first. Secondly, the crossed-dipole feeding network makes the antenna possible to have a stable circular polarization and wide 3-dB AR bandwidth. Besides, it is also essential for wideband impedance matching. So, the width of the short leads (W_{Con}) and width of the long leads (W_{Ring}), and radius of the arc (R_{Ring}) are investigated. Thirdly, like the ground plane of the LP pseudo-ME dipole proposed n Chapter 4. The height between radiating layer and the ground plane (H_{Air}) and the length of square the ground plane (L_{Ground}) has also been investigated to study the influence on gain and bandwidth. Finally, in the last part of this study, a metallic cavity geometry will replace the planner ground plane. It provides the proposed antenna with a more unidirectional radiation pattern and a higher front-to-back ratio [35]. The height of the cavity vertical wall (H_{Wall}) will be studied.

The parametric study will analyze the performance of the antenna by studying S_{11}, the real and imaginary parts of Z_{11}, the realized gain, and the axial ratio. The other parameters remain the same as those values in table 5.1 when each parameter is studied.

4.4.1 L$_{Patch}$

The four horizontal patches on the radiating layer are the main radiating elements that produce the four fundamental resonances, so the size of patches determine the frequencies of four resonances.

Fig. 4.13 depicts the real and imaginary parts of the impedance with different L$_{Patch}$. Since the resonant frequency of either a half-wavelength electric dipole or a magnetic dipole is determined by its length, when tuning the L$_{Patch}$ longer, all four modes move to a lower frequency band (ref to section 5.4.1 for the four modes of the antenna). Although the resonant frequency changes with L$_{Patch}$ varying from 15.5 mm to 20 mm (19.5 λ_g to 25.2 λ_g), the value of impedance is generally not affected significantly except the fourth mode, so the bandwidth is still wide generally while the high-frequency band is affected relevant more. This can be confirmed by the S$_{11}$ shown in Fig. 4.12. By tuning L$_{Patch}$, the operating frequency of the proposed antenna shifts accordingly, but the impedance bandwidth remains wide close to 60%.
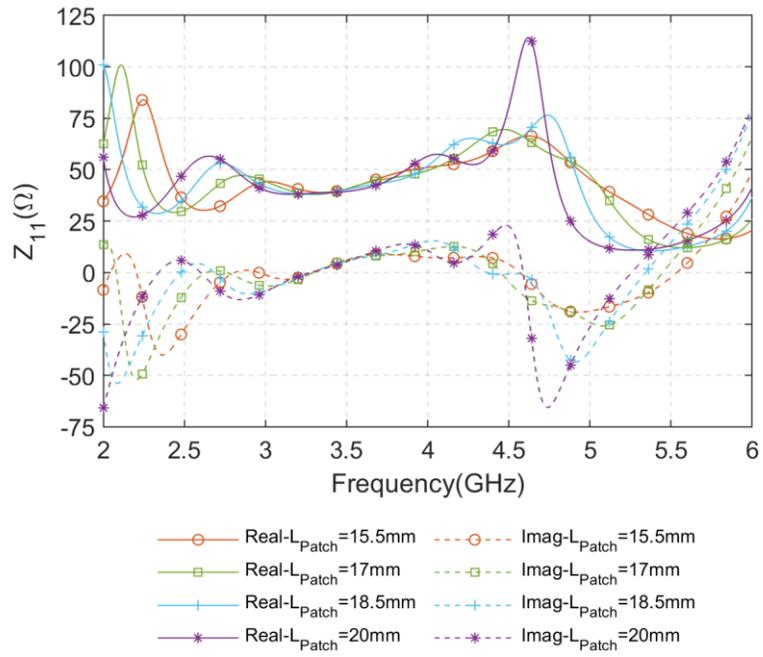
Fig. 4.12: Simulated Z_{11} and gain of the proposed CP pseudo-ME dipole antenna with different
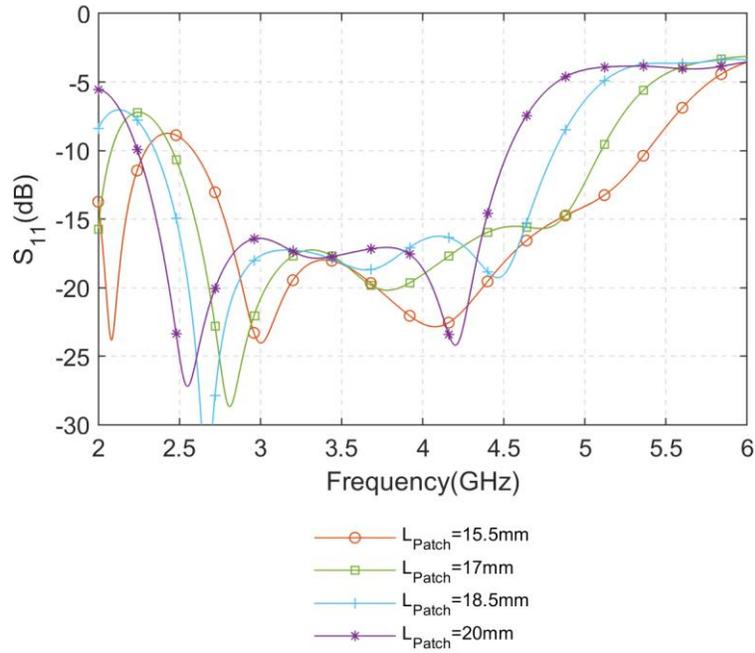
L_{Patch}

Fig. 4.13: Simulated S_{11} of the proposed CP Pseudo-ME dipole antenna with different L_{Patch}

Fig. 4.14 shows how gain and the axial ratio change with different L_{Patch}. By tuning L_{Patch} larger, the gain at the high-frequency band drops since the resonance frequency moves. Moreover, due to the impedance changes of the fourth mode, and the R_{Ring} becomes relatively shorter with a longer L_{Patch}, the amplitude/phase balance of the high-frequency-band CP cannot be maintained, the gain and AR performance at high frequency are deteriorated.
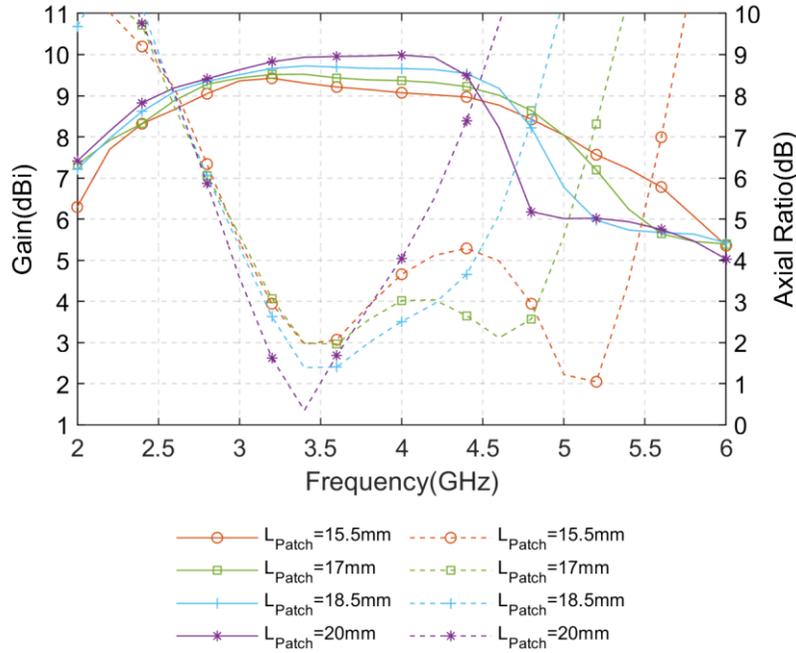
Fig. 4.14: Simulated gain and the axial ratio of the proposed CP Pseudo-ME dipole antenna

with different L_{Patch}

4.4.2 W_{Con}

The feeding network is the critical part that transfers the balanced signal from the coaxial cable to each patch and the open-slots. It plays an essential role in creating the 90° phase difference and allocates equal power for the four horizontal patches to generate circular polarization. The signal will be spilt into four paths and travel to each patch after the feed network geometry. Thus, the width of each lead becomes a critical value that affects the impedance matching.

W_{Con} represents the width of the short lead. Fig. 4.15 and Fig. 4.16 show the influence of W_{Con} on S_{11} and Z_{11}. Generally, the wider W_{Con} is, the wider S_{11} bandwidth will achieve. As it can be observed from the Z_{11} profile, larger values of W_{Con} will make both real parts and the imaginary part of the antenna balanced and close to $50 + j0$ Ω. In this parameter study, 5.2 mm (0.065 λ_g) is almost the

maximum width that can be achieved, as it is limited by the space available. It must mention in this specific case, wider W_{Con} brings a properly balanced impedance. However, in other cases of implementing crossed-dipole geometry as a feeding method, the value chosen guide may be different.

Fig. 4.17 shows that by tuning W_{Con} from 3.7mm (0.046 λ_g) to 5.2 mm (0.066 λ_g), the gain and axial ratio are not affected significantly while only the high-frequency band gain slightly increased. The axial ratio remains low in the investigated range of W_{Con}, and the AR profile shows that W_{Con} is related to the balance between low-frequency and high-frequency band CP. To sum up the analysis state so far, when set up the value of short lead W_{Con}: firstly, the width should be as comprehensive as possible since a wide impedance bandwidth is desired. Secondly, according to the axial ratio to choose the value of W_{Con} for the antenna for a balanced circular polarization.
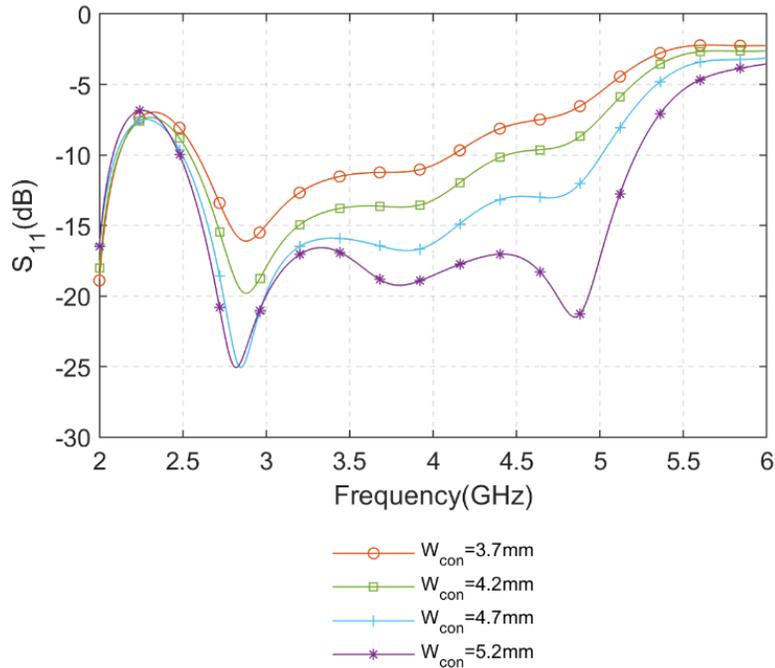

Fig. 4.15: Simulated S_{11} of the proposed CP Pseudo-ME dipole antenna with different W_{Con}
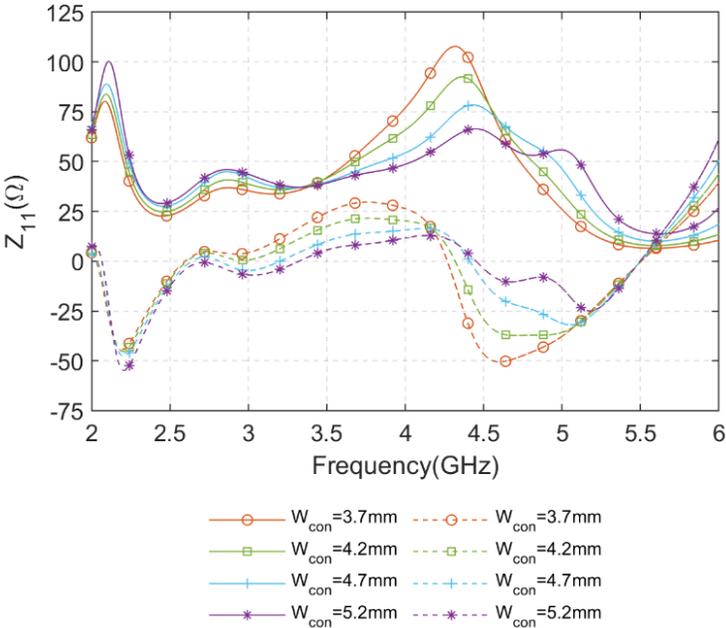
Fig. 4.16: Simulated Z_{11} of the proposed CP Pseudo-ME dipole antenna with different W_{Con}
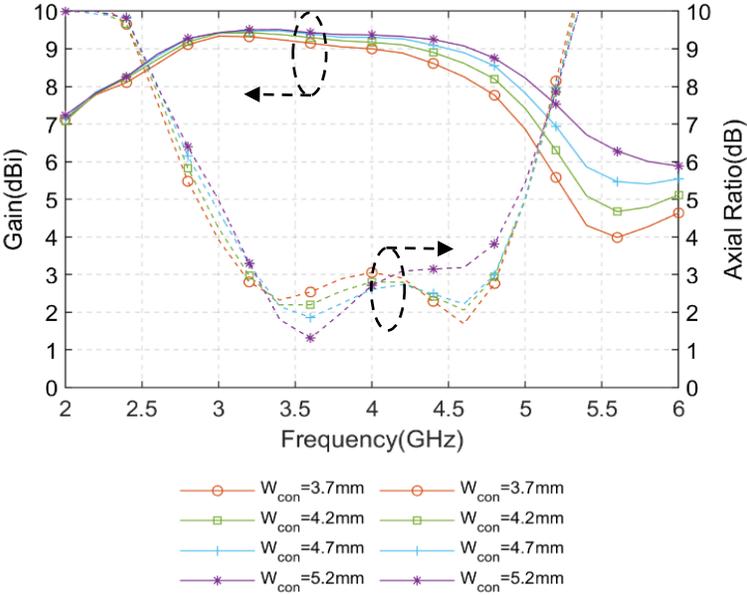

Fig. 4.17: Simulated gain and the axial ratio of the proposed CP Pseudo-ME dipole antenna

with different W_{Con}

4.4.3 W_{Ring}

W_{Ring} represents the width of the long lead (quarter-wavelength ring). Fig. 4.18 and Fig. 4.19 show the influence of W_{Ring} on S_{11} and $Z_{11,}$ respectively. It can be observed from the Z_{11} profile. W_{Ring} affects the real part of the second and fourth modes and the imaginary part of the first and the third mode of the antenna. Generally, a wider W_{Ring} means wide bandwidth in the investigation range, and 1.5 mm is almost the maximum width that can be achieved.

In Fig. 4.20, W_{Ring} is tuned from 0.6 mm (0.008 λ_g) to 1.5 mm (0.019 λ_g); the gain remains high except in the high frequency since the impedance matching worsens when W_{Ring} is narrow. Because W_{Ring} affects the second and fourth modes of the proposed antenna, both circular polarizations could be affected. Relatively narrow W_{Ring} separates while wide W_{Ring} concentrates the two AR center points.
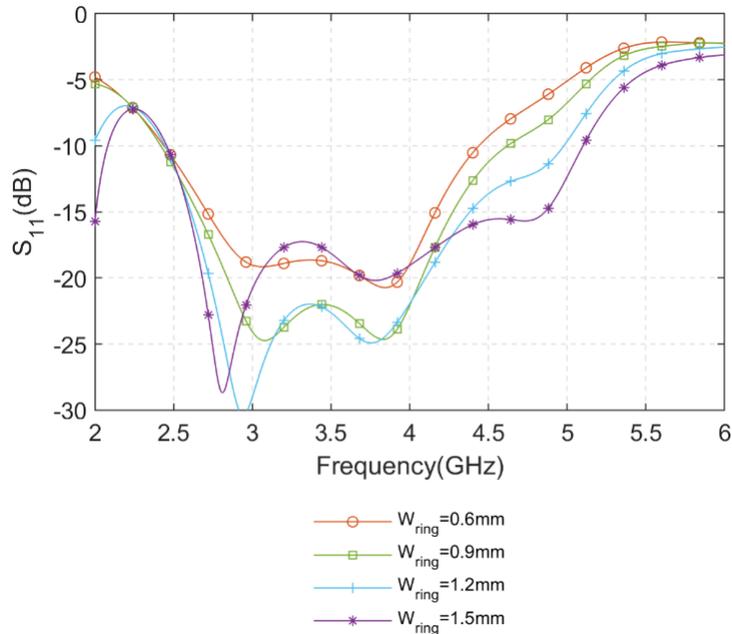

Fig. 4.18: Simulated S_{11} of the proposed CP Pseudo-ME dipole antenna with different W_{Ring}
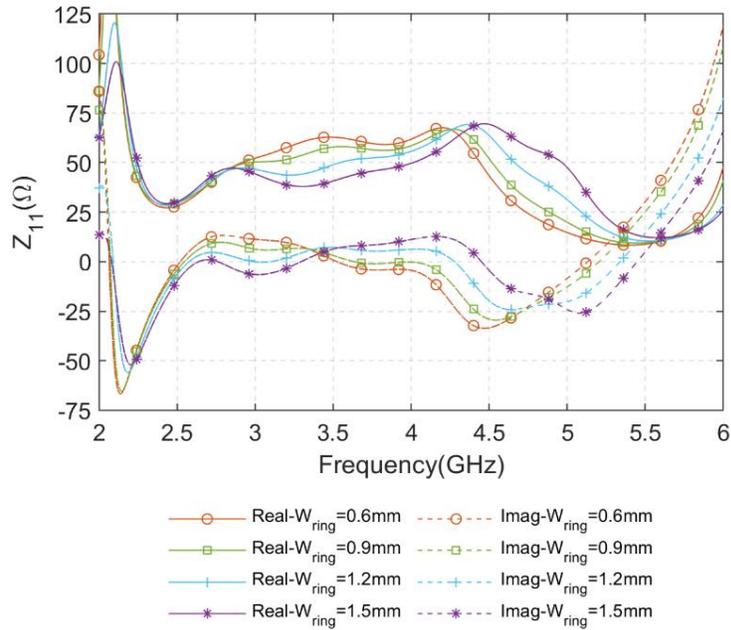
Fig. 4.19: Simulated Z_{11} of the proposed CP Pseudo-ME dipole antenna with different W_{Ring}
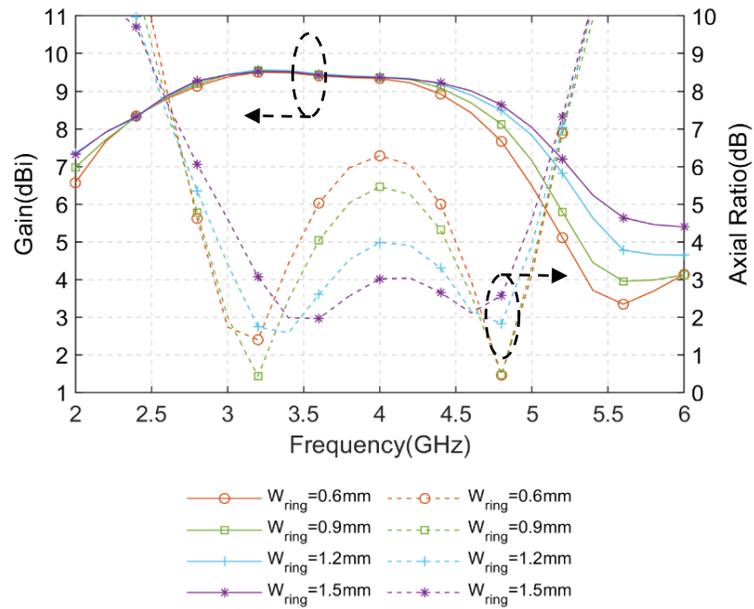
Fig. 4.20: Simulated gain and the axial ratio of the proposed CP Pseudo-ME dipole antenna

with different W_{Ring}

To sum up the analysis state related to the crossed-dipole feeding network: when setting up the available value of W_{Con} or W_{Ring} for this CP Pseudo-ME dipole antenna, it is always good to keep a large value so that the antenna will have a wide impedance bandwidth. More importantly, the W_{Con} or W_{Ring} affects the axial ratio more significantly than the impedance bandwidth. The final optimized value should be carefully set up according to the axial ratio, as wide AR bandwidth is the priority of this CP antenna.

4.4.4 R_{Ring}

R_{Ring} represents the radius of the quarter-wavelength arc (from center to the middle of the arc). The signal from coaxial cable travels longer to the patch B and D due to the quarter arc. Thus, the length of the quarter-wavelength arc is the key to create the 90° phase difference, and it is the most critical parameter for generating circular polarization. Fig. 4.21 and Fig. 4.22 show the influence of R_{Ring} on S_{11} and Z_{11}, respectively. It can be observed that the changes of R_{Ring} affects all four modes of the antenna. Shorter R_{Ring} makes the impedance match better at high-frequency band, and wide bandwidth will be achieved.

Fig. 4.23 shows when R_{Ring} varies from 4.9 mm to 5.5 mm. The gain remains high; only the gain in the highest frequency decreased slightly since the impedance does not match well. R_{Ring} is related to the phase difference between orthogonal resonances, so the two circularly polarized frequency points could be affected. A shorter R_{Ring} brings the two AR center frequency points closer and results in a narrower AR bandwidth. Simultaneously, a desirable value of R_{Ring} will arrange the two AR center points to be properly separated so that a wide axial ratio bandwidth can be achieved.
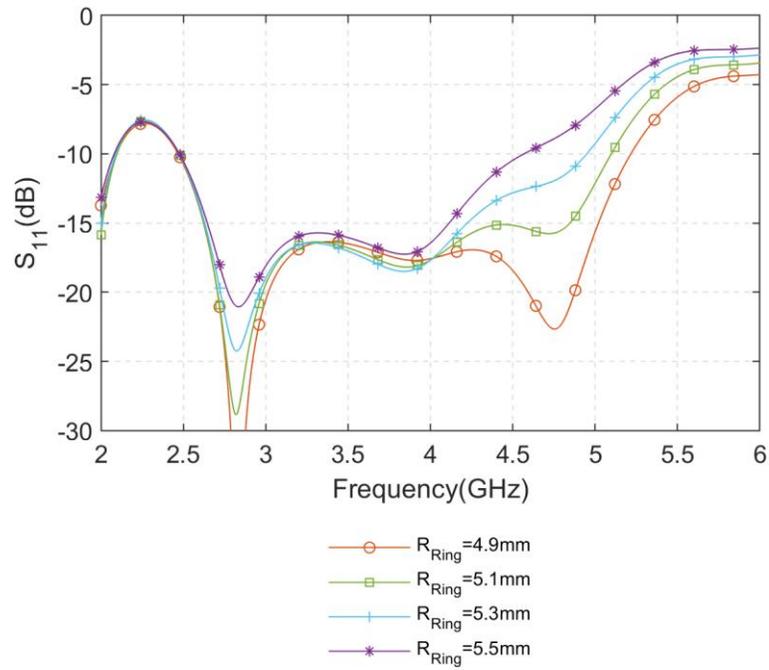
Fig. 4.21: Simulated S_{11} of the proposed CP Pseudo-ME dipole antenna with different R_{Ring}
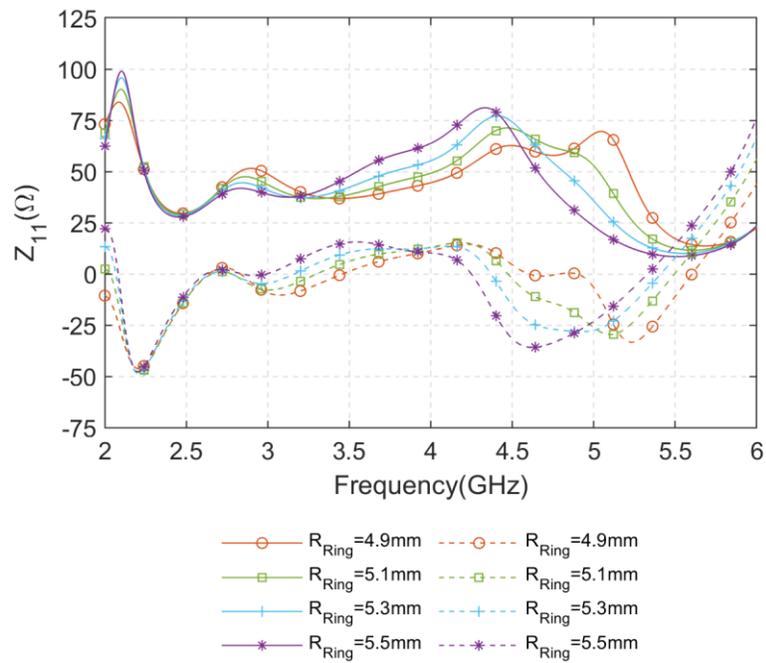

Fig. 4.22: Simulated Z_{11} of the proposed CP Pseudo-ME dipole antenna with different R_{Ring}
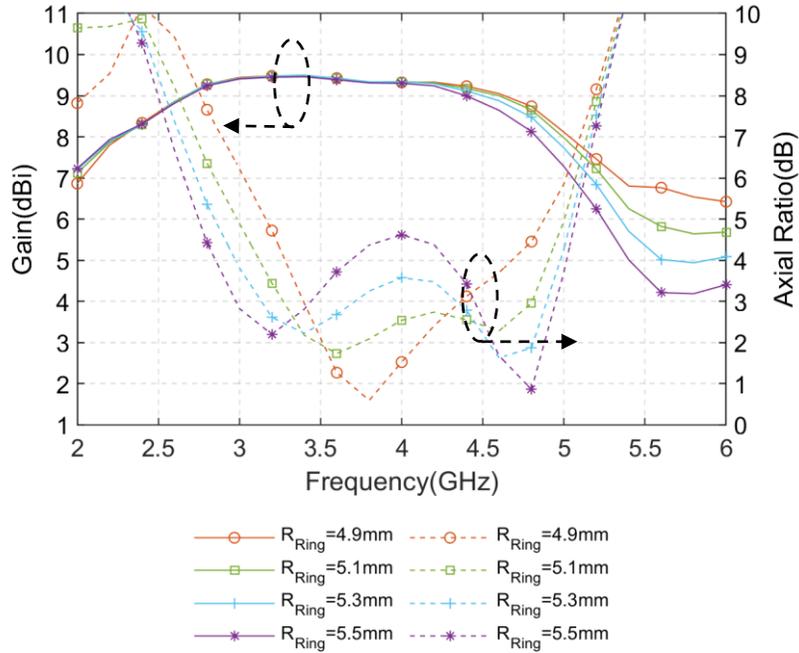
Fig. 4.23: Simulated gain and the axial ratio of the proposed CP Pseudo-ME dipole antenna

with different R_{Ring}

According to the parametric studies in W_{Con}, W_{Ring}, R_{Ring}, their effect on gain of the proposed antenna is not significant; only the gain in the high frequency band drops slightly because of the impedance mismatch. Good impedance matching could be achieved by adjusting the value of W_{Con} and W_{Ring}. Generally, a wider W_{Con} makes the impedance match better in the whole frequency band. While then, according to the parametric study data, tuning W_{Ring}, R_{Ring} with suitable values, a wide and balanced AR bandwidth could be obtained.

4.4.5 H_{Air}

In the next two sections, the influence of the ground plane on the antenna will be studied. Like the ground plane of the cavity-less Pseudo-ME dipole proposed in chapter 4, the ground plane of this CP Pseudo-ME dipole antenna is also employed as a reflector.

H_{Air} represents the height between the radiating layer to the ground plane. Fig. 4.24 and Fig. 4.25 show the influence of H_{Air} on S_{11} and Z_{11} of the proposed antenna. By tuning H_{Air} from 14 mm (0.177 λ_g) to 23 mm (0.290 λ_g), all four modes of the antenna are shifted due to the effective length of the patches and slots change accordingly. In contrast, since the value of Z_{11} remains relatively stable and close to $50 + j0$ Ω, the impedance bandwidth remains wide.
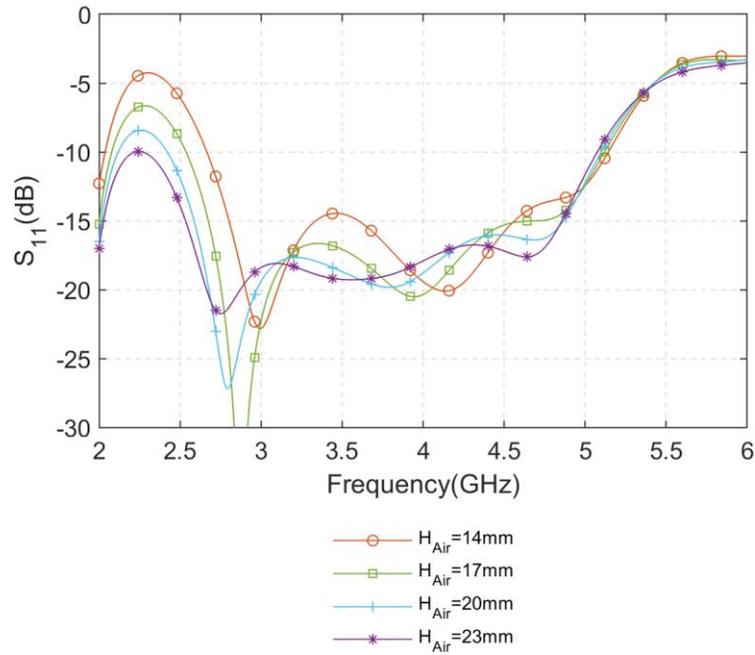

Fig. 4.24: Simulated S_{11} of the proposed CP Pseudo-ME dipole antenna with different H_{Air}
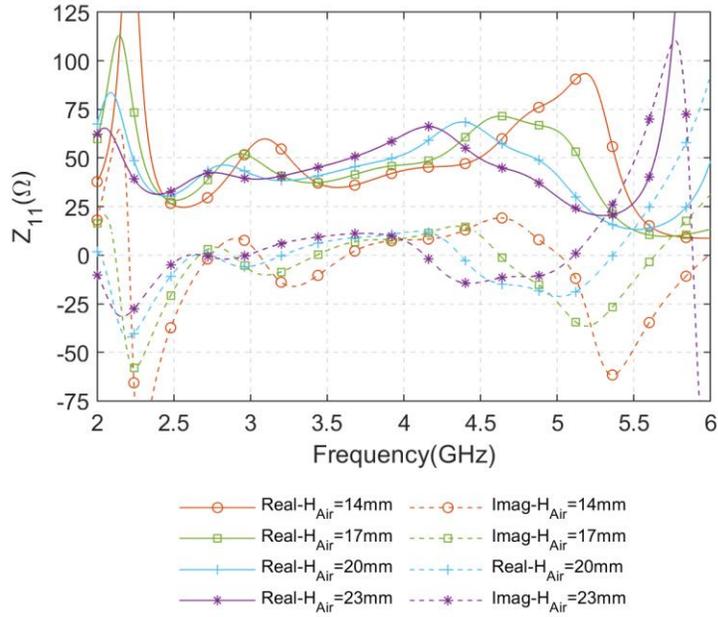
Fig. 4.25: Simulated Z_{11} of the proposed CP Pseudo-ME dipole antenna with different H_{Air}

Fig. 4.26 depicts how gain and AR change with different H_{Air}. Generally, the gain at the high-frequency band is affected more when comparing the low-frequency when H_{Air} is increased. As explained in the radiating principle in section5.3, the resonance at low frequency band is contributed by the electric dipoles while the magnetic dipole modes contribute the resonance at high-frequency band. When set the ground plane more than a quarter wavelength away from the radiating layer, this difference is relatively more impactful at higher frequencies since the wavelength is shorter, so that the gain drops more in higher frequency. When focusing on the axial ratio, by tuning the height close to a quarter-wavelength (20 mm ($0.252 \lambda_g$)), the gain becomes flatter in the operating frequency band, so a better balance gain stability and the widest AR bandwidth could be obtained.
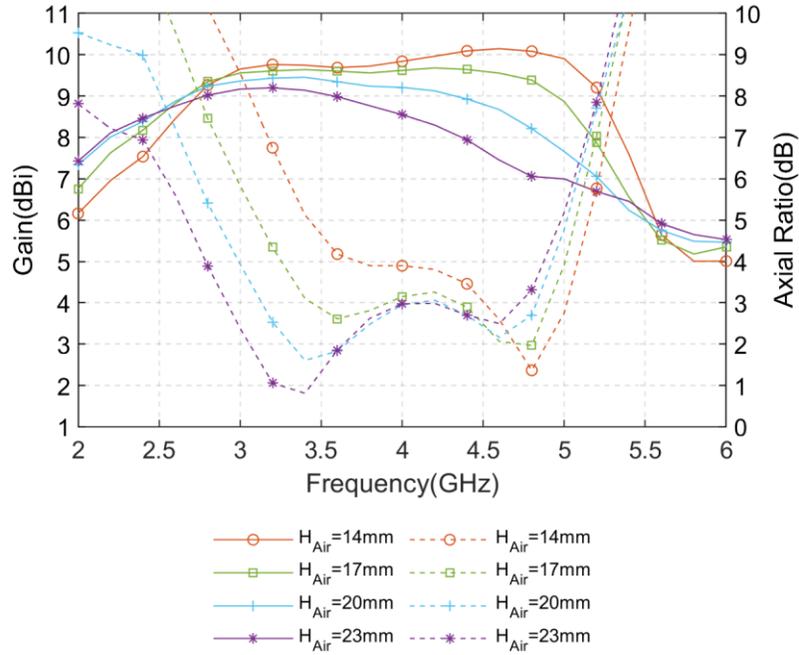
Fig. 4.26: Simulated gain and the axial ratio of the proposed CP Pseudo-ME dipole antenna

with different H_{Air}

4.4.6 L_{Ground}

L_{Ground} represents the length of the square ground plane. Fig. 4.27 and Fig. 4.28 depict the influence of L_{Ground} on S_{11} and Z_{11}, respectively. Theoretically, a square ground plane with a size equal or larger size than λ_0^2 will give better gain enhancement. To study how the size of the ground plane affects the proposed antenna performance. The value of L_{Ground} has been set from 40 mm (0.504 λ_g) (same size of the radiating layer) to 100 mm (1.261 λ_0) for investigation. Fig. 5.35 shows that Z_{11} is barely affected by the length of the square ground, excepted at 40 mm since it is only about half wavelength of the low-frequency band. The impedance bandwidth also gets narrower at the low-frequency band.
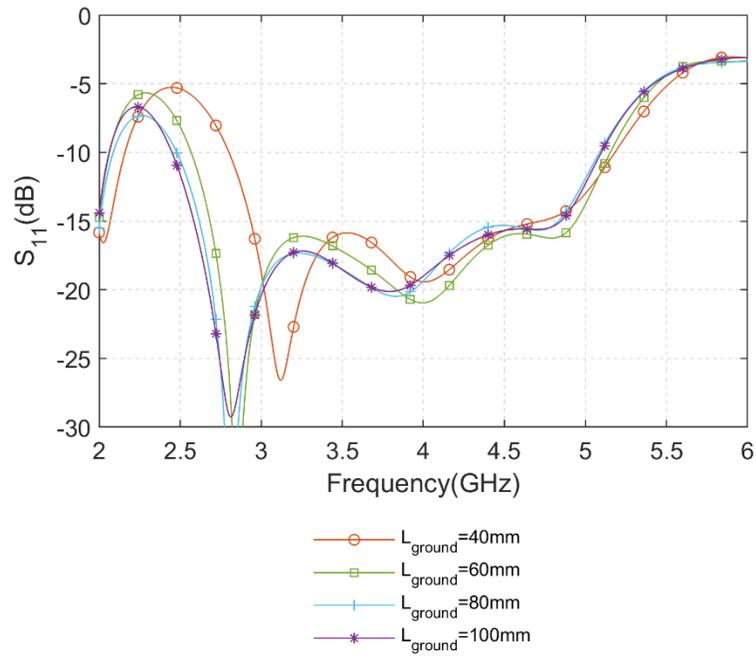
Fig. 4.27: Simulated S_{11} of the proposed CP Pseudo-ME dipole antenna with different L_{Ground}
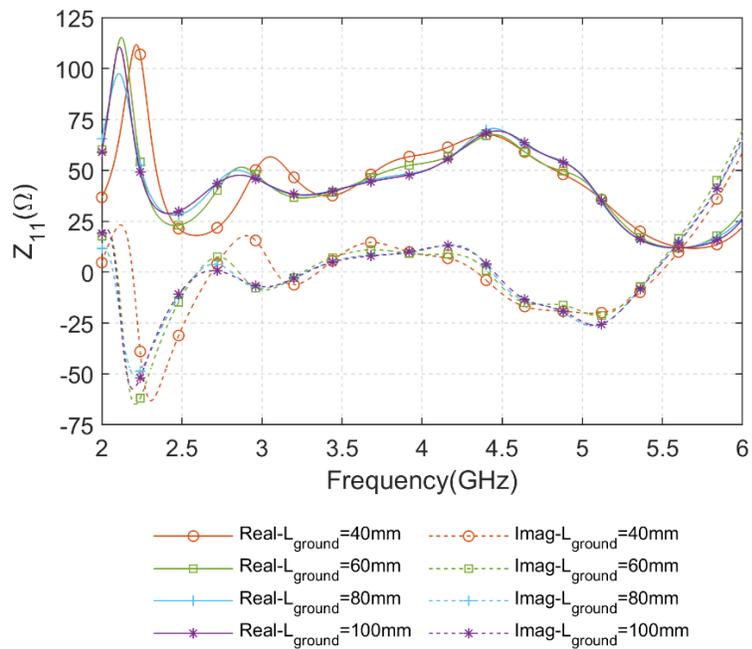

Fig. 4.28: Simulated Z_{11} of the proposed CP Pseudo-ME dipole antenna with different L_{Ground}

Fig. 4.29 shows the gain and AR with different values of L_{Ground}. Likewise, since the ground plane does not affect the impedance matching significantly, the proposed axial ratio of the antenna is slightly affected when L_{Ground} is varying from 60 mm to 100 mm. However, the gain of the antenna is affected significantly by the ground plane size. In the investigation range, the gain increase with a larger size of the ground plane. When the size increased to 100 mm, the average gain will stay around 8.7 dBi in the operating frequency band.
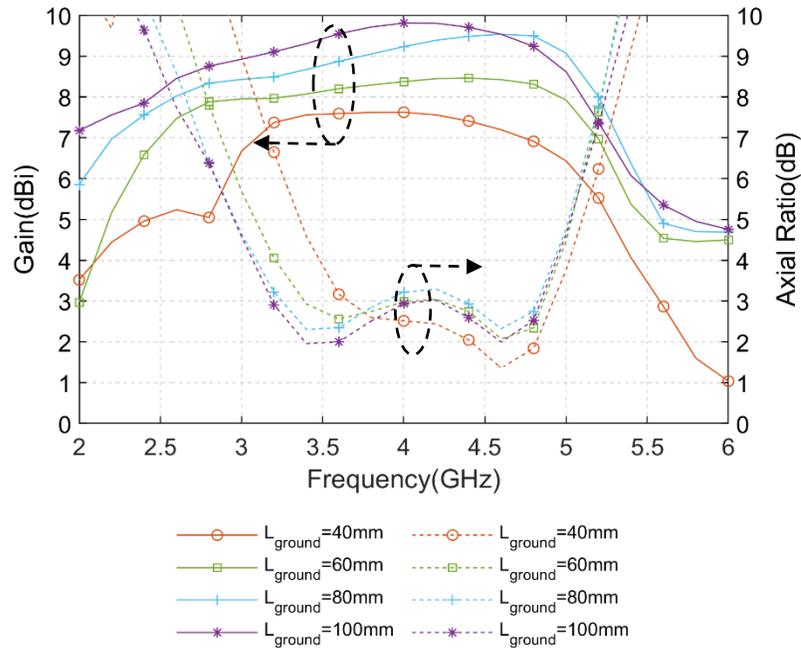
Fig. 4.29: Simulated gain and the axial ratio of the proposed CP Pseudo-ME dipole antenna

with different L_{Ground}

4.4.7 Parametric study summary

Six critical parameters of the cavity-less crossed-dipole fed circularly polarized Pseudo-ME dipole antenna have been studied in the previous sections. To design the antenna operating at the proper frequency band for specific applications, the size of four patches needs to be first determined by setting up the proper value

of L_{Patch} (roughly a quarter-wavelength). Secondly, to obtain a wide and balanced axial ratio bandwidth, the long lead R_{Ring} of the crossed-dipole geometry should be set around a quarter wavelength so that a 90° phase difference will be achieved between the orthogonal resonances. Thirdly, the width of the short lead W_{Con} and long lead W_{Ring} of the crossed-dipole geometry should be set as wide as possible in the limited space since that will give the proposed antenna a flat impedance across the frequency. Wide impedance bandwidth and balanced axial ratio bandwidth will be achieved. Finally, a ground plane with a size of about λ_g^2 should be located at a quarter-wavelength under the radiating layer. A balanced gain enhancement will be achieved in the operating band, and a high and stable gain will be obtained.

The Fig. 4.30 give the average gain, impedance bandwidth, and axial ratio bandwidth of the proposed antenna with different values of each parameter. These data could be useful as a reference for designing the proposed wideband cavity-less CP Pseudo-ME dipole antenna at S-band or similar frequency bands.
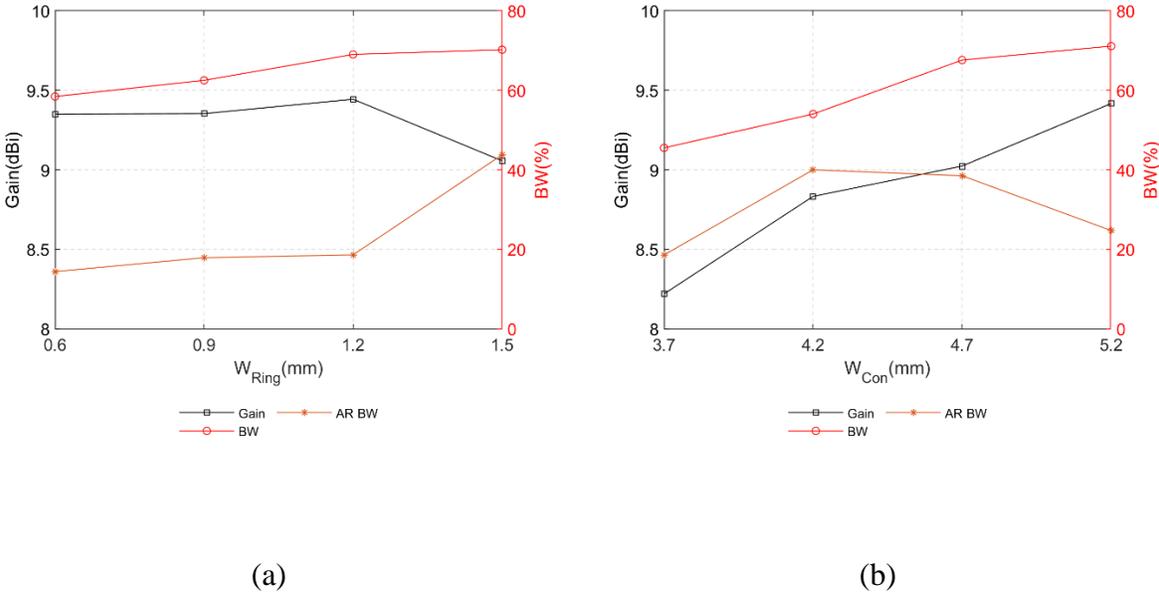
(a)   (b)
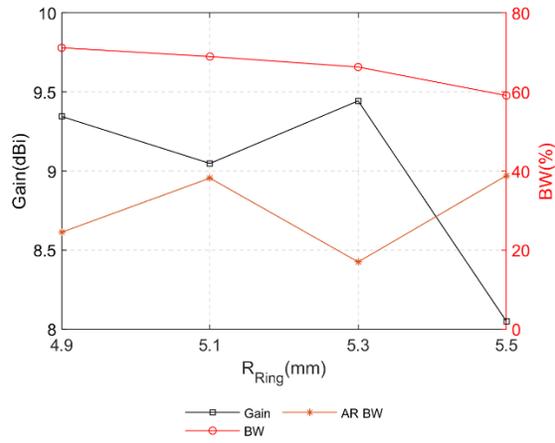
(c)
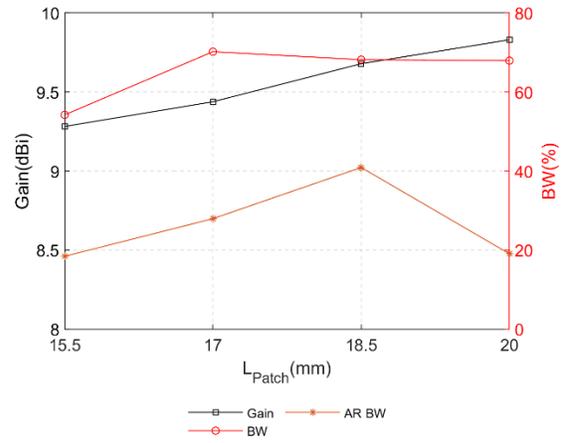
(d)
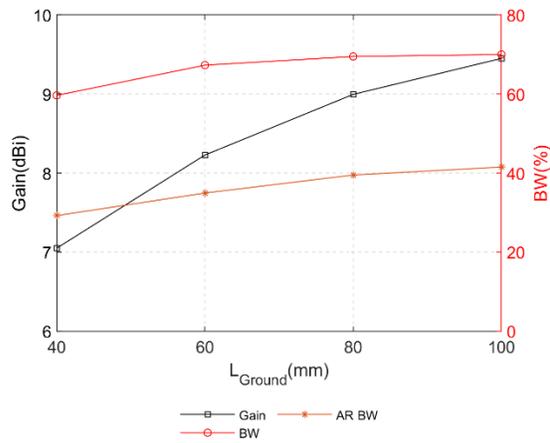
(e)
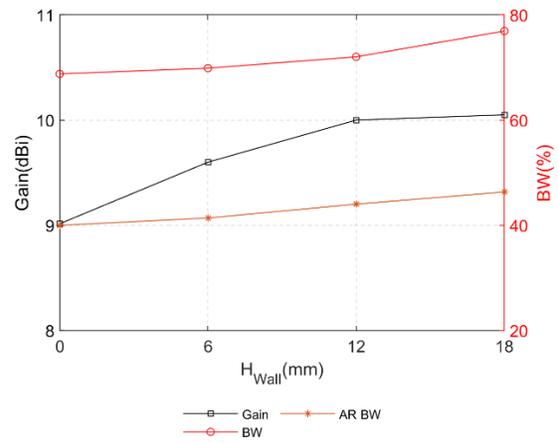
(f)
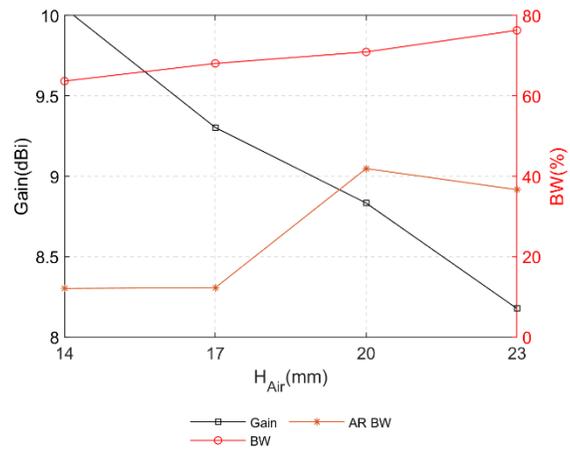
(g)

Fig. 4.30: Average gain, impedance bandwidth and AR bandwidth with different (a). W_{Ring}.

(b). W_{Con}. (c). R_{Ring}. (d). L_{Patch}. (e) L_{Ground}. (f) H_{Wall}. (g). H_{Air}.

4.5   Simulated and Measured Results

Antenna prototypes were fabricated and measured to verify the performance. Fig. 4.31 is the photo of the fabricated cavity-less CP Pseudo-ME dipole antenna prototype. Fig. 4.32 shows the detailed top side and the bottom side metallic pattern of the radiating layer. It could be noticed that the only difference between them is a round aperture on the bottom layer, which is for connecting the outer conductor of the semi-rigid cable and being isolated from the inner conductor. Two prototypes were fabricated for the gain and radiation pattern measurement.

Fig. 4.31: The fabricated CP Pseudo-ME dipole antenna

<div align="center">(a)   (b)</div>
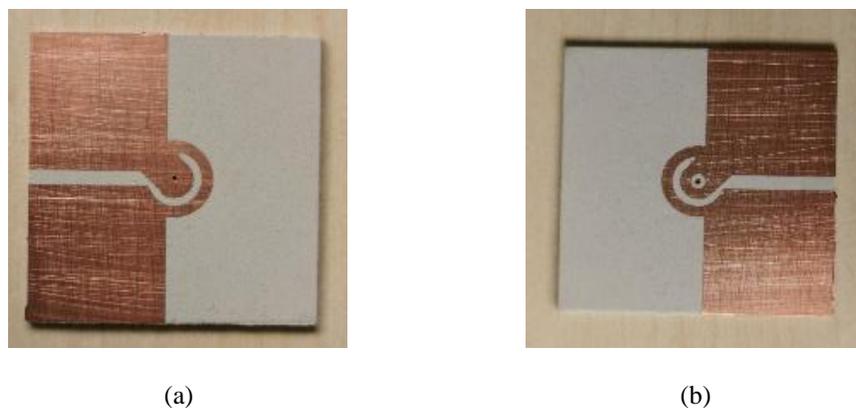
Fig. 4.32: (a) Top side of the radiating layer (b) the bottom side of the radiating layer of the

fabricated radiating layer

4.5.1 S_{11} & Z_{11}
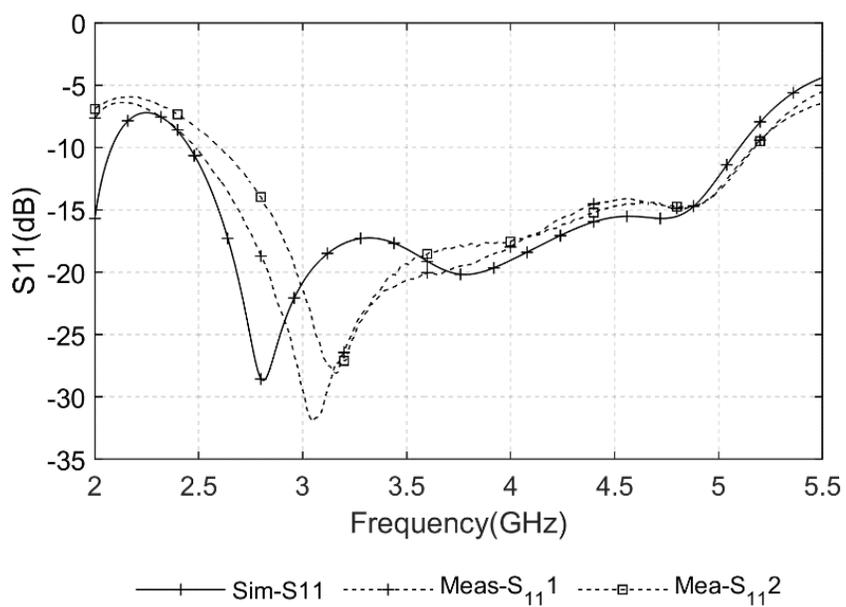
Fig. 4.33: S_{11} of the CP Pseudo-ME dipole antennas under test

Firstly, the S_{11} of the two CP Pseudo-ME dipole antenna prototypes were confirmed. Since the gain measurement will be reliable if the two antennas under test are similar (better if two S_{11} are the same), the simulated and measured S_{11} of both fabricated antennas are shown in Fig. 4.33. The simulated results show the CP antenna has a wide impedance bandwidth ($S_{11} < -10$ dB) of 69.8% from 2.46 GHz to 5.10 GHz, and both fabricated antennas have S_{11} match reasonably well with the simulated results.
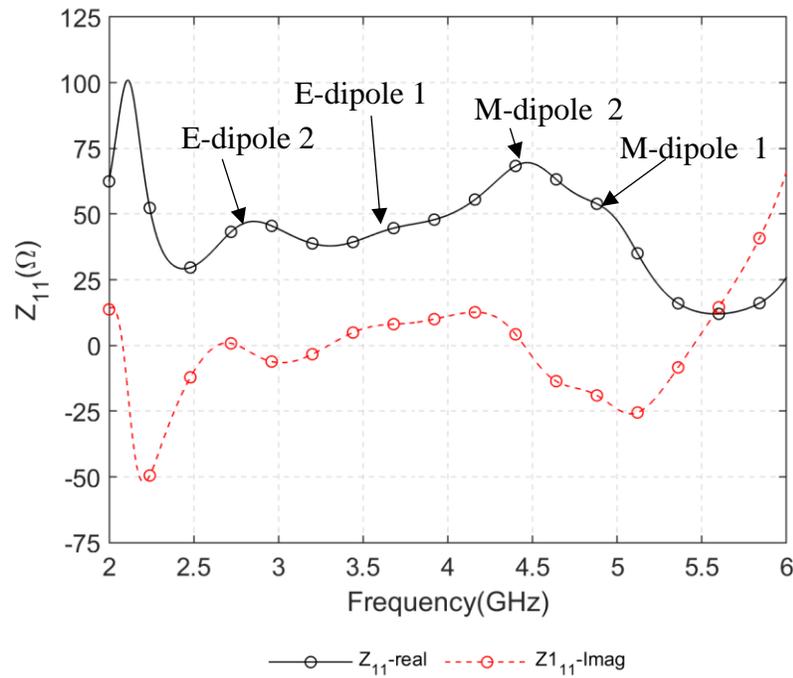
Fig. 4.34: Z_{11} of the CP Pseudo-ME dipole antennas under test

Section 5.3 states the circular polarization is generated from four resonances. To verify the four fundamental resonances of the proposed antenna, Fig. 4.34 gives the simulated real and imaginary parts of impedance. It shows the antenna has four modes in the operating band, since the two electric dipoles are operating at in diagonals, so they operate at 2.8 GHz, 3.6 GHz, and the two magnetic dipoles are operating at 4.2 GHz, and 5 GHz.

135

Since the two electric dipoles are operating at the diagonal directions, which is slightly longer than the magnetic dipoles. Thus, two electric dipoles operate at the lower frequency (2.8 GHz and 3.6 GHz), and magnetic dipoles operate at the high-frequency band (4.2 GHz and 5 GHz). In the parametric study section following, this statement will be further verified.

4.5.2 Gain, Axial Ratio and Efficiency

Fig. 4.35 depicts the gain and the axial ratios of the proposed antenna. The measured and simulated results of gain matched well; the measured axial ratio shows very similar trend but generally 1.5 dB better than the simulated result. In the impedance frequency band from 2.46 GHz to 5.10 GHz, the proposed CP pseudo-ME dipole antennas have a stable high gain of 8.7 ± 0.9 dBi, and the maximum gain is 9.6 dBi at 3.27 GHz. The radiation efficiency and total efficiency are shown in Fig. 4.36, which are higher than 99% and 90% respectively.
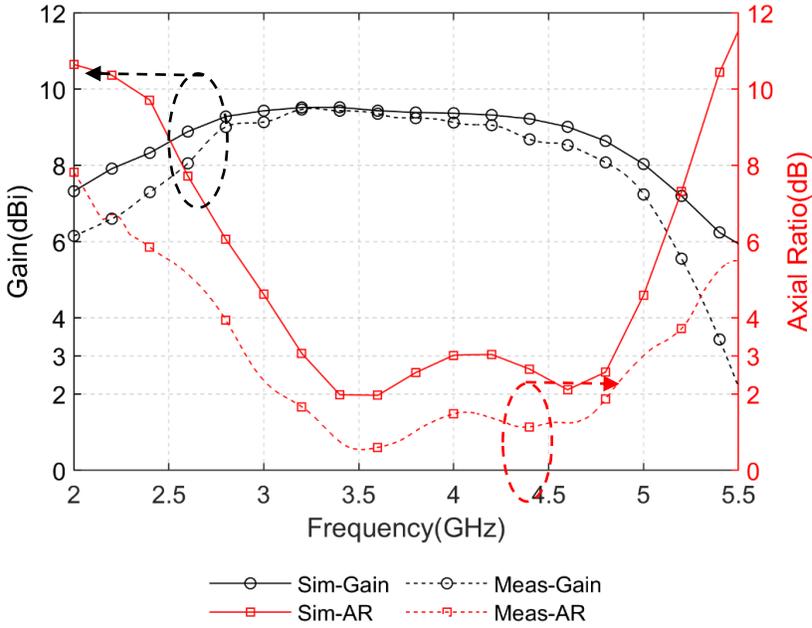
Fig. 4.35: Simulated and measured gain and the axial ratio of the CP ME dipole
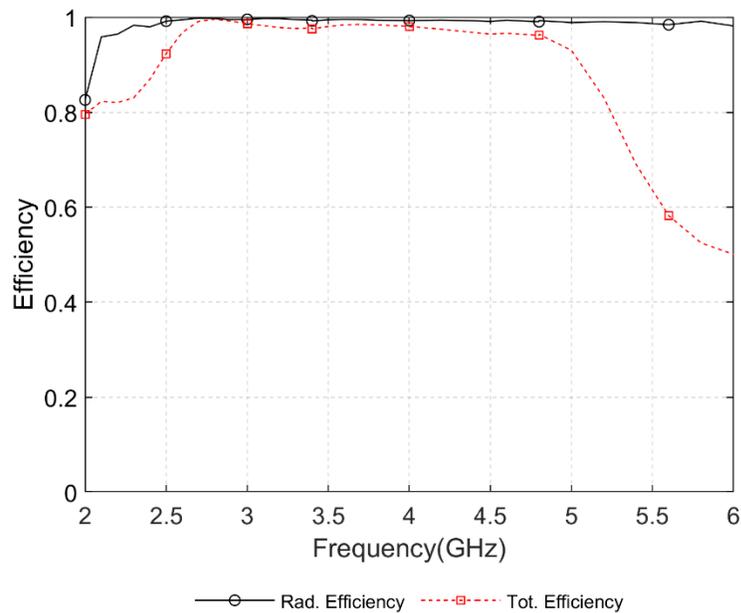
Fig. 4.36: Simulated radiation and total efficiency of the CP ME dipole

The axial ratio results show two CP center frequency points. According to the radiating principle explained in section 5.3. The pair of electric dipoles operating at the diagonal directions generates the low-frequency band CP center frequency point at 3.50 GHz (measured AR = 0.53 dB). The pair of magnetic dipoles operating at the x-, y-axis directions generate the high -frequency band CP center frequency point, which is at 4.60 GHz (measured AR = 1.2 dB). The measured result demonstrated that the proposed antenna has a wide CP radiation bandwidth for AR ≤ 3 dB of 54.1% from 2.87 GHz to 5.00 GHz. Although, there is discrepancy between the measured and simulated AR, the measured result has similar trend showing two pair of CP are generated by the antenna.

4.5.3 Radiation Patterns

To further verify the stability of the circular polarization, the simulated radiation patterns of the four principal planes will be discussed. Benefits from the two pairs of orthogonal electric dipoles and magnetic dipoles, the proposed Pseudo-

ME dipole antenna offers symmetrical CP radiation patterns in all four principal planes over the AR bandwidth.

Fig. 4.37 shows the radiation pattern of the pseudo-CP-ME dipole antenna in 3D. which demonstrate the antenna has high gain, low-backward radiation, and very similar E- and H-plane radiation pattern.
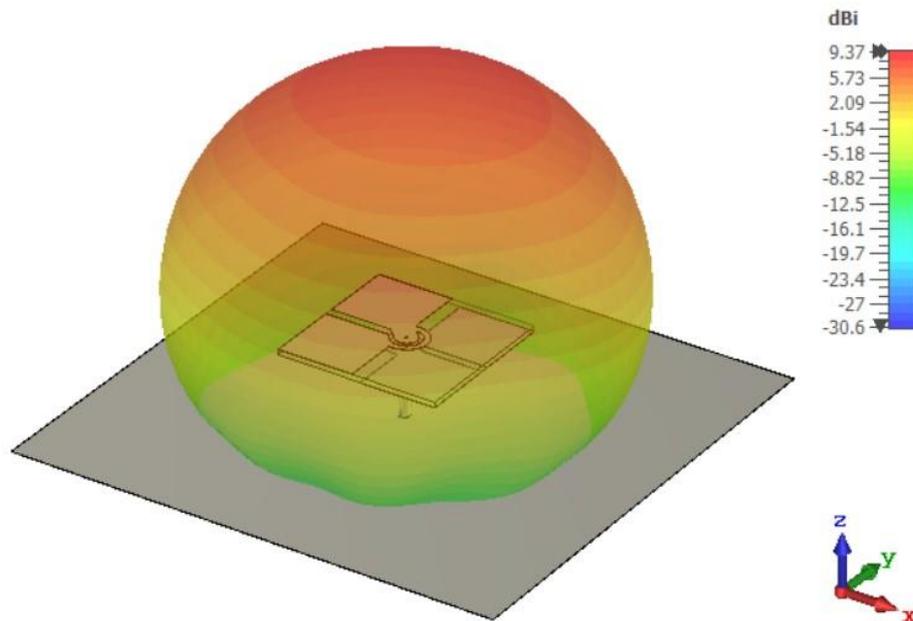
Fig. 4.37: Simulated radiation patterns at 4 GHz in 3D

Fig. 4.38 shows the simulated radiation patterns of $\phi = 0°$, 45°, 90°, 135° at the lowest frequency (3.2 GHz), center frequency (4 GHz) and highest frequency (4.8 GHz) of the AR bandwidth.

From each figure in Fig. 4.38, the radiation patterns of each principal plane show high consistency over the AR bandwidth. Moreover, when comparing the patterns of different planes, they also show a high similarity. The front-to-back ratio is always larger than 20 dB of different planes over the frequency. Table 5.2 tabulates the measured results of 3-dB beamwidth of radiation patterns, and

table 5.3 gives the simulated results for comparison. The measured results have acceptable consistency with the simulated results.

(a)

(b)

(c)

(d)
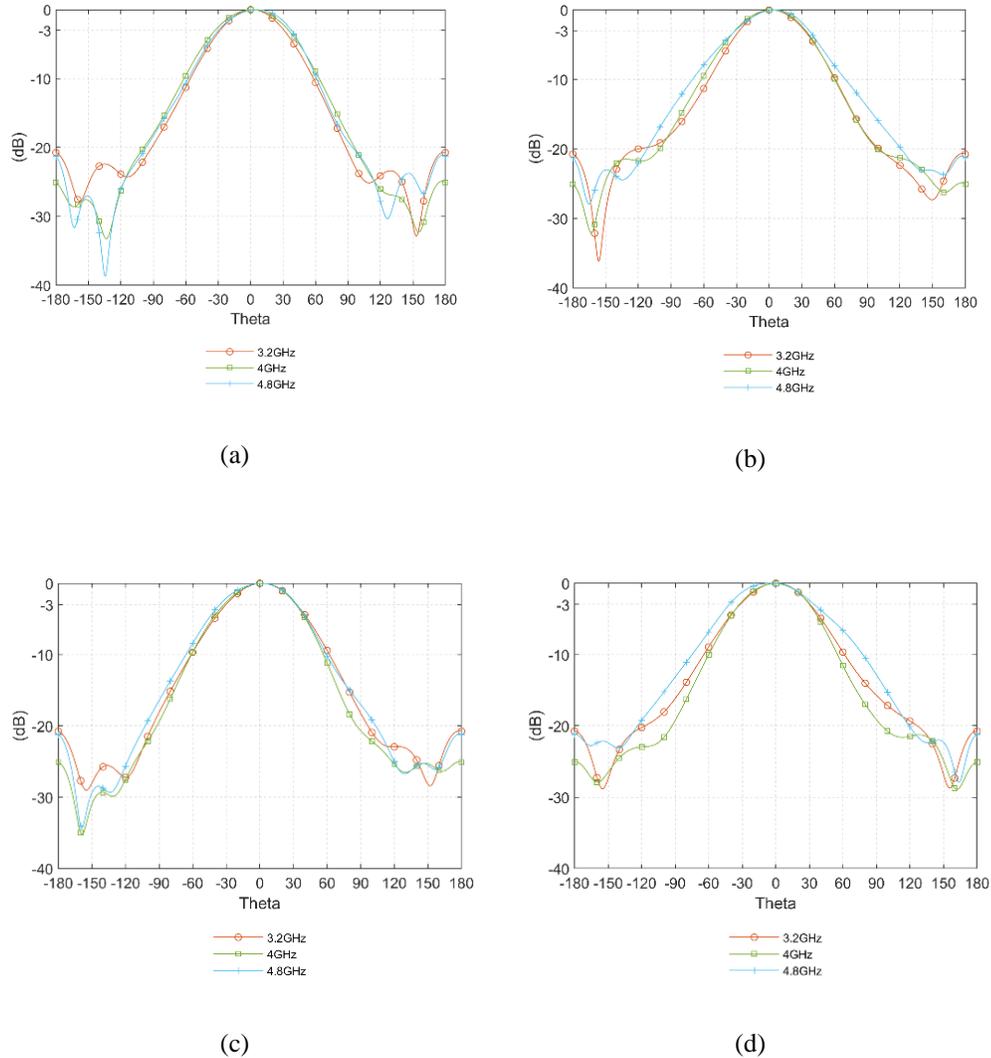
Fig. 4.38: Simulated radiation patterns at 3.2 GHz, 4 GHz, and 4.8 GHz when (a) $\phi=0°$, (b) $\phi=45°$, (c) $\phi=90°$, (a) $\phi=135°$.

Like the analysis in Chapter 4, parameters $|\Delta_1|$ $|\Delta_2|$ are also introduced for comparing the radiation patterns of different planes and frequencies. $|\Delta_1|$ means the beamwidth differences across the frequency at each plane, and $|\Delta_2|$ represents the beamwidth differences in different planes at each frequency. In general, the

139

3-dB beamwidth in the angular range between 66.5° to 77.5°. $|\Delta_1|$ shows good consistency at each plane with a small variation between 9.2° to 12.1°, which means the proposed CP ME antenna has a similar 3-dB beamwidth of the four principal planes over the frequency.

Moreover, as mentioned in section 5.3 radiating principle, the low-frequency band mainly results from the electric dipoles while the high-frequency band CP results from the magnetic dipoles. Therefore, CP should have the most average distribution at the center frequency (4 GHz), and that explains $|\Delta_2|$ has the minimum value of 1.8° at the center frequency.

Table 4.2:Measured 3-dB beamwidth results

3-dB beamwidth	3.2 GHz	4 GHz	4.8 GHz	$|\Delta_1|$ (°)
$\phi = 0°$	65.5	70.3	74.7	9.2
$\phi = 45°$	63.7	68.5	75.8	12.1
$\phi = 90°$	66.0	69.9	76.8	10.8
$\phi = 135°$	68.0	69.0	77.5	9.5
$|\Delta_2|$(°)	4.3	1.8	2.8	

Table 4.3: Simulated 3-dB beamwidth results

3-dB beamwidth	3.2 GHz	4 GHz	4.8 GHz	$|\Delta_1|$ (°)
Phi=0°	59.1	67.9	67.3	8.8
Phi=45°	59.9	65.1	67.8	7.9
Phi=90°	63.2	64.3	69.0	5.8
Phi=135°	63.0	62.9	76.3	13.3
$|\Delta_2|$(°)	4.1	5	9	

Conventionally, the beamwidth of a wideband antenna decreases at the high-frequency band due to the antenna aperture becoming relatively electrically larger when frequency increases. However, for this CP Pseudo-ME dipole antenna, the beamwidth seems to increase with frequency. The reason to explain the circumstance is that: magnetic dipoles dominate the high-frequency band, and the aperture for the magnetic dipole is determined by the side length while not the diagonal of the radiating layer. Therefore, the aperture of the antenna at the high-frequency band is not relevant increased, so the beamwidth at the high-frequency band do not decrease.

4.5.3.1   Radiation Pattern ($\phi = 0°$)

The measured radiation pattern and simulated results of four principal planes: ϕ = 0°, 45°, 90°, and 135° are shown in Fig. 4.39 to Fig. 4.42. Each figure contains three frequencies: 3.2 GHz, 4 GHz, and 4.8 GHz, which covered the low, middle, and high frequency in full AR band. Generally, the measured results matched the simulated results well, especially the pattern between -90° to 90°. Although the pattern between -180° to -90° and 90° to 180° have some discrepancy, it is still in an acceptable range.
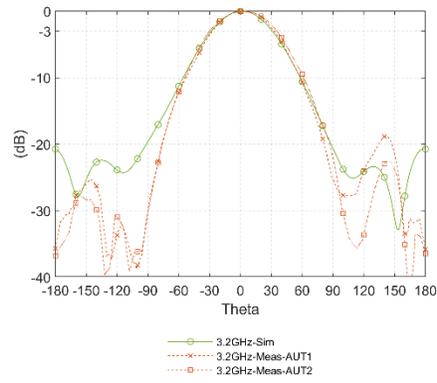
(a)
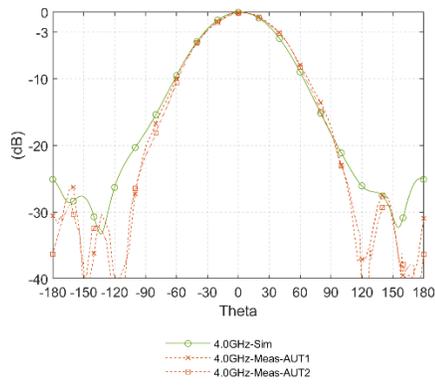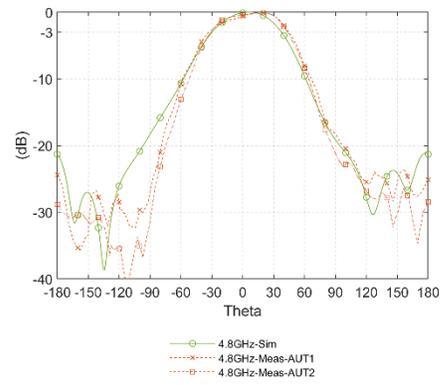
(b)   (c)

Fig. 4.39: Simulated and measured radiation patterns of $\phi = 0°$. (a) 3.2 GHz (b).4 GHz (c).4.8

GHz

142
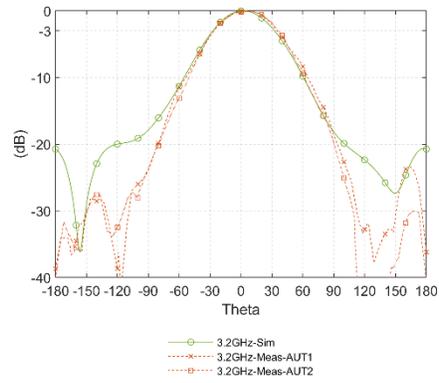
(a)
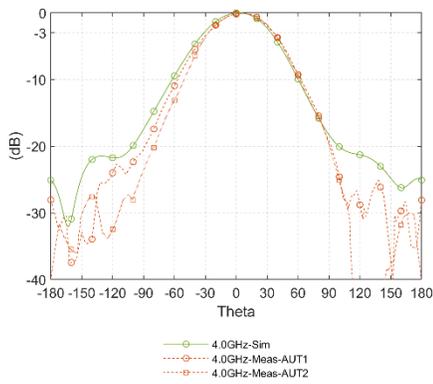
(b)
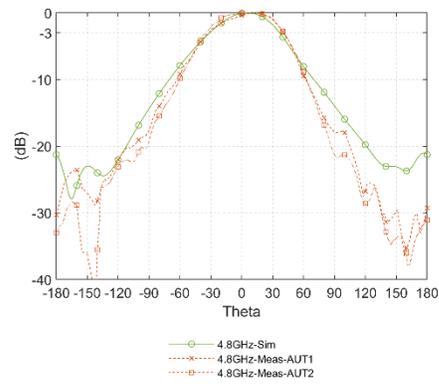
(c)

Fig. 4.40: Simulated and measured radiation patterns of $\phi = 45°$. (a) 3.2 GHz (b).4 GHz (c).4.8 GHz

143
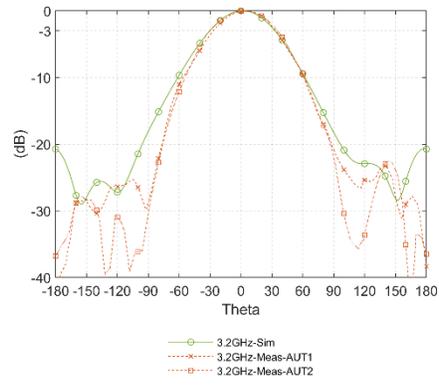
(a)
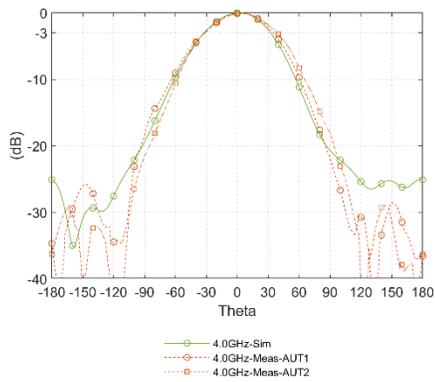
(b)
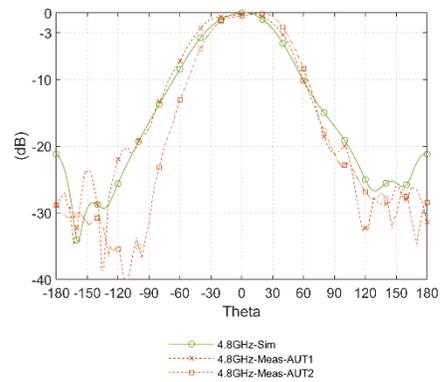
(c)

Fig. 4.41: Simulated and measured radiation patterns of $\phi = 90°$. (a) 3.2 GHz (b).4 GHz (c).4.8 GHz

144
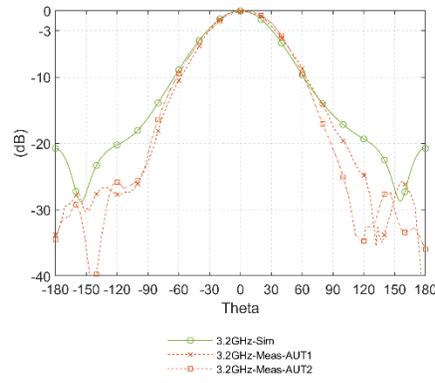
(a)
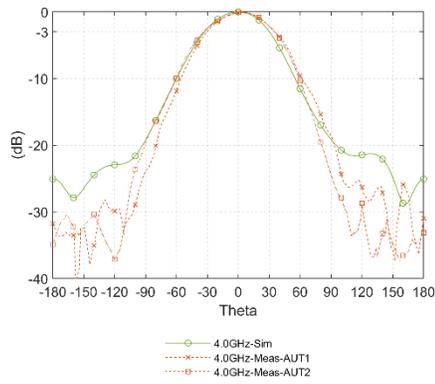
(b)
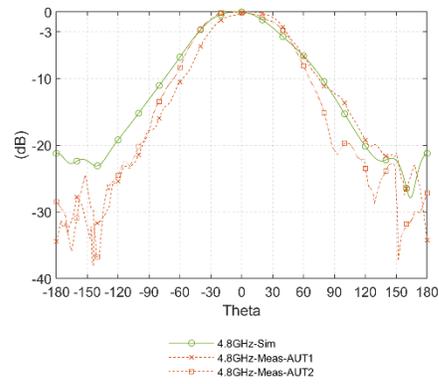
(c)

Fig. 4.42: Simulated and measured radiation patterns of $\phi = 135°$. (a) 3.2 GHz (b).4 GHz (c).4.8 GHz

4.6   Metallic cavity

For further understanding the performance of the flat ground plane, a metallic cavity is used to replace the ground plane and used as a reflector of the antenna for comparison. By implementing this type of reflector, the advantage is the footprint of the antenna can be kept minimum with improved directivity, so the antenna could be fit into limited space and produce a more unidirectional radiation pattern, and higher gain and front-to-back ratio [72][73].

In this design, the rest of the antenna is kept the same as the value presented in table 5.1. Fig. 4.43 shows the geometry of this improved design.
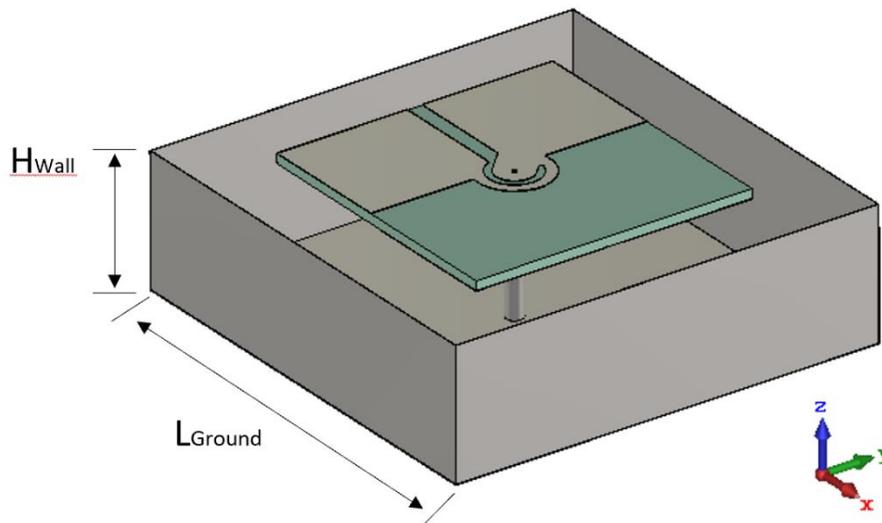
Fig. 4.43: The geometry of the CP Pseudo-ME dipole antenna with the metallic cavity

In this section, the influence of the cavity vertical wall (H_{Wall}) on the antenna performance will be studied. The L_{Ground} is set as 80 mm, which is about one free-space wavelength at the center frequency of the antenna.

Fig. 4.44 and Fig. 4.45 depict the influence of H_{Wall} on S_{11} and Z_{11}, respectively. Like the previous observation on the ground plane. With an 80 mm $\times$ 80 mm (λ_0^2) ground plane, the proposed antenna's impedance is affected slightly when compared to that of $L_{Ground} = 100$ mm, the impedance bandwidth remains wide.

While with a higher H_{Wall}, the part of the electric field travels relatively shorter distance and then been reflected by the vertical wall, so gain of the proposed antenna in the high-frequency band increased dramatically. Furthermore, since the cavity geometry did not change the antenna's four fundamental modes, so it can be observed that the two AR center frequencies do not shift as shown in Fig. 4.46.
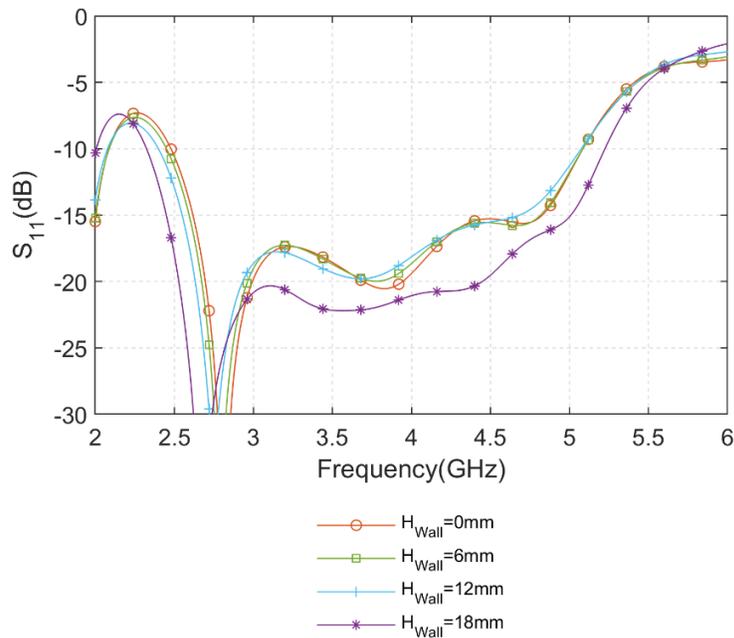
Fig. 4.44: Simulated S_{11} of the proposed antenna with different H_{Wall}
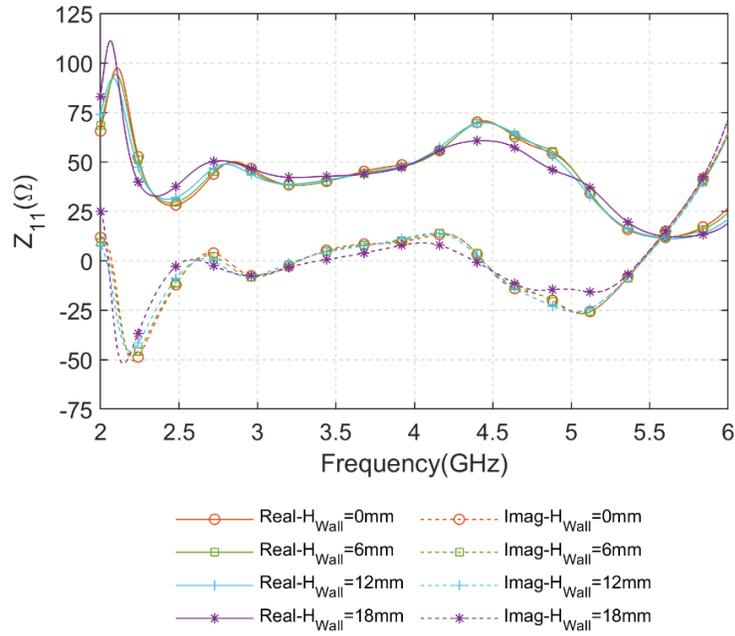
Fig. 4.45: Simulated Z_{11} of the proposed antenna with different H_{Wall}
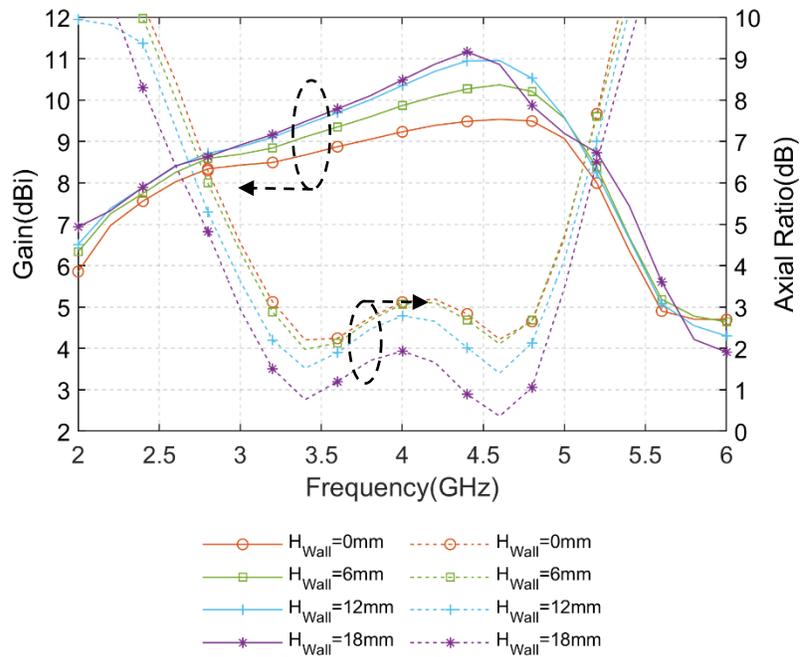
Fig. 4.46: Simulated gain and the axial ratio of the proposed antenna with different H_{Wall}

Fig. 4.47 to Fig. 4.50 shows the radiation pattern of the proposed CP Pseudo-ME dipole antenna with different H_{Wall} when $\phi=0°$, 45°, 90°, and 135°. Within the increase value of the H_{Wall}, the 3-dB beamwidth at each plane get narrower. It is obvious when $\phi=0°$ and 90° (the principal plane of the magnetic dipoles), which explains the gain increase more at high-frequency band.
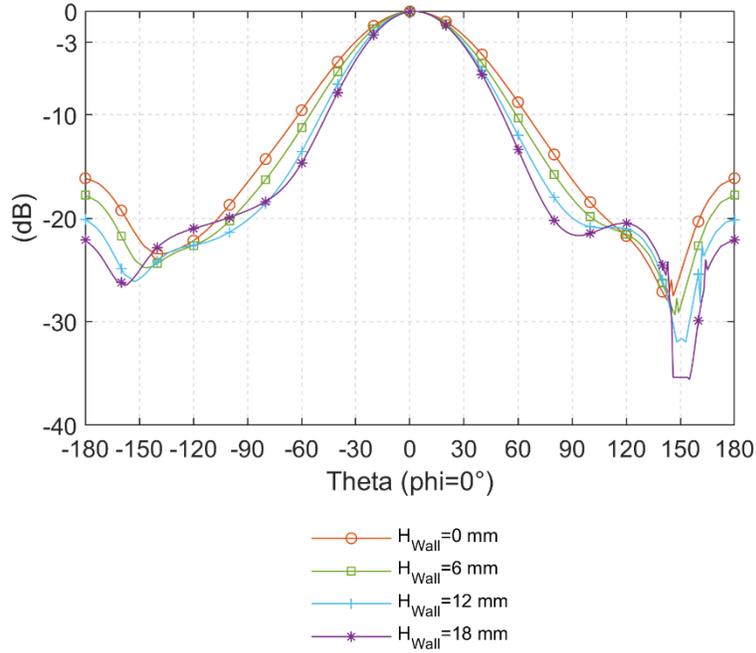
Fig. 4.47: Radiation pattern of the CP Pseudo-ME dipole antenna with different H_{Wall} when

$\phi=0°$

149
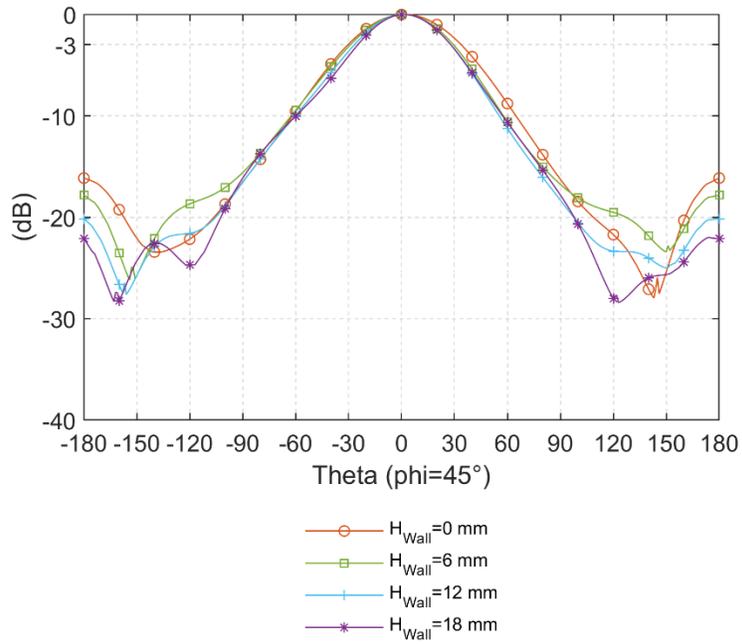
Fig. 4.48: Radiation pattern of the CP Pseudo-ME dipole antenna with different H_{Wall} when

ϕ=45°
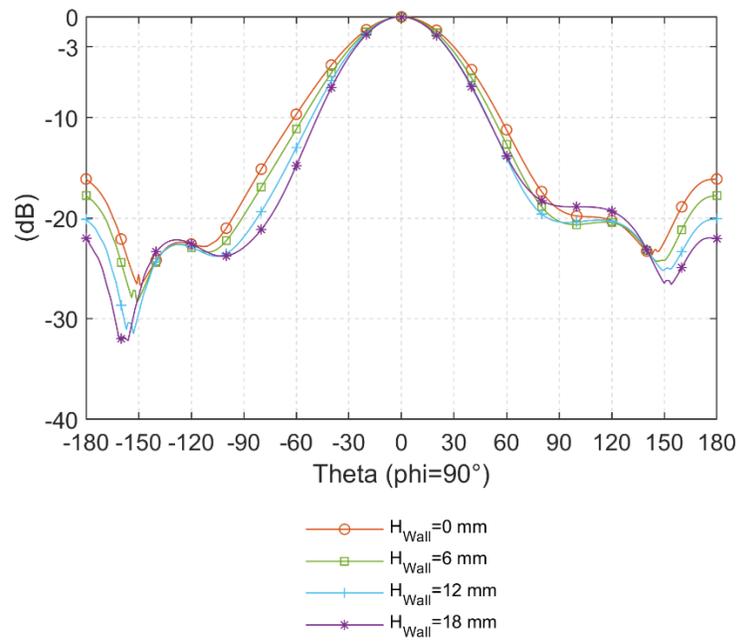
Fig. 4.49: Radiation pattern of the CP Pseudo-ME dipole antenna with different H_{Wall} when

$\phi=90°$
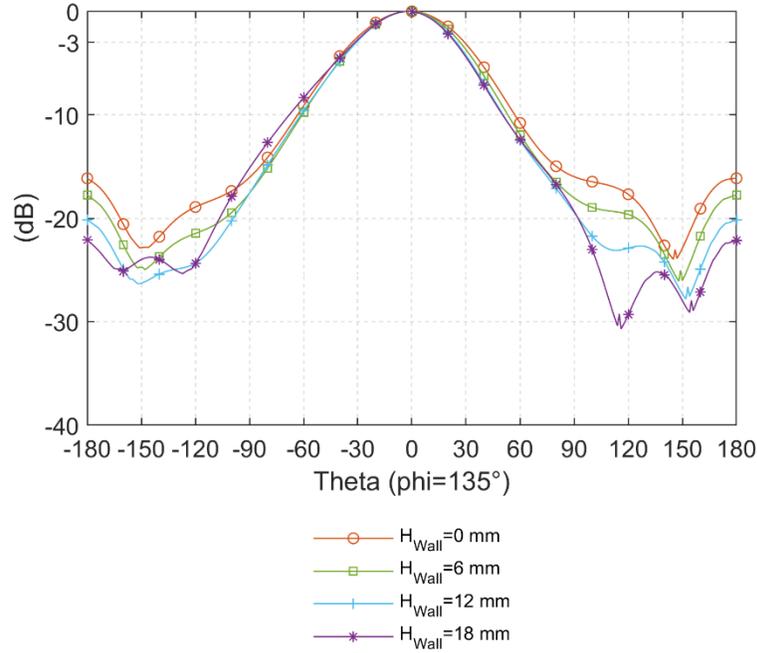
Fig. 4.50: Radiation pattern of the CP Pseudo-ME dipole antenna with different H_{Wall} when

$\phi=135°$

Fig. 4.51 shows the impedance, AR bandwidth and the average gain in-band increased with different H_{Wall}. Compared with a flat rectangular ground plane reflector, the cavity reflector design archives slightly wider bandwidth and higher average gain. Most importantly, it helps reduce the aperture size of the antenna which make it easier to fit into limited space.
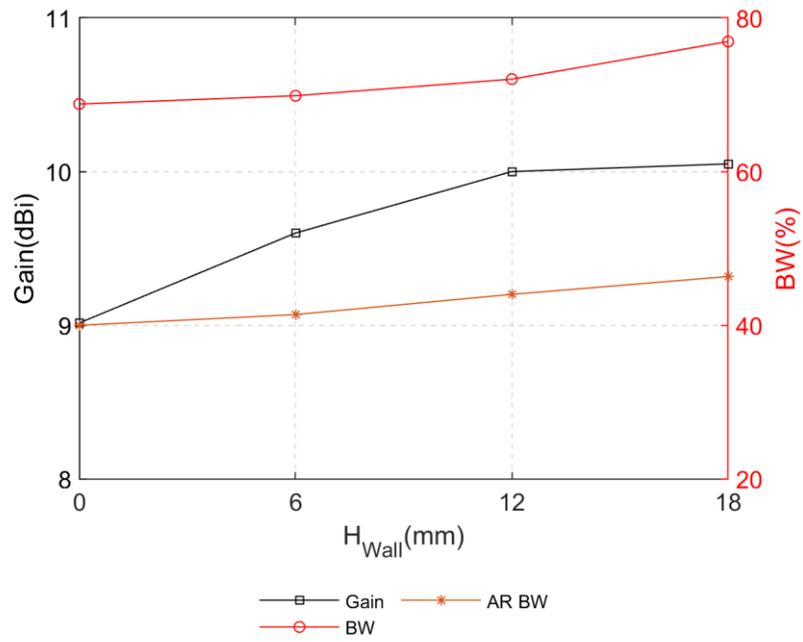
Fig. 4.51: Average gain, impedance bandwidth and axial ratio bandwidth with different H_{Wall}

4.7   Concluding remarks

In this chapter, a wideband circularly polarized pseudo magneto-electric dipole antenna has been presented. The proposed antenna has a wide impedance bandwidth of 69.8% from 2.46 GHz to 5.10 GHz, an average gain of 8.7 dBi and the variation in-band is only ± 0.9 dBi. Most importantly, with a λ_0^2 ground plane, the axial ratio bandwidth achieves 54.1% from 2.87 GHz to 5.00 GHz, which is around twice of the most of state-of art CP antenna. Moreover, Inheriting the advantages of the cavity-less pseudo-ME dipole antenna, the circularly polarized antenna also has simple geometry. In addition, a smaller size cavity geometry could be used as a reflector to replace the conventional flat ground plane for reducing the footprint of the antenna.

5.Millimeter-wave aperture-coupled magneto-electric dipole

The 5th Generation (5G) mobile network provides gigabytes of data per second in millimeter-wave bands. In millimeter wave band, it is easier to obtain wider spectrum for higher data rate. In the meantime, millimeter-wave antenna design and fabrication present the following challenges: (i). Gain: antennas with high-gain characteristics are critical to wireless applications in the millimeter-wave frequency bands, which could compensate for high free space path loss. (ii). Bandwidth: antennas with the wideband feature are also essential to cover the required wide operating bands. (iii). Geometry: the physical size of millimeter-wave antennas is usually small due to the short wavelength. Therefore, it is desirable to have simple antenna geometries to respond to the challenges in fabrication. (iv). Collaborative design [4], the large transmission line loss in high-frequency circuit cannot be ignored, therefore, the antenna and the chip should be located as close as possible. The antenna and the RF front-end should be integrated; solutions like antenna-on-chip (AoC) and antenna-in-package (AiP) are proposed to reduce signal loss under high-frequency [55][74][75].

According to the challenges mentioned above, several studies on Pseudo-ME dipole antenna in the millimeter-wave band have been demonstrated. A 60-GHz plated-through-hole printed Pseudo-ME dipole antenna with impedance bandwidth of 33% ($S_{11} < $ -15 dB) and stable gain of 7.5 dBi has been reported in [45]. Via holes, fabricated by using plated through-hole technology, are used to

construct a vertical cavity. An 18-element slotted leaky-wave antenna (LWA) array with electric dipoles was proposed [76]. By applying the Pseudo-ME dipole antenna concept with an electric dipole introduced to each slot of the LWA, the antenna array could operate at a wide impedance bandwidth, and the in-band gain variation has been suppressed from 5.9 dB to 3 dB.

These previously reported PCB-based millimeter-wave band ME dipoles usually require a quarter-wave vertical-cavity to generate the magnetic dipole mode. Moreover, the cavity structures in the millimeter-wave band are usually fabricated by a series of via holes [45]; these small size structures increase the fabrication difficulty and bring more uncertainty. The experience of designing the Pseudo-ME dipole without the quarter-wave cavity have been discussed in Chapters 4 and 5. Therefore, the cavity-less geometry has been further applied to the millimeter-wave band antenna present in this chapter.

5.1 Model A: coaxial-fed mmW Pseudo-ME dipole

To verify the feasibility of implementing the cavity-less geometry in the millimeter-wave band, Model A, a linearly polarized Pseudo-ME dipole antenna, has been designed by reducing the geometry proportionally to up-shift the operating frequency to the 5G millimeter-wave band between 22 GHz and 30.5 GHz.

5.1.1 Antenna geometry

Fig. 6.1 depicts the geometry of Model A, which is designed on a single-layer PCB like the antennas design in Chapter 4. Based on the accuracy of conventional photolithographic PCB fabrication techniques in the author's lab is about ± 0.05 mm, which is 5% of the free space wavelength at 30 GHz, furthermore, the frequency shift cause by the fabrication inaccuracy will be even more in dielectric substrate. this fabrication error cannot be ignored for a millimeter-wave band antenna. Therefore, a low dielectric constant substrate Rogers RT5880LZ ($\varepsilon_r = 2.0$, $\tan \delta = 0.0021$ @ 10 GHz) is chosen as the substrate, to reduce the frequency shift caused by fabrication error. it worth to mention that the low dielectric constant substrate is not compulsory; other materials, such as polystyrene foam board, could also be used depending on the fabrication accuracy.

On top of the antenna, there are two printed horizontal rectangular patches. On the bottom side of the antenna, an SMK coaxial connecter is used to feed the antenna. A short coaxial cable is inserted in-between the SMK connecter and the horizontal patches. The inner and outer conductors of the coaxial cable are connected to two patches, respectively. The inner conductor is connected with one horizontal patch directly.

Fig. 5.1: Geometry of Model A

5.1.2 Simulated results

Fig. 6.2 and 6.3 depict the gain, S_{11}, and the radiation patterns at E-plane and H-plane, respectively. In the first attempt, Model A has demonstrated the possibility of the proposed concept. Fig. 6.2 shows a wide impedance bandwidth ($S_{11} \leq$ -10 dB) of 10 GHz (32.7%) from 22 GHz to 32 GHz and a relatively high gain of 6.6 ± 1.6 dBi in the operating band.
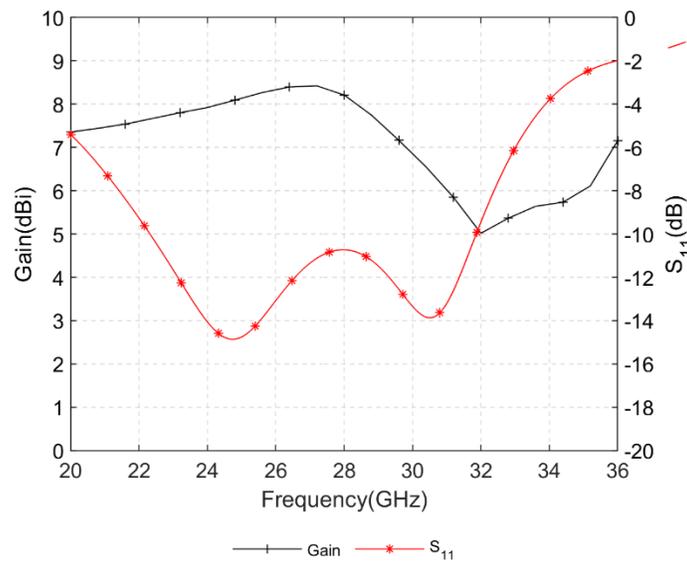
Fig. 5.2: Simulated gain and S_{11} of Model A
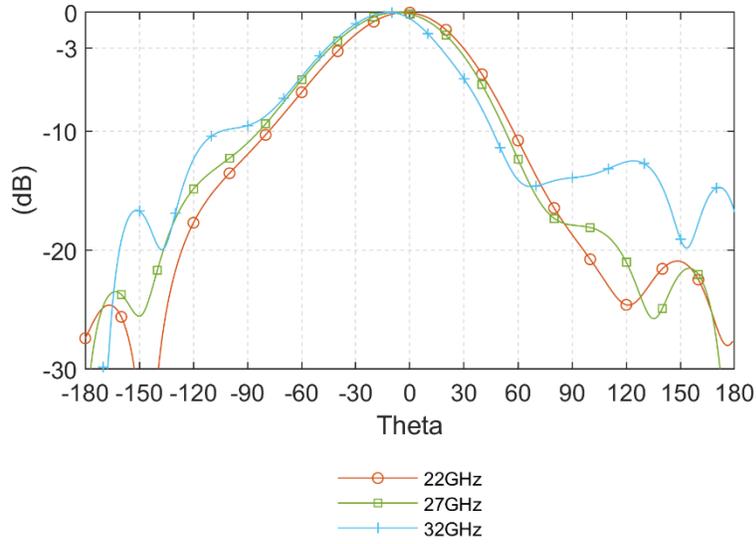
(a). E-plane radiation pattern
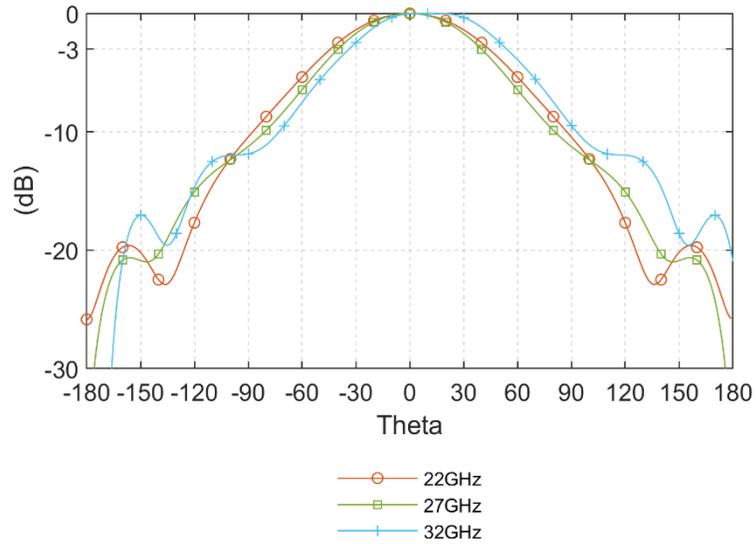
(b). H-plane radiation patterns

Fig. 5.3: Radiation patterns at center frequency 22 GHz, 26.3 GHz, and 30.6 GHz

Both the radiation patterns at E-plane and H-plane show the appropriate consistency in the low, center, and high-frequency bands. The front-to-back ratio is generally larger than 20 dB. Due to the coaxial connector feeding the two

horizontal patches in the x-axis, H-plane has more symmetrical patterns than the E-plane. Also, due to the size of the antenna is optimized at the center frequency (i.e., the length and width of the patch are around quarter and half wavelength at center frequency), the size of the antenna is relatively larger at high-frequency band, the side lobe of E- and H-plane at 32 GHz are slightly higher than low frequency.

Generally, the simulation achieved the expected results. The width of the gap between the horizontal patches is 0.5 mm. It is not easy to implement such a coaxial connection in the millimeter-wave pseudo-ME dipole antenna. In [45], A W-type connector (from Anritsu: W1-103F) used to connect a T-shaped coupled strip, a GSG transmission line structure is formed to feed the antenna. However, considering the fabrication complexity and the material cost, the aperture-coupled feeding method will be introduced to solve the feeding problem, and this design will be presented in the next section.

5.2   Model B: aperture-coupled mmW ME dipole

The aperture-coupled feeding method is another way to feed the patches (the electric dipole) and the gap between the patches (the magnetic dipole). As shown in Fig. 6.4, Model B is designed on two substrates with different materials using the aperture-coupled technique as the feeding method. Like Model A, there is no quarter-wave vertical-cavity serving as the magnetic dipole in this design. In contrast, the magnetic dipole is formed by the gap between the two horizontal patches. This design makes the geometry of the mmW Pseudo-ME dipole antenna simple to be fabricated. Simulated results show that the proposed Pseudo-ME dipole has impedance bandwidth ($S_{11} \leq$ -10 dB) of 33.6% from 22.8 GHz to 32 GHz and a stable high gain of 7.1 $\pm$ 1 dBi across the operating frequency band.

5.2.1 Antenna Geometry

The antenna geometry and detailed dimensions are presented in Fig. 6.4 and table 6.1, respectively. (It must mention that the guided electrical length of each parameter in the first row is calculated based on the Substrate 1 and the guided electrical length of each parameter in the second row is calculated based on the Substrate 2). The proposed antenna is designed on two pieces of the dielectric substrate with different materials. On the bottom layer (Substrate 1: Rogers TMM4, ε_r = 4.5, tanδ = 0.002 @ 10 GHz), the antenna was fed by a microstrip line through a slot aperture on the ground plane. The two copper patches served as the radiating elements are realized on the top layer (Substrate 2: Rogers RT5880LZ, ε_r = 2.0, tanδ = 0.0021 @ 10 GHz). The feeding layer is designed to be thinner (0.508 mm) and of a higher value of dielectric constant, the advantage of the two-layer design is: high dielectric constant and thin substrate help to reduce the amount of spurious radiation so that yield a better transmission efficiency in the feedline; in comparison, the upper radiating layer is thicker (1.27 mm) and with lower dielectric constant to achieve better radiation efficiency.
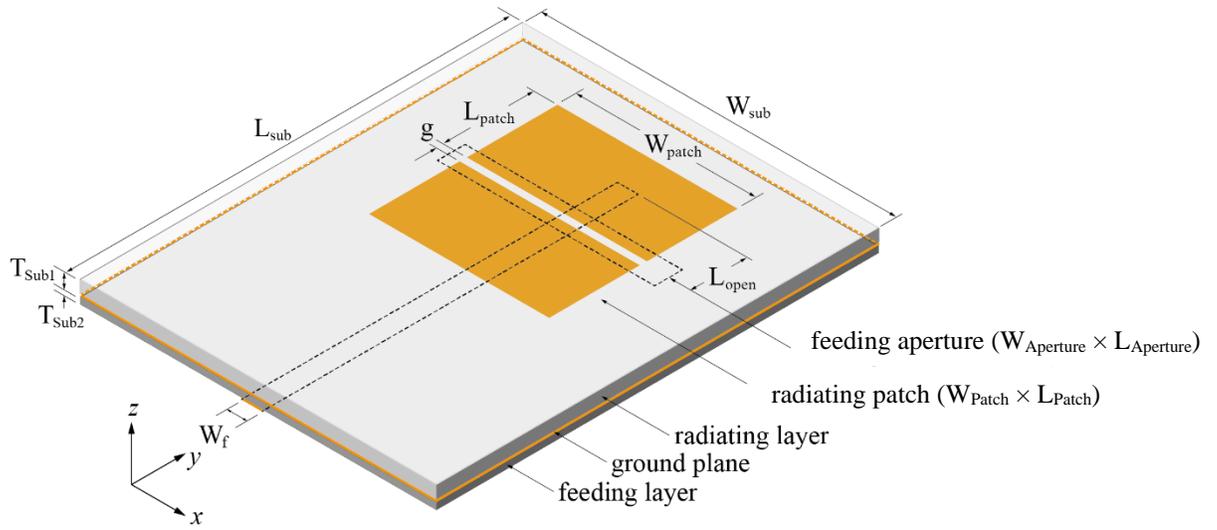
Fig. 5.4: The geometry of the aperture-coupled millimeter-wave Pseudo-ME dipole

antenna.

Table 5.1: Dimensions of Model B

Parameter	L_{Patch}	W_{Patch}	g	$W_{Aperture}$	$W_{Aperture}$	T_{Sub1}
Value (mm)	2.1(0.262λ_g)	4.1(0.513λ_g)	0.5(0.513λ_g)	6.5(0.813λ_g)	0.6(0.075λ_g)	0.508(0.064λ_g)
Parameter	L_{open}	W_f	L_{Sub}	W_{Sub}	T_{Sub2}	
Value (mm)	1.6(0.308λ_g)	1.2(0.231λ_g)	16(3.080λ_g)	10(1.923λ_g)	1.27(0.244λ_g)	

5.2.2 Operating principle

In the proposed Pseudo-ME dipole antenna, the two horizontal patches, in the y-axis direction, form a wide electric dipole antenna. In comparison, the narrow gap between the two patches forms a magnetic dipole antenna in the x-direction. Meanwhile, the separation between radiating elements and the ground plane is 1.27 mm (0.244 λ_g at the center frequency). The ground plane reflects the signal and increases the gain and front-to-back ratio of the proposed antenna.

In contrast to the previously reported high frequency planar Pseudo-ME dipole antennas [34][45], which require an array of via-hole to create the specific cavity to excite the magnetic dipole mode, a much simple design, which can be easily fabricated, is proposed in this design. The magnetic dipole mode of the proposed antenna, in the form of open-end slot between two horizontal patches, is activated through the aperture on the ground plane of the bottom layer. The antenna has a comparable wide impedance bandwidth and stable high gain.

Fig. 5.5 shows the electric field distribution of the proposed antenna at different times in period T, explaining how the magnetic dipole and the electric dipole cooperatively radiate. As shown in Fig. 5.5 (a) and (b), when t = 0 or T/2, the electric field has the most substantial distribution along the gap between the two horizontal patches. Hence, the magnetic dipole is excited at these moments. While t = T/4 or 3T/4 as shown in (c) and (d), the electric field has significant distribution at the end of the horizontal patches. Therefore, the electric dipole is operating.

(a)

(c)

(b)

(d)
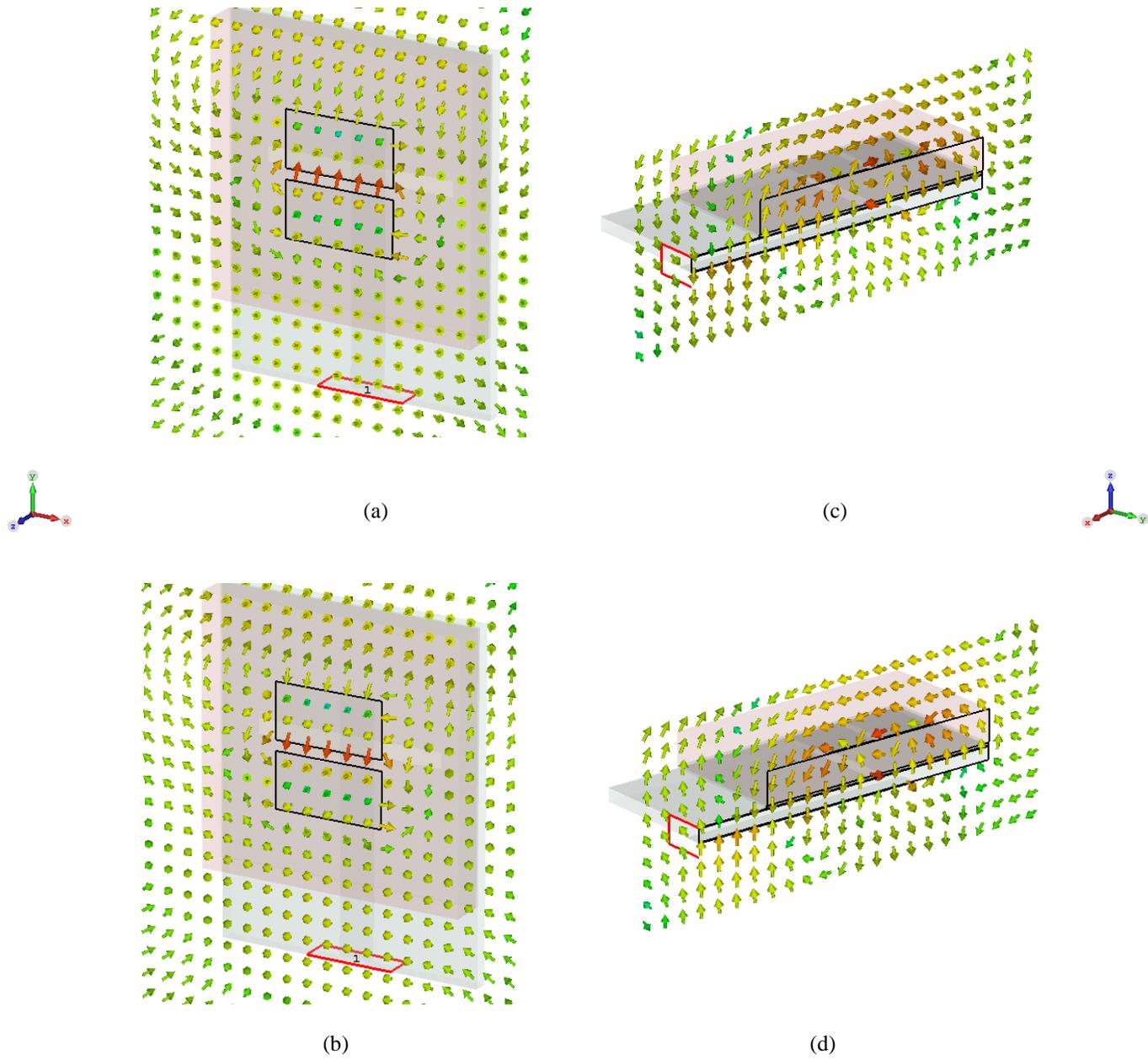
Fig. 5.5: E-field of the proposed antenna at center frequency 27.2 GHz (a) t = 0; (b) t = T/2 in xy plane;

(c) t = T/4, (d) t = 3T/4 in yz-plane

5.2.3 Prototype fabrication

There are two main challenges of fabrication Model B: (i). The accuracy of the PCB fabrication equipment in UCL is around 0.1 mm. The discrepancy will cause a considerable effect on the antenna operating at the millimeter-wave band. (ii). The Pseudo-ME dipole antenna Model B consists of two PCB layers; the accurate alignment of the two-layer PCB is another challenge.

To respond to the first challenge mentioned above. Nine antennas of slightly different dimensions have been fabricated, aligned, glued, the width of the gapand cut. Fig. 5.6 (a) & (b) have shown the antenna prototype. As shown in Fig. 6.6 (a), since antenna transmission layer and radiating layer are on two separated PCB, extra markers (triangle shape with a via hole placed at the corner) are introduced to increase the alignment accuracy to respond to the alignment challenge.

(a)   (b)
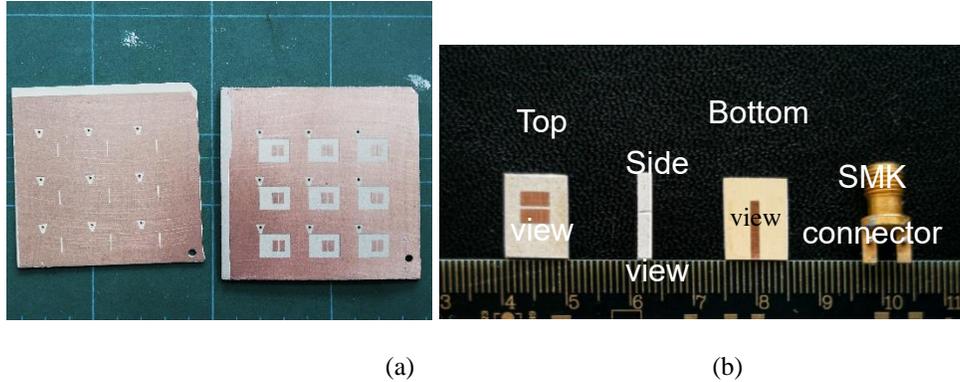
Fig. 5.6: (a) The bottom layer and the top layer of the prototype, (b) the prototype.

However, the performance of this prototype does not match well with the simulation in the first integration. Fig. 5.6 (b) shows that the SMK connecter is too close to the patches. In this case, the radiation pattern of the antenna will be significantly affected. To minimize the impact on the radiation pattern, the transmission line is extended to avoid the interference from the connector.

Another way is to use microstrip-gap-waveguide feeding method to concentrate the signal in the desired transmission area [77][78].

In the second iteration, some changes have been made in fabrication to achieve better measurement results: (i). replace the 10×10 mm^2 bottom substrates with a larger 16×10 mm^2 substrate. In this case, the length of the microstrip line has been extended to about 1 λ_g, so there is more separation between radiating patches and the SMK connector. (ii). the bottom transmission line layer was fabricated first to compare and confirm its performance with the simulated result. And then, stick the top layer and measure the assembled mmW Pseudo-ME dipole antenna.
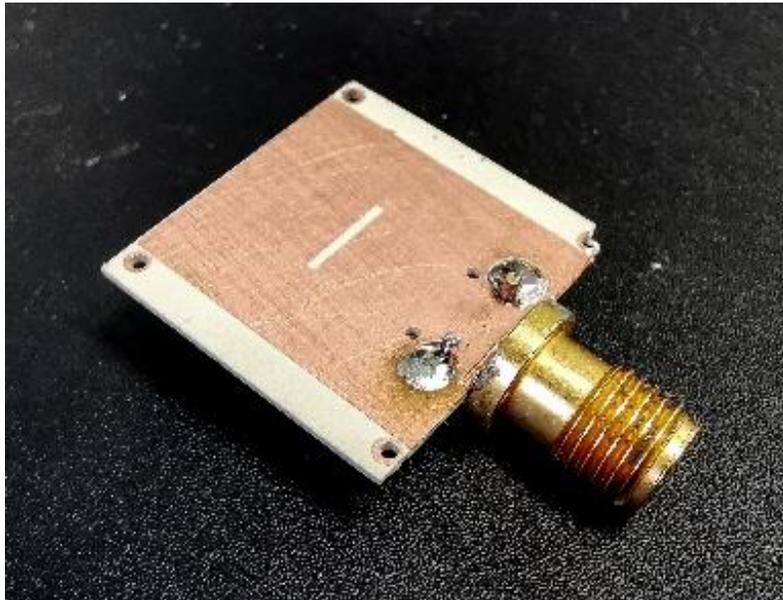
Fig. 5.7: The bottom layer of the millimeter-wave Pseudo-ME dipole (second attempt)
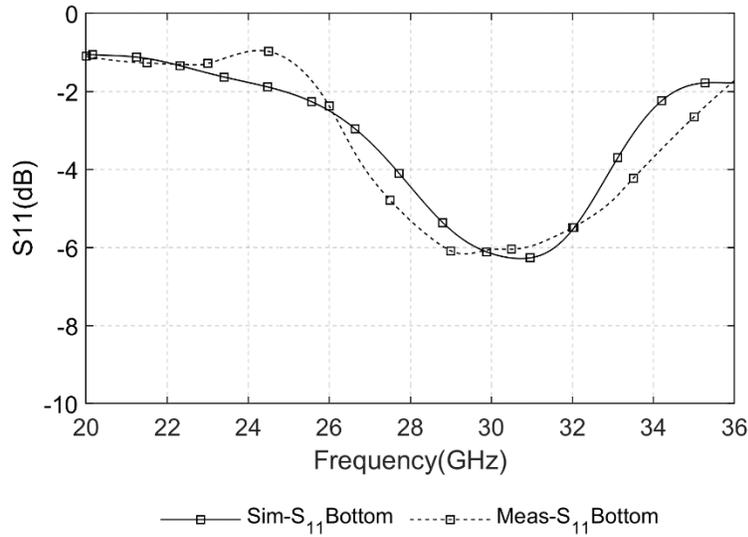
Fig. 5.8: Comparison of measured and simulated S_{11} of the bottom layer millimeter-wave

Pseudo-ME dipole

Fig. 5.7 shows the bottom layer of the fabricated antenna. The SMK connecter is soldered with it robustly. Fig. 5.8 depicts the comparison between simulated and measured results of S_{11} of the bottom layer of the Model B. The measured result shows a lower S_{11} at high frequency band, shows a similar trend as the simulated results.

As a popular feeding technique, the aperture coupled feeding method has been widely used for feeding patch antenna for extending bandwidth [79]–[81]. The real part and the imaginary part of the bottom layer are shown in Fig. 5.9 for analysis and verify whether the aperture contributes to the antenna gain performance. The Z_{11} profile shows the aperture has two modes in the interested frequency band, one is at 26.6 GHz, and another is at 31 GHz. In an aperture-coupled feed antenna, a common way to control the coupling is by adjusting the size of the aperture [81]. However, since the aperture in the antenna also contributes to the gain in center and high-frequency band (as shown in Fig. 5.10), its size could not be adjusted independently. In this research, the aperture on the ground plane (slot) is set slightly larger than the open-end slot on the radiating

layer for transferring the signal as much as it can. More details about study of the slot size will discussed in the parametric study section later.
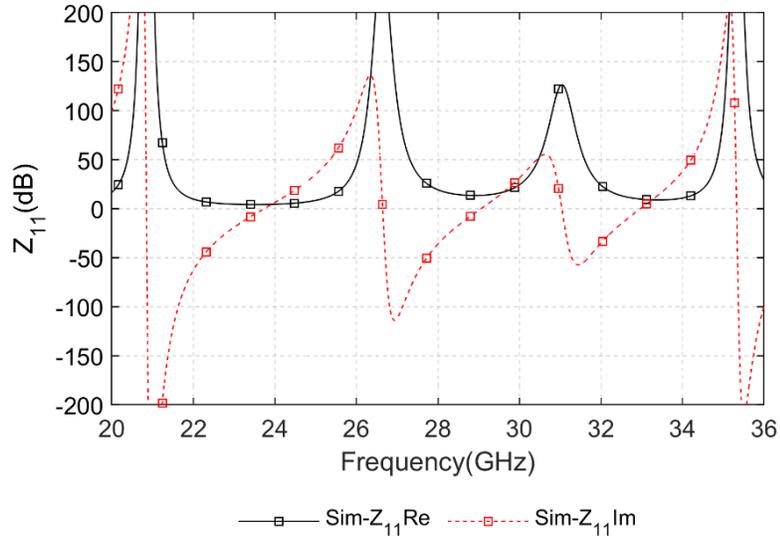
Fig. 5.9: Simulated Z_{11} of the bottom layer millimeter-wave Pseudo-ME dipole
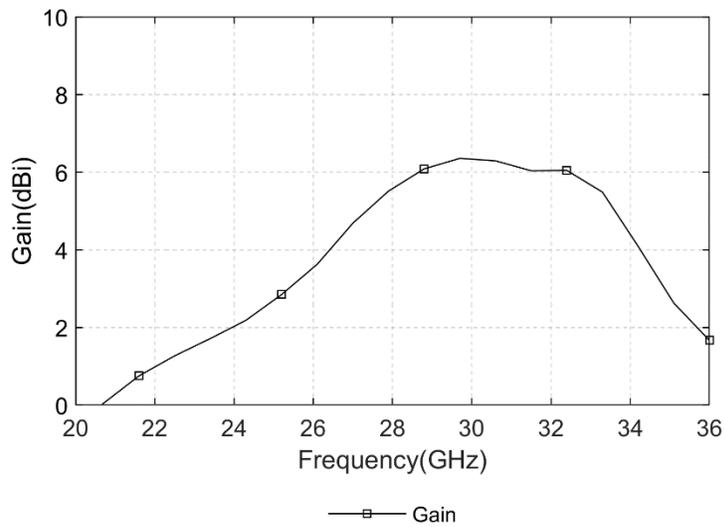
Fig. 5.10: Simulated gain of the transmitting layer

5.2.4 Parametric Study

A series of parametric studies will be discussed in this section to understand the proposed antenna operation principles further. The bottom layer is responsible for feeding the signal to the radiating elements, the width of the microstrip transmission line, W_f, is fixed at 1.2 mm to guarantee the input impedance at the port is 50 Ω, so W_f will not be studied. The two horizontal patches on the top of the substrate play a key role in generating the stable high gain beam over the frequency. So, the width (W_{Patch}), the length (L_{Patch}) of the patch, and the gap between them (g) are studied first. After that, the size of the feed aperture ($W_{Aperture}$ and $L_{Aperture}$ will be discussed). Finally, the length of the open end of the microstrip feed line from the center of feed aperture (L_{Open}) is investigated since the L_{Open} significantly affects the impedance matching. The rest of the parameters remain the value in table 6.2 when each parameter is investigated.

5.2.4.1 W_{Patch}

W_{Patch} represents the width of the patch, and it is also the parameter that determines the resonant frequency of magnetic dipole mode. Fig. 5.11 shows the influence of W_{Patch} on gain and S_{11} of the proposed antenna. By slightly tuning W_{Patch} down, the 1-dB gain bandwidth extends towards high frequency. S_{11} has followed accordingly. The impedance bandwidth of $S_{11} < $ -10 dB has also extended towards the higher frequency.

Fig. 5.12 depicts the real part and imaginary part of the impedance of the proposed antenna. Like the design in Chapter 4, it can be observed that the second and the third mode of the antenna are sensitive to magnetic dipole mode which determined by W_{Patch}. The third mode shifts to a higher frequency with a shorter W_{Patch}. The first and second modes impedance is also changed, but the resonant frequency does not change a lot. The Z_{11} profile concludes the magnetic dipole is mainly operating at the high-frequency band.
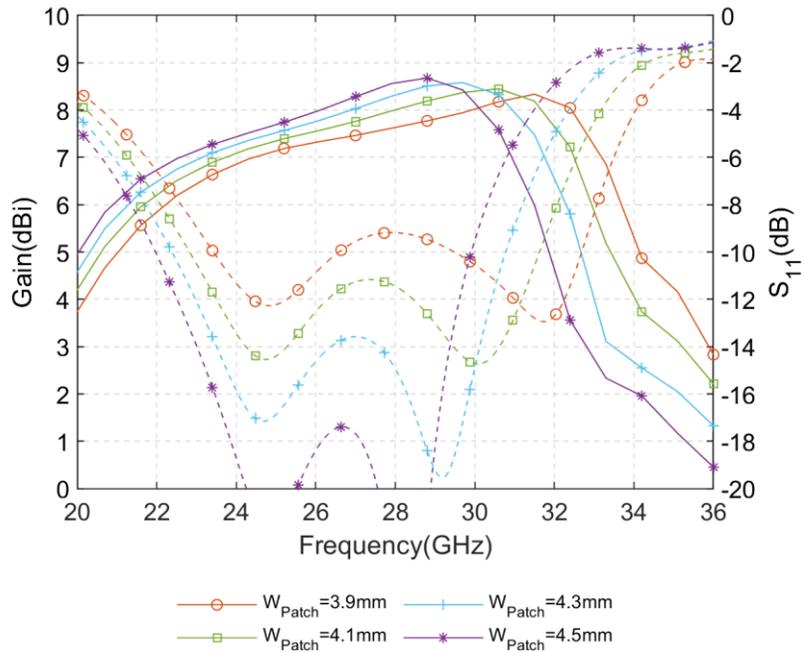
Fig. 5.11: Simulated S_{11} and gain of the mmW Pseudo-ME dipole antenna with different W_{Patch}
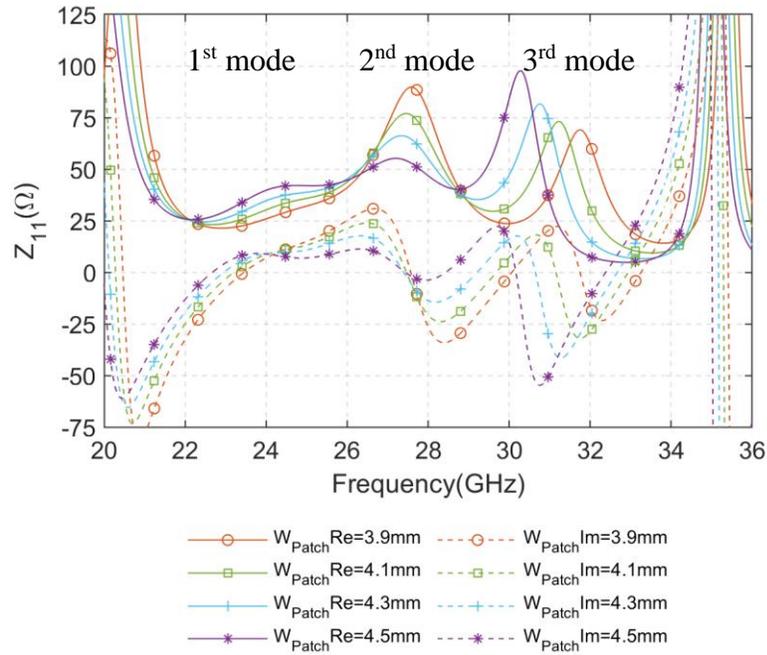
Fig. 5.12: Simulated Z_{11} of the mmW Pseudo-ME dipole antenna with different W_{Patch}

170

5.2.4.2 L_{Patch}

L_{Patch} represents the length of the horizontal patches, which is the parameter that controls the resonant frequency of the electric dipole mode. Fig. 6.17 shows the influence of L_{Patch} on the gain and S_{11} and gain. Relatively longer L_{Patch} shifts the operating band to lower frequency and slightly increases the gain in the low-frequency band integrally.

Fig. 6.18 shows that the resonant frequency of the first mode changes with different L_{Patch}. The frequency of the second and third modes remain similar, but the impedance of them changed the antenna significantly, which could also explain the worse impedance match in the S_{11} profile with a longer L_{Patch}.

According to the parametric study so far, the operating frequency and impedance bandwidth could be achieved by tuning the values of W_{Patch} and L_{Patch}. Generally, W_{Patch} determines the higher end of the impedance bandwidth while L_{Patch} determines the lower end. W_{Patch} and L_{Patch} value need to be set properly to make the proposed antenna wide bandwidth and stable high gain over the frequency.

For wide impedance bandwidth, the rules should be followed when setting L_{Patch} and W_{Patch}: the resonant frequencies of the electric dipole mode and the magnetic dipole mode are supposed to be properly separate. When these two frequencies are too close, a good impedance match S_{11} smaller than -20 dB or even -30dB will be achieved in the band, but the bandwidth will be sacrificed. When these two frequencies are too far, the impedance bandwidth will be divided into two separate bands.
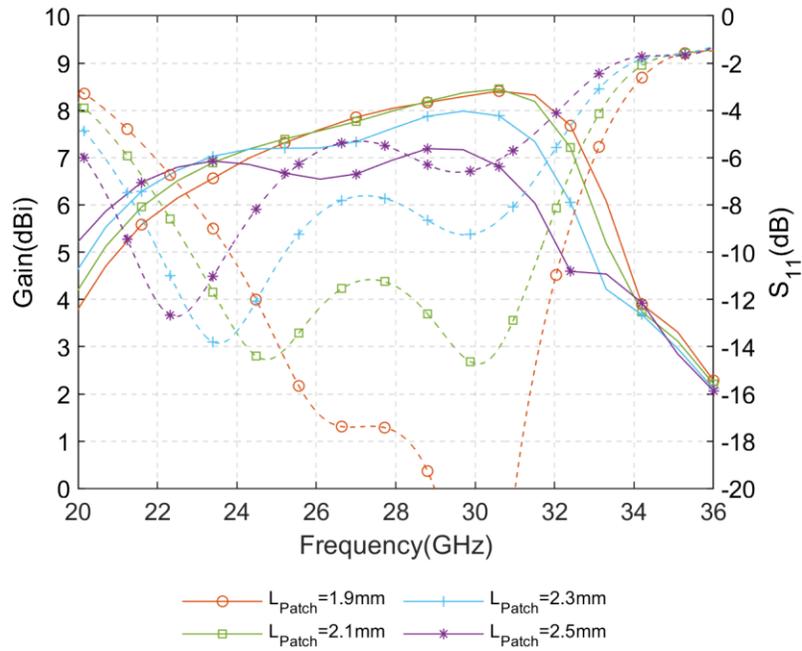
Fig. 5.13: Simulated S_{11} and gain of the mmW Pseudo-ME dipole antenna with different L_{Patch}
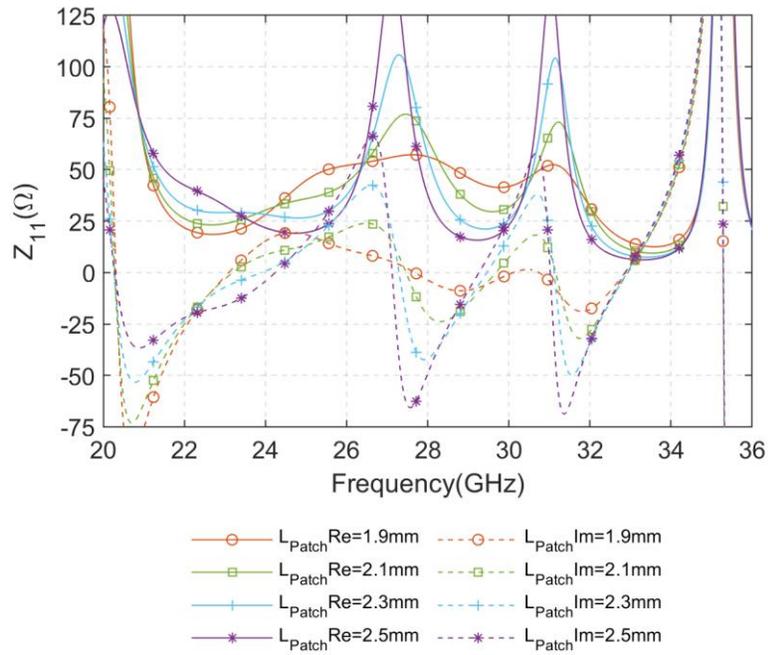
Fig. 5.14: Simulated Z_{11} of the proposed mmW Pseudo-ME dipole antenna with different L_{Patch}

172

5.2.4.3   g

The gap, g, represents the separation between the two horizontal patches. Fig. 6.19 shows the gain and S_{11} profiles with different g. From the S_{11} profile, it can be observed that the low-frequency band of the proposed antenna gets narrower significantly with an increased g. On the other hand, the gain remains steady at the higher frequency band while slightly increases in the lower frequency band, as the impedance bandwidth drops with a relatively narrower gap. This observation could be explained from the Z_{11} profile.

Fig. 6.20 shows the Z_{11} with different g. Relative narrower g makes the first mode pop up into the Z_{11} profile, making the electric dipole operating at the low-frequency band. In contrast, when g is larger than 0.5 mm ($W_{Aperture}$ is 0.6 mm), or in other words, when g is larger than $W_{Aperture}$, the electric dipole cannot resonant properly anymore. Therefore, the impedance bandwidth gets narrow and the gain drops in the low-frequency band.
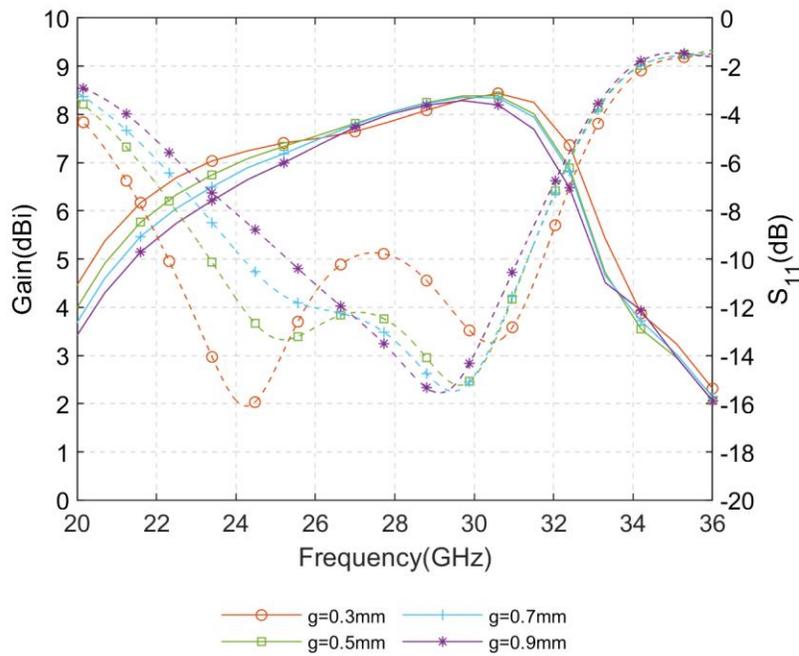
Fig. 5.15: Simulated S_{11} and gain of the proposed mmW Pseudo-ME dipole antenna with
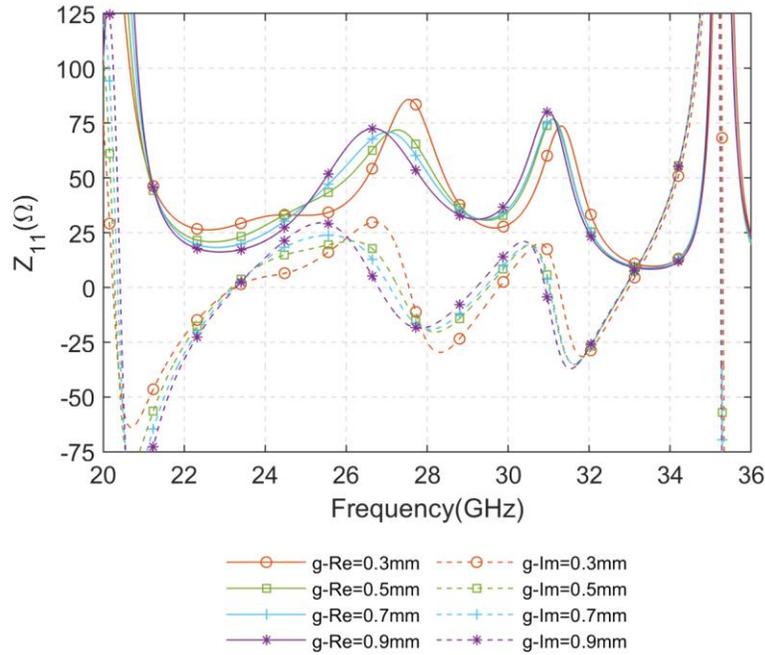
different g

Fig. 5.16: Simulated Z_{11} of the proposed mmW Pseudo-ME dipole antenna with different g

In the previous sections, parameters related to the radiating layer have been studied. In the rest part of the parametric studies, parameters related to the feed layer will be discussed.

5.2.4.4 $L_{Aperture}$

The bottom layer is in charge of feeding the signal from the input port of the antenna to the radiating layer. The microstrip transmission line width is set as 1.2 mm for a line impedance of around 50 Ω. Fig. 6.21 and Fig. 6.22 depict the S_{11}, gain and Z_{11} with different length of the aperture, $L_{Aperture}$. Generally, all three modes of the antenna are sensitive to this parameter, and the changed impedance results in a huge difference in impedance bandwidth. Narrow $L_{Aperture}$ brings a complete impedance mismatch with gain decrease, while wide $L_{Aperture}$

separates the resonance into two bands. According to the S_{11} and Z_{11} profiles, also the parametric study of g, the $L_{Aperture}$ is better to set slightly wider than g.
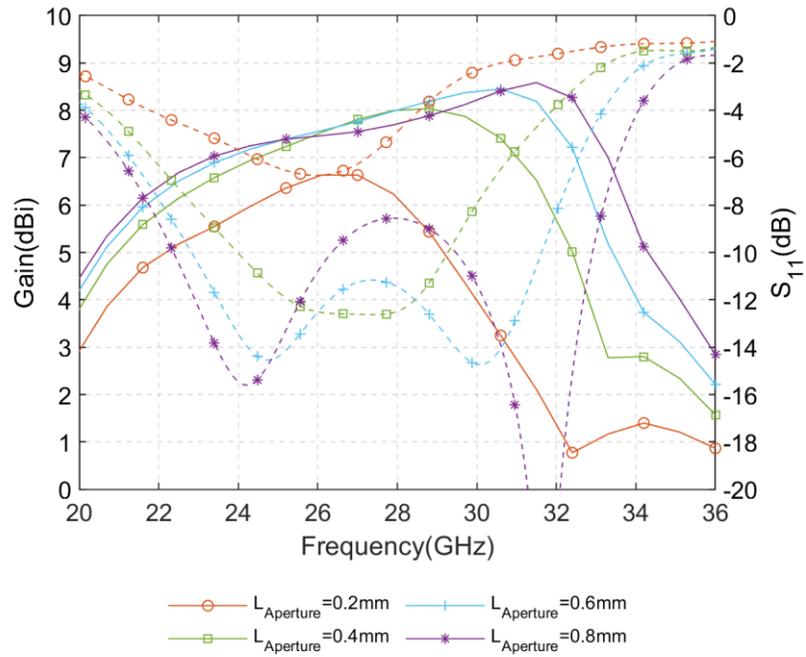

Fig. 5.17: Simulated S_{11} and gain of the mmW Pseudo-ME dipole antenna with different
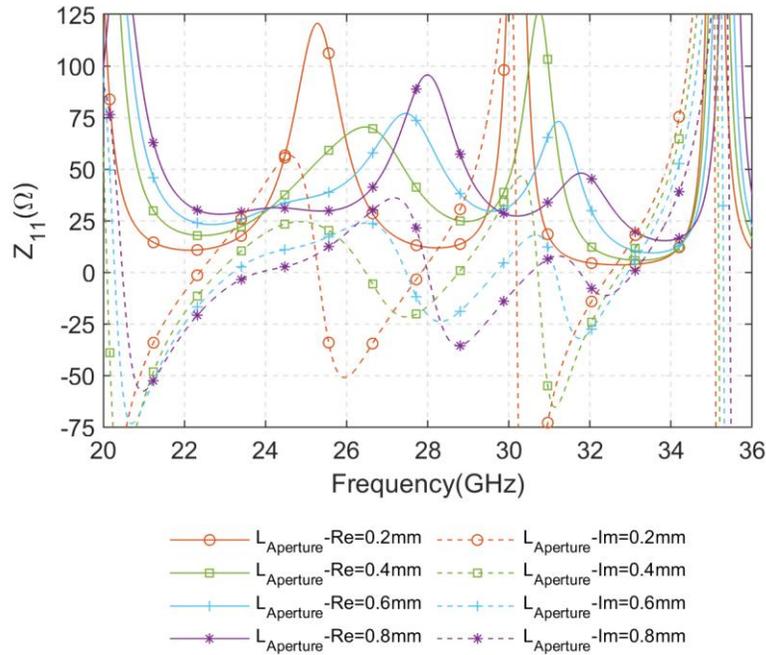
$L_{Aperture}$

Fig. 5.18: Simulated Z_{11} of the proposed mmW Pseudo-ME dipole antenna with different

$L_{Aperture}$

Since the aperture on the ground plane also radiates (in high-frequency band, reference to Fig. 6.9 and Fig. 6.10), the aperture size could be a significant parameter related to the back-lobe level of the antenna. Thus, for $L_{Aperture}$ and $W_{Aperture}$, the radiation patterns are also given for analysis.

Fig. 6.23 to 6.25 show the radiation pattern with different $L_{Aperture}$ at the low (228.GHz) center (27.2 GHz) and high (31.6 GHz) frequency points. The results demonstrate that the length of the aperture affects the radiation at the high-frequency band more significantly at the center and low frequency (which is also a shred of evidence that the aperture on the ground plane is a part of radiating elements). Narrow $L_{Aperture}$ increases the back lobe level in a high-frequency band.
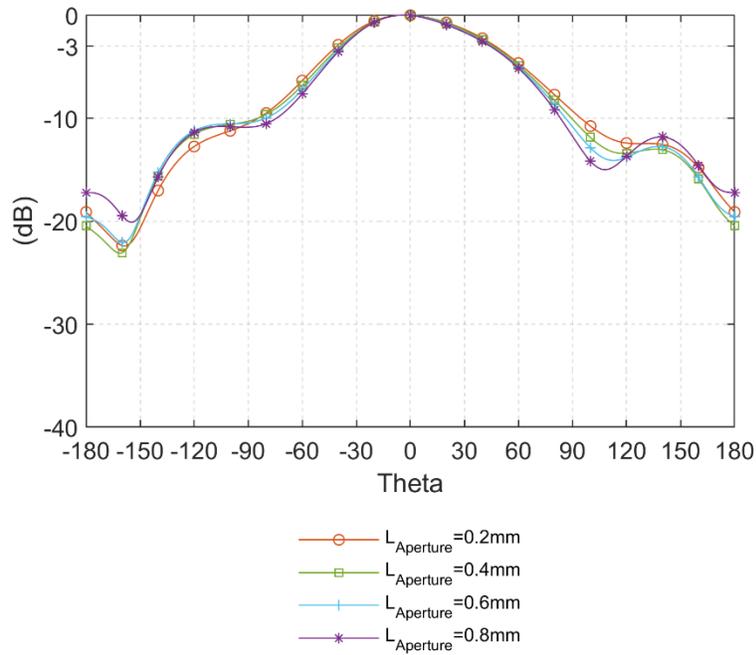
Fig. 5.19: E-plane radiation pattern at 27.5 GHz with different L$_{Aperture}$
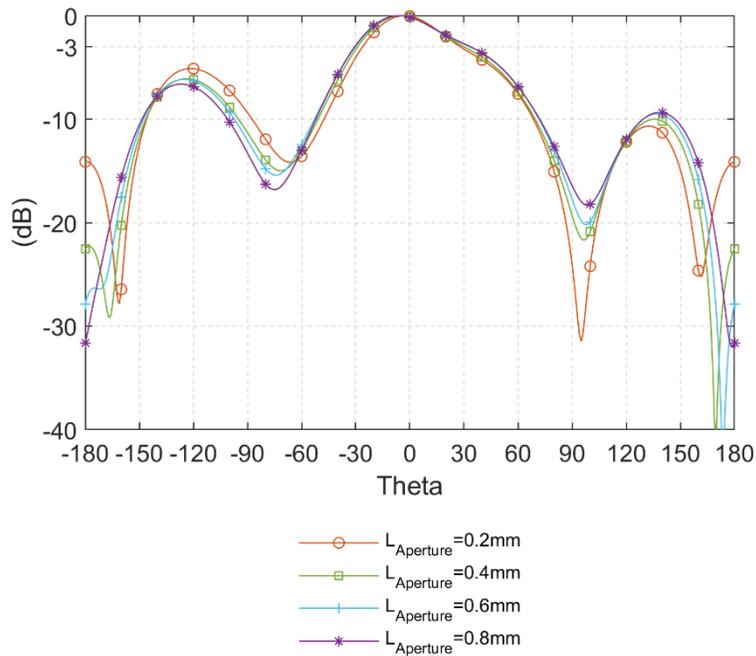
Fig. 5.20: E-plane radiation pattern at 27.5 GHz with different $L_{Aperture}$
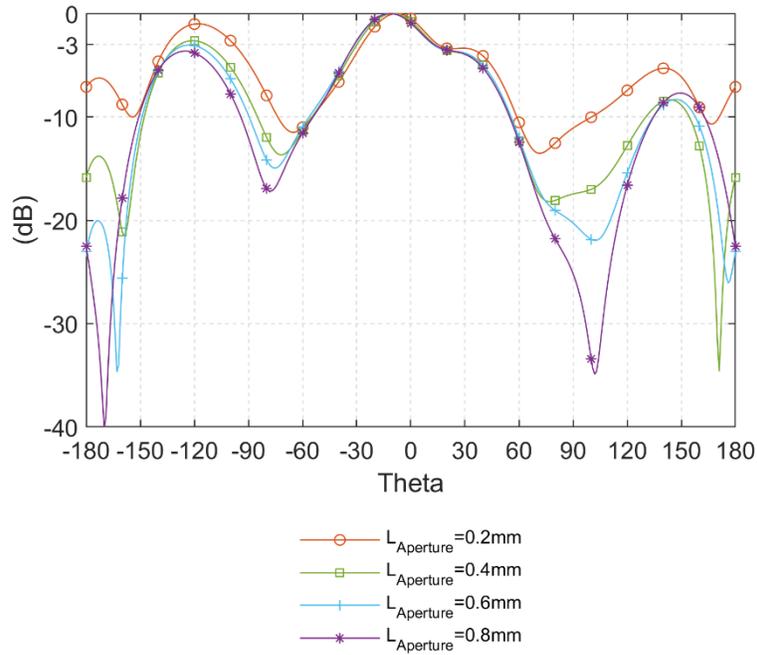
Fig. 5.21: E-plane radiation pattern of at 31.5 GHz with different $L_{Aperture}$

5.2.4.5 $W_{Aperture}$

Since the aperture radiate, the length of the aperture decides the resonant frequency of it. It can be observed from Fig. 6.26; longer $W_{Aperture}$ affects the second and the third modes of the antenna and moves them to lower frequency. $W_{Aperture}$ is finally optimized for the best impedance match at 6.1 mm (2 mm longer than W_{Patch}) for the widest impedance bandwidth and stable high gain at desired frequency band.
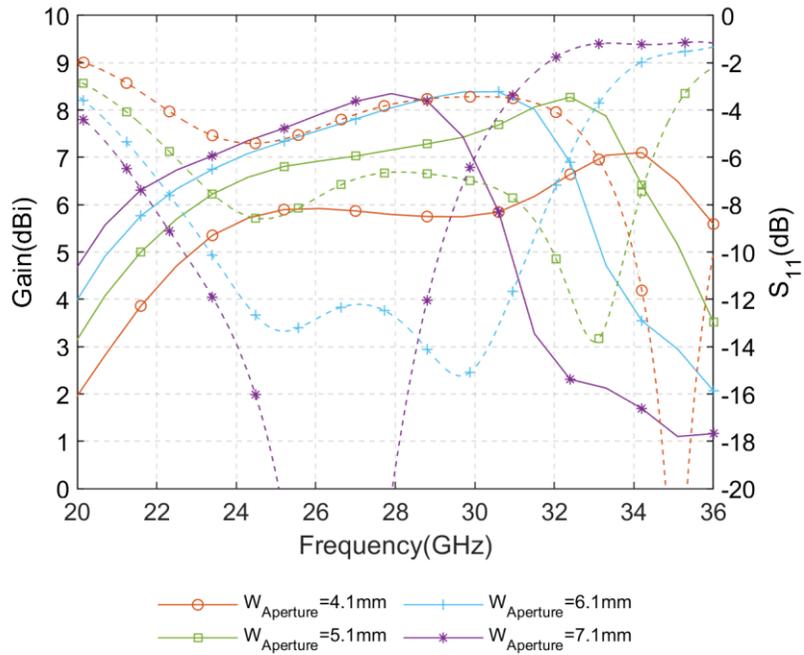
Fig. 5.22: Simulated S_{11} and gain of the mmW Pseudo-ME dipole antenna with different $W_{Aperture}$
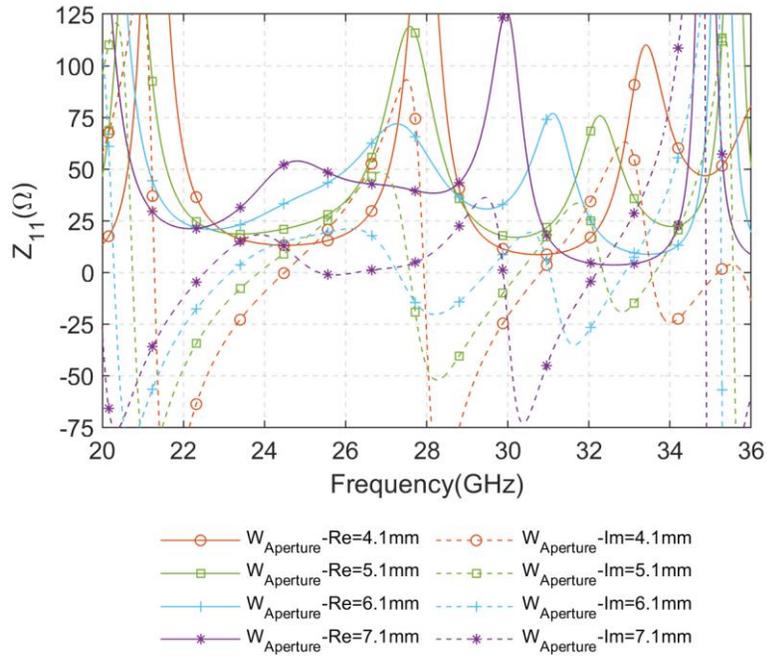
Fig. 5.23: Simulated Z_{11} of the proposed mmW Pseudo-ME dipole antenna with different

$W_{Aperture}$

More importantly, from the radiation patterns Fig. 6.28 to 6.30 below, the back lobe level increase with $W_{Aperture}$. This influence is moderate in the center frequency band, while in the high-frequency band, the increased back lobe level result from longer $W_{Aperture}$ cannot be ignored. Considering impedance bandwidth and back lobe level, an aperture of 0.6×6.1 mm^2 is decided as the finally optimized size.
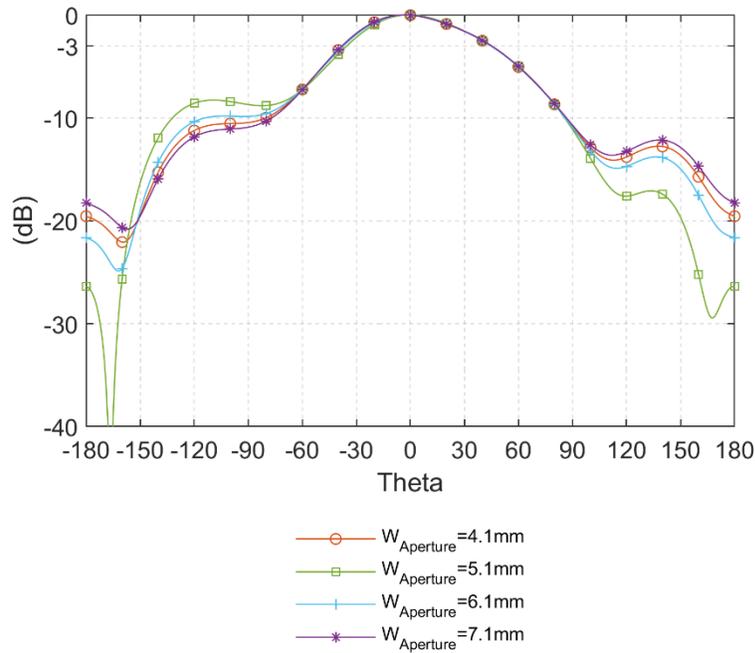
Fig. 5.24: E-plane radiation pattern of at 22.8 GHz with different $W_{Aperture}$
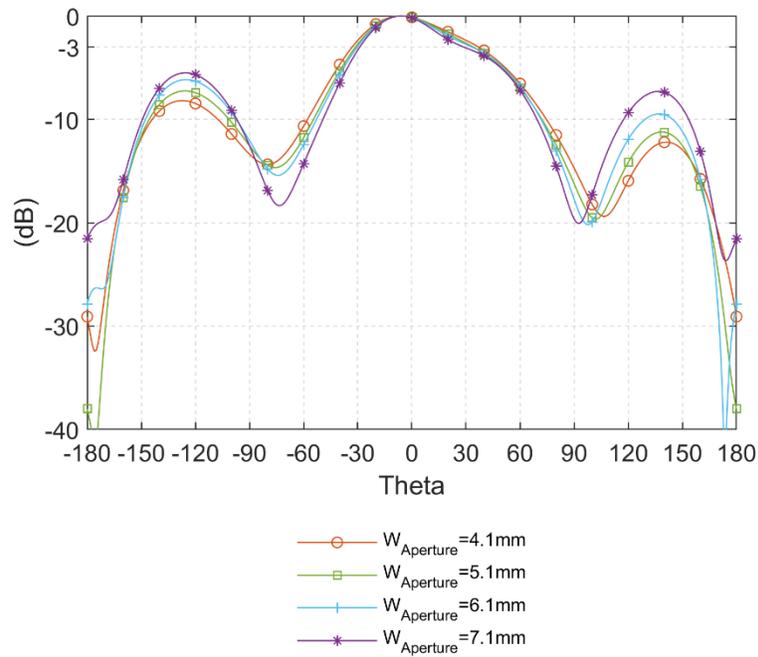
Fig. 5.25: E-plane radiation pattern of at 27.5 GHz with different $W_{Aperture}$
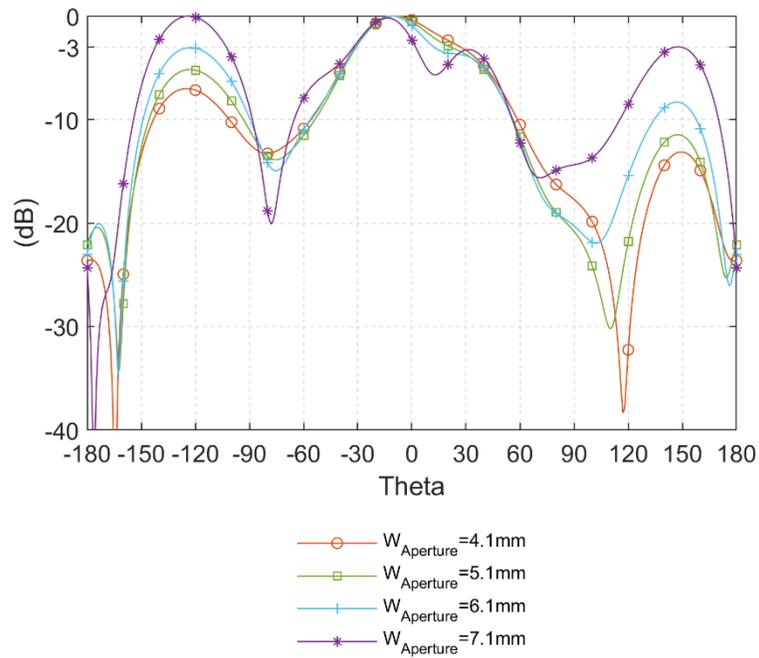
Fig. 5.26: E-plane radiation pattern of at 31.5 GHz with different $W_{Aperture}$

181

5.2.4.6 L_{Open}

L_{Open} represents the dimension between the middle of the aperture to the open-end of the microstrip line. Theoretically, L_{Open} is supposed to around a quarter-guided wavelength at center-frequency to achieve a balanced impedance match in the whole impedance band. Fig. 5.27 shows the influence of the L_{Open} on gain and S_{11} over the frequency band. For L_{Open} changing from 1.2 mm to 1.8 mm (0.22 λ_g to 0.33 λ_g in the Substrate 2), the antenna impedance matching is affected significantly. When L_{Open} equal to 1.6 mm (0.29 λ_g), the proposed antenna has the widest impedance bandwidth. The gain remains high and stable over the frequency band as the impedance matching well.
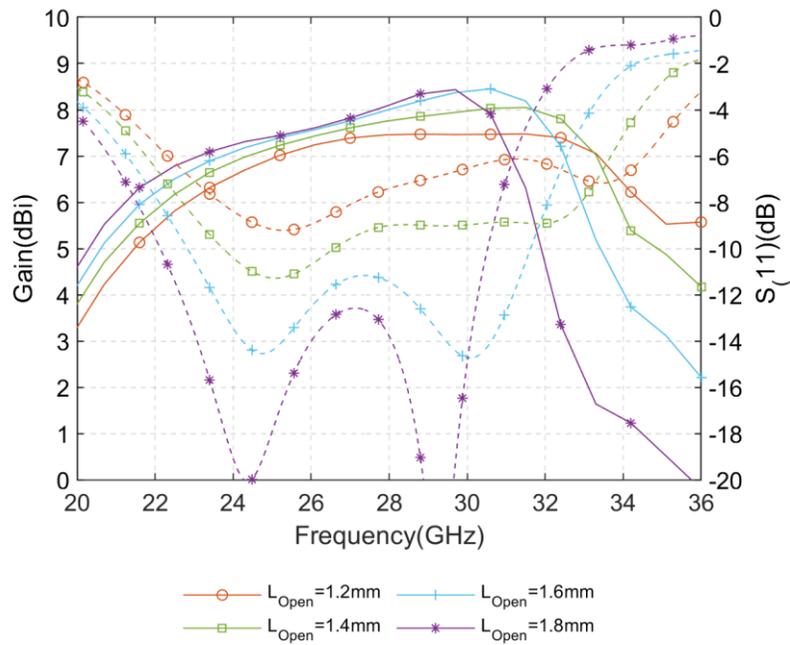

Fig. 5.27: Simulated S_{11} and gain of the mmW Pseudo-ME dipole antenna with different L_{Open}
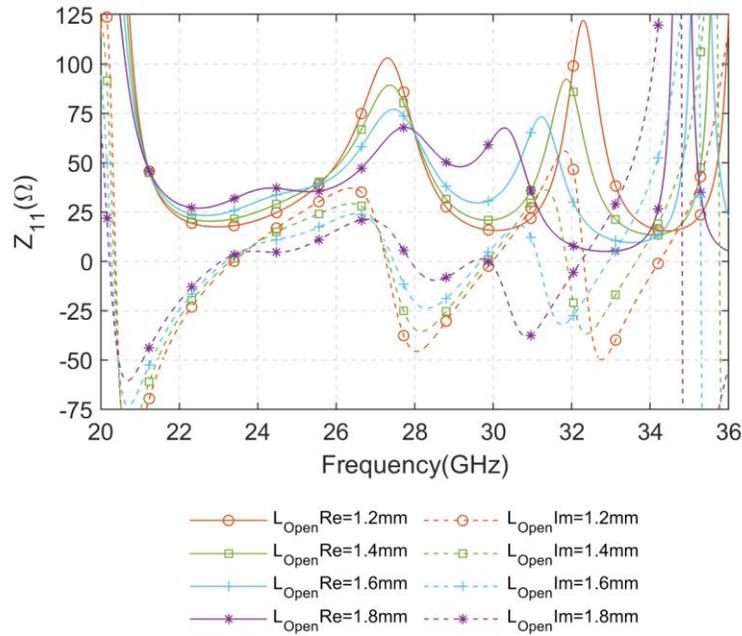
Fig. 5.28: Simulated Z_{11} of the mmW Pseudo-ME dipole antenna with different L_{Open}

5.2.5 Parametric study summary

Six significant parameters have been studied in the last section. To ensure the antenna operating at the desired frequency with wide bandwidth and high gain. Firstly, W_{Patch}, L_{Patch}, and g should be set since they are the parameters to control the two horizontal patches, which providing the antenna two main resonances. Secondly, the slot in the ground plane should be kept slightly larger than the gap between the two horizontal patches to ensure the feeding layer signal could be passed to the radiating layer efficiently. Thirdly, the open end of the microstrip line L_{Open} should be set around a quarter-guided-wavelength at the center frequency to achieve good impedance matching.

Figures of the gain and impedance bandwidth with different values of each parameter are given for reference design of the aperture-coupled Pseudo-ME dipole antenna in the millimeter-wave band or similar band.

(a)

(b)

(c)

(d)
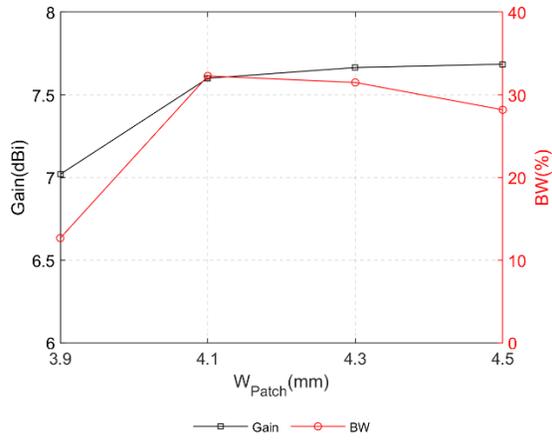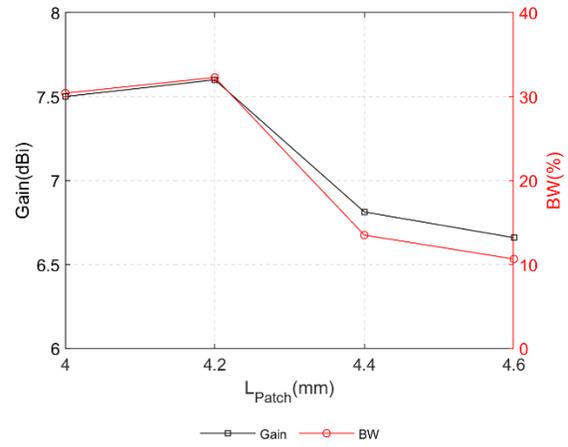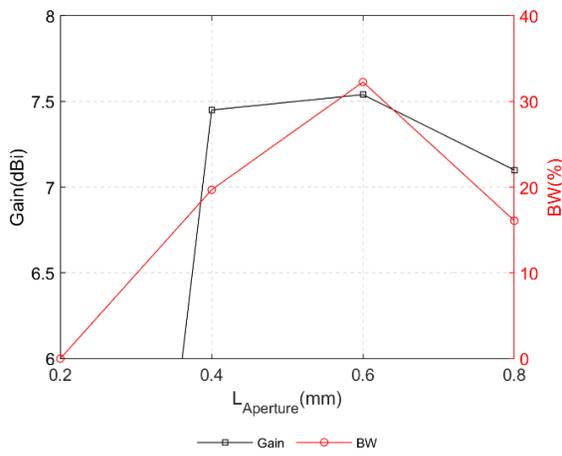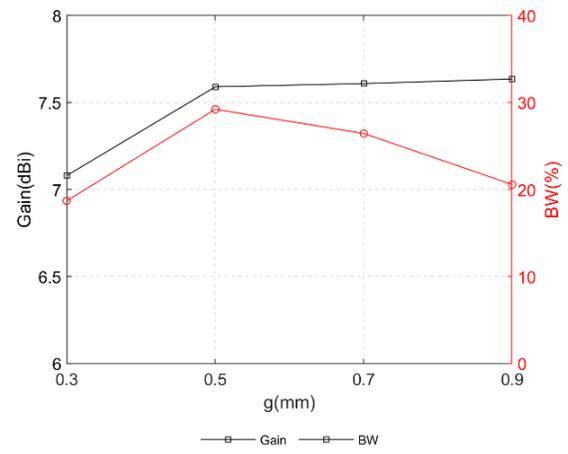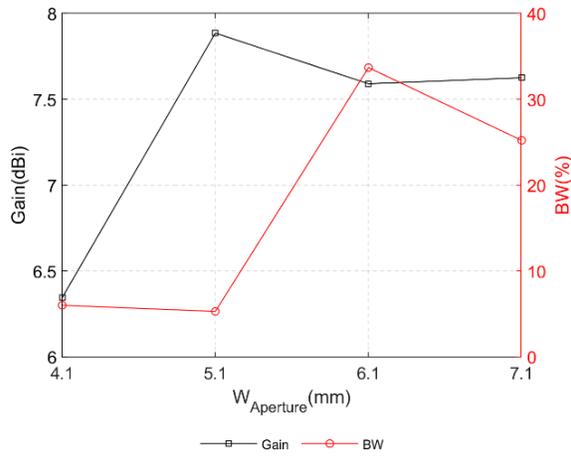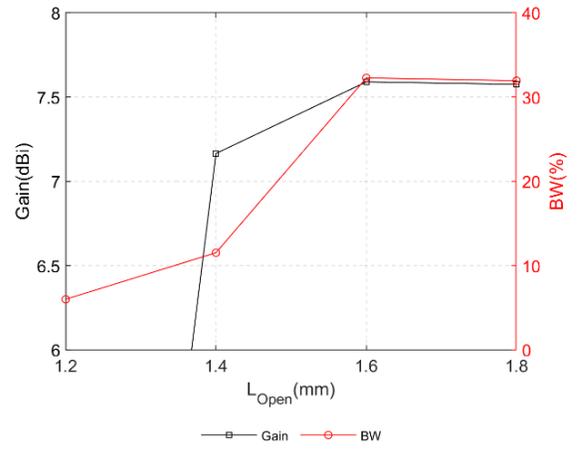
(e)   (f)

Fig. 5.29: Average gain and impedance bandwidth with different (a). W_{Patch}. (b). L_{Patch}. (c).

$L_{Aperture}$. (d). g. (e). $W_{Aperture}$. (f). L_{Open}.

185

5.2.1 Measurement Results
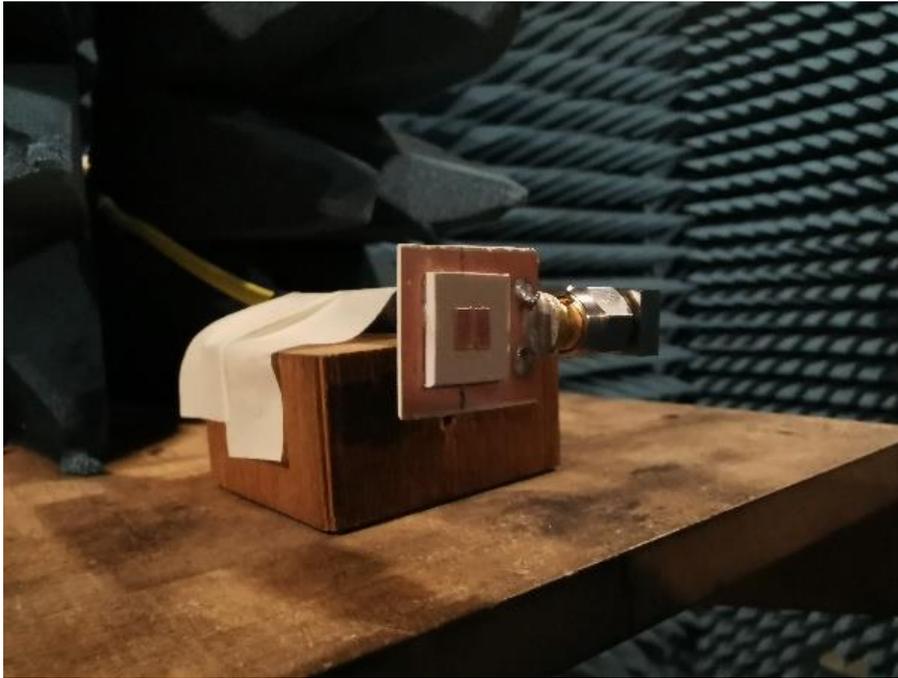
Fig. 5.30: Final prototype antenna under test in the anechoic chamber

After confirming that the bottom layer performs as expected, the radiating layer was added to measure the overall antenna performance. Fig. 5.30 shows the assembled proposed antenna prototype under the measurement in the anechoic chamber. Fig. 5.31 gives the simulated and measured gain and S_{11}.
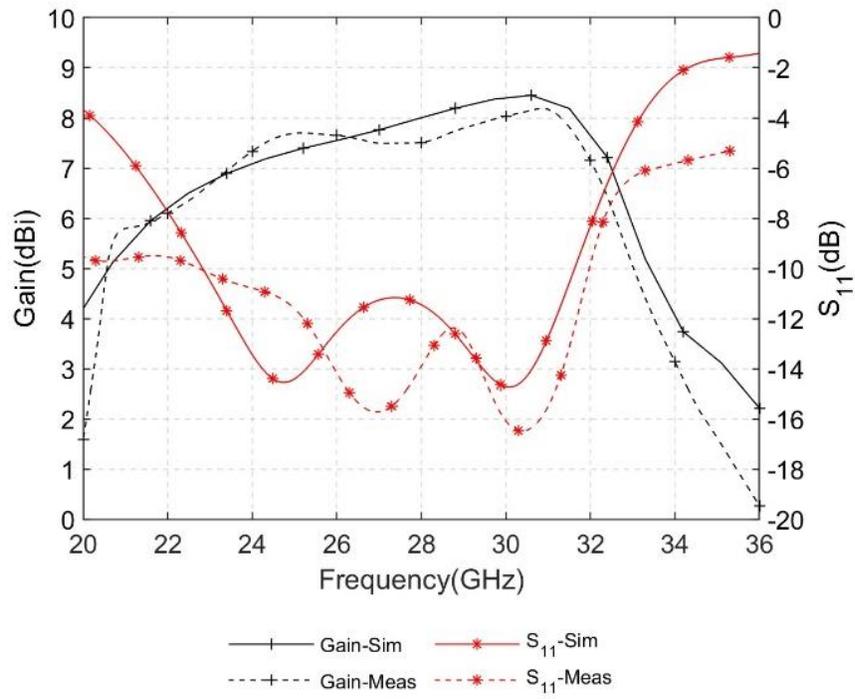
Fig. 5.31: Simulated Gain and S_{11} of the proposed antenna.
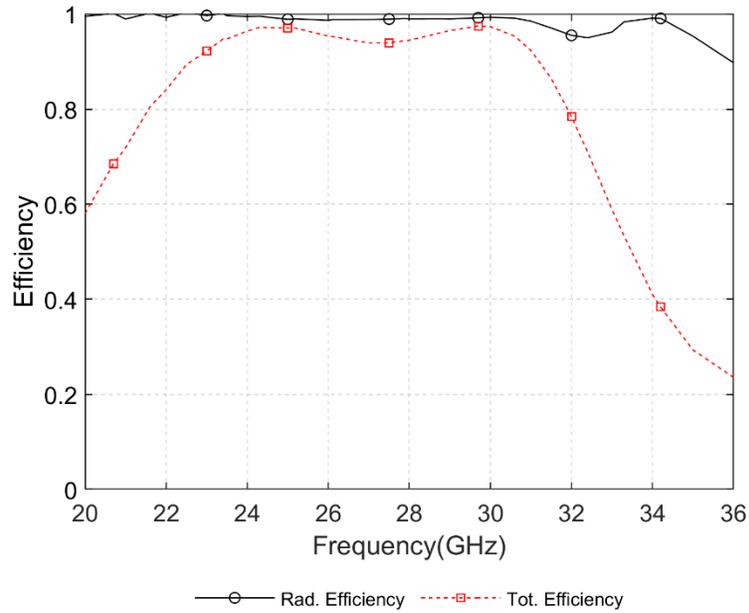
Fig. 5.32: Simulated radiation and total efficiency of the CP ME dipole

The measured and simulated gain shows a good degree of consistency. For the S_{11} profile, although the measured and simulated results are not matched as good as the gain profile at the low frequency band, they still show a similar trend, and the operating bandwidth is highly agreed. It has a simulated impedance ($S_{11} < -10$ dB) of 32.3 % from 22.8 GHz to 31.6 GHz (centered at 27.2 GHz) and a measured impedance bandwidth of 33.6 % from 22.8 GHz to 32 GHz (centered at 27.4 GHz). Moreover, the measured gain is 7.4 ± 0.8 dBi over the frequency band. The maximum measured gain of the antenna is around 8.2 dBi at 30.9 GHz.

Wide bandwidth is a critical feature of the Pseudo-ME dipole antenna. The radiation patterns at different frequencies of the Pseudo-ME dipole antenna are expected to be consistent. Fig. 5.33 (a) shows the simulated E-plane radiation patterns at low (21.6 GHz), center (27.4 GHz), and high (32 GHz) frequency points. Due to the microstrip line aperture-coupled feeding method, there is a higher back lobe level in the E-plane radiation patterns when compare to the design in Chapter 4. Moreover, due to the slot (or magnetic dipole mode) and the aperture radiating operate at higher frequency band, the back lobe level gets even higher in the high-frequency (32 GHz) band. Thus, the 3-dB beamwidth at the E-plane was reduced at the high-frequency band while the back-lobe increases. The variation ($|\Delta_1|$) of the 3-dB beamwidth during the operating band of the E-plane is 36.5°.

The measured results of the E-plane radiation pattern are shown in Fig. 5.33 (b), (c), (d). Generally, the measured results of low and center frequency bands are very close to the simulated radiation patterns. However, the measured result only shows a similar trend at the high-frequency (32 GHz) band; In addition to the asymmetric geometry of the antenna in the E-plane, that could result from the SMK connector and measurement conditions in the anechoic chamber. When measuring the back lobe, the turntable that fixes the antenna prototype might block some of the signals to reduce the back lobe level, and it can be observed

that the measured back lobe of other frequencies points is generally lower than -10 dB.

(a)

(b)

(c)

(d)
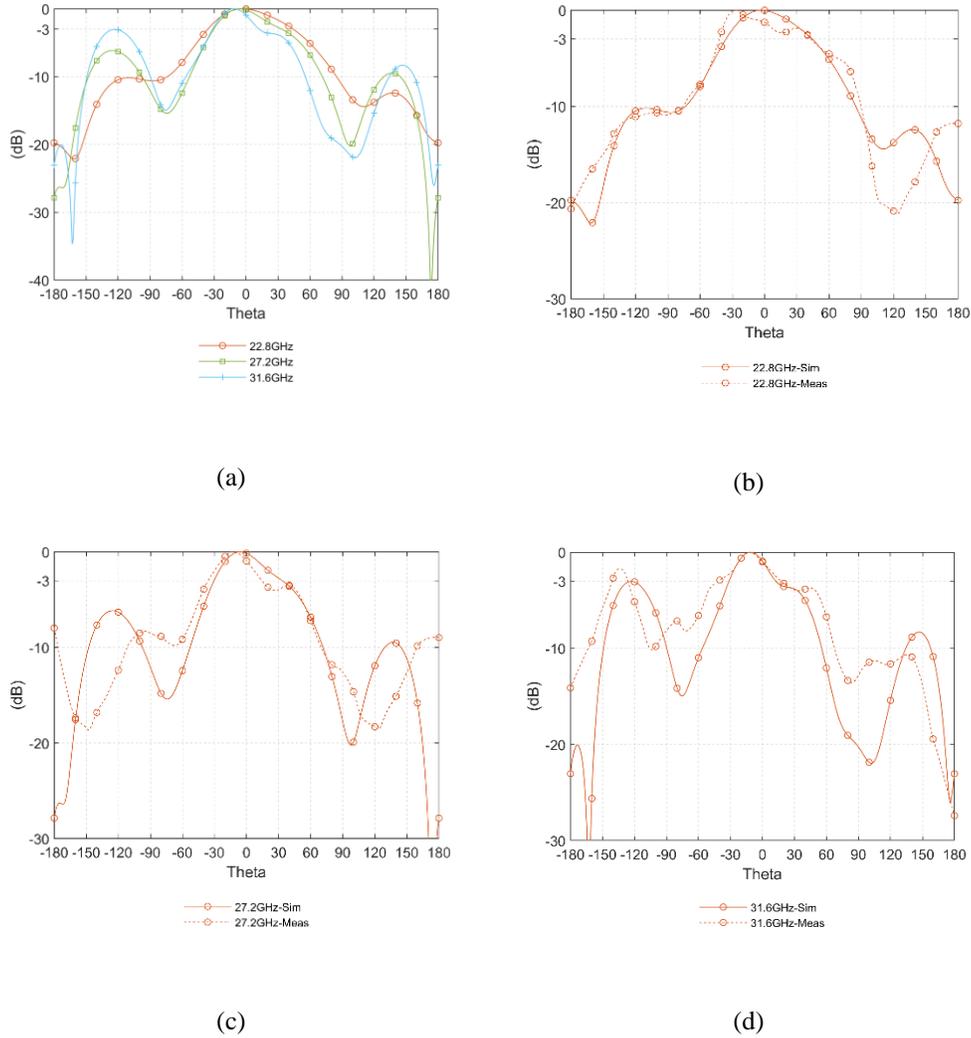
Fig. 5.33: E-plane radiation patterns of the proposed mmW antenna at different frequencies

Since the physical coaxial cable used to feed the antenna is in the E-plane, the affection from the cable distorted the E-plane radiation pattern more than the H-plane. Therefore, the simulated back-lobes in the H-plane at different frequencies are always less than -20 dB, as shown in Fig. 6.14. (a), and the radiation patterns show good consistency over the frequency band. Therefore,

the variation among the H-plane 3-dB beamwidth $|\Delta_1|$ at different frequencies is less than 4.3°. The measured results presented in Fig. 6.14 (b), (c), (d) also show a good match with the simulated results, mostly when -90° < θ < 90°. In the angular range 90°< θ < 120°, the measured radiation pattern shows a moderate drop when comparing the simulated results at all frequencies.

(a)   (b)

(c)   (d)
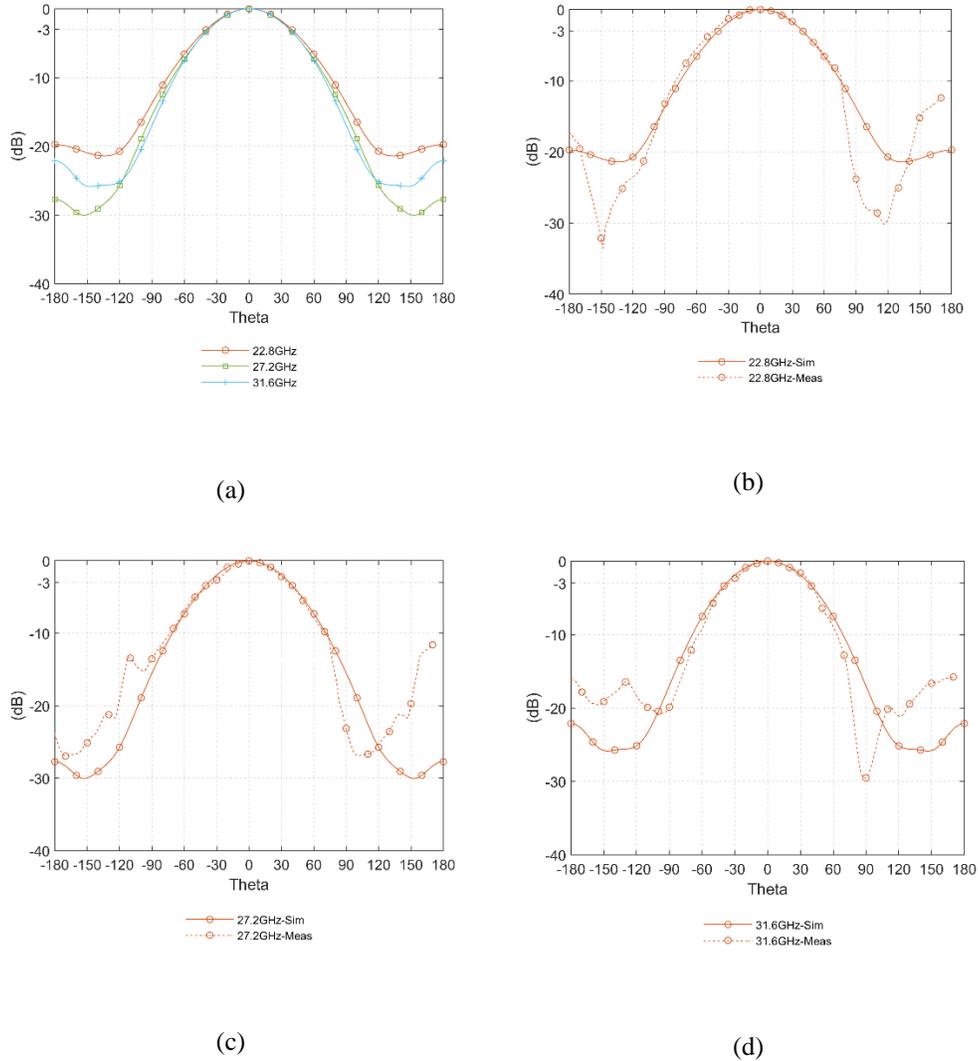
Fig. 5.34: H-plane radiation patterns of the proposed mmW antenna at different frequencies.

The detailed 3-dB beamwidth at different frequencies and the variations are shown in table 6.2. $|\Delta_2|$ is also given for observing the difference between E- and H-plane of different frequencies. The proposed antenna has very similar E-and

190

H-plane patterns at low-frequency band, the difference $|\Delta_2|$ is only 1°, while with the increased frequency, $|\Delta_2|$ becomes larger due to the increased back lobe level.

Table 5.2: 3-dB beamwidth of mmwW Pseudo-ME dipole atenna in E- & H-planes

3-dB beamwidth (°)	22.8 GHz	27.2 GHz	31.6 GHz	$|\Delta_1|$
E-plane (Phi=0°)	80.1	63.6	43.6	36.5
H-plane (Phi=90°)	79.1	74.8	75.5	4.3
$|\Delta_2|$	1	11.2	31.9	

5.3   Conclusive remarks

A millimeter-wave low-profile cavity-less pseudo magneto-electric dipole antenna has been designed and verified. The antenna is designed on a two-layer PCB to reduce losses in the substrate. By implementing the aperture-coupled feeding method, there are no via-holes in the design. The geometry is simple, and it is easy to fabricate.

6.Conclusions

6.1 Proposed novel Pseudo-ME dipole antennas

In this research thesis, three novel Pseudo-ME dipole antennas have been designed, manufactured, and verified to answer modern wireless communications requirements. Generally, all the proposed antennas have wide impedance bandwidth and stable high gain in the operating bandwidth.

All the conventional Pseudo-ME dipole antenna has a quarter-wave cavity to produce the magnetic dipole mode. The vertical-cavity increased the complexity of manufacture of the cost; on the other hand, it also makes it challenge to be implemented into the millimeter-wave band. To solve this problem, a low-profile simple geometry Pseudo-ME dipole antenna without quarter-cavity has been introduced in Chapter 4. The magnetic dipole mode of the antenna is generated by activating the slot between two patches. Therefore, there is no vertical structure in the complete design except the feed line; the whole geometry of the Pseudo-ME dipole antenna becomes extremely straightforward. The measured results prove the feasibility of the design. The measured impedance bandwidth (S_{11} < -10 dB) is 50.30% from 1.86 GHz to 3.11 GHz, and a stable high gain of 8.74 ± 1 dBi.

Polarization miss-match loss happens when the transmit/receive antennas do not align properly, bringing unnecessary signal losses in the communication systems. Circularly polarized antennas show the advantage of solving the problem. Therefore, a circularly polarized Pseudo-ME dipole antenna has been designed and verified. Usually, the circular polarization of a CP antenna is generated by two orthogonal resonances with equal amplitude and 90 phase differences. While the proposed one has two pairs of orthogonal resonances so that the antenna has a wide axial ratio bandwidth of 54.1% from 2.87 GHz to 5 GHz,

antennas have a stable high gain of 8.7 ± 0.9 dBi. Likewise, the CP Pseudo-ME dipole antenna geometry is also simple; the radiating layer that generates the circular polarization is built on a single layer PCB.

The cavity-less LP Pseudo-ME dipole antenna shows good performance in bandwidth, stable high gain. However, due to the coaxial feeding method, there is a limitation to realize this geometry into the millimeter-wave band since the coaxial cable is relatively larger, and it is hard to manufacture in practice. While a coaxial feed mmW Pseudo-ME dipole antenna has still been designed and simulated, and the simulated results prove the feasibility of the antenna in theory. More importantly, an aperture coupled Pseudo-ME dipole antenna in mmW band has been designed, manufactured, and verified. It is built on a two-layer PCB, the bottom layer operating as the transmission layer and the top layer operating as the radiation layer, it has a bandwidth ($S_{11} \leq$ -10 dB) of 33.6% from 22.8 GHz to 32 GHz.

Moreover, the measured gain is 7 ± 1 dBi over the frequency band. Generally, the compact size, wide impedance, and high gain features make it possible to be implemented into 5G mmW band. On the other hand, due to the microstrip line feeding method, the antenna back lobe is relevant larger when compared with the coaxial feeding method, especially in the high-frequency band, and this issue needs to be solved in the future.

6.2   Fulfilling the research aims

The aims and requirements have been proposed in the first chapter of this research thesis, in this section, the completeness of these aims will be discussed.

- Wide bandwidth: All proposed designs in this thesis have wide bandwidth larger than 33.6%.
- High and stable gain: all proposed antennas have an average gain higher than 7dBi, and the in-band gain variation is less than 1 dBi.
- Stable polarization: In this thesis, $|\Delta_1|$ has been used for observing the beamwidth difference over the wide impedance bandwidth, the maximum $|\Delta_1|$ for coaxial feed Pseudo-ME dipole antenna in this thesis is 13.3°. Due to the microstrip line feeding method, the beamwidth of mmW Pseudo-ME dipole antenna decrease due to the high back lobe.
- Simple geometry: all proposed antenna has simple and straightforward geometry, there is a cavity-less structure in the proposed antenna, the radiation layer of all proposed antenna could be easily fabricated by print circuit technology.
- Low cost: The simple geometry, generally without significant challenging aspects in antenna fabrication, and the material used to fabricate could be easily found.

6.3 Future work

Modern and future wireless communications have the trend of utilizing a broader spectrum to achieve massive data transmission. In this thesis, three novel pseudo magneto-electric dipole antennas have been presented; all of them meet the requirements of modern wireless communications.

At the current stage, 5G sub-6 GHz has already serviced our daily life, and the millimeter-wave band will be significantly developed in the later phase. The millimeter-wave band will realize high-speed data transmission with large bandwidth and use extremely dense spatial multiplexing to increase capacity. As mentioned in chapter 1, antenna arrays (for massive MIMO) will be used on the base station side. Beamforming technology is introduced in 5G to meet the needs of large capacity and high speed; the mobile devices can receive superimposed electromagnetic waves with enhanced signal strength. Therefore, the array design of the linearly polarized cavity-less Pseudo-ME dipole antenna and the millimeter-wave band aperture-coupled antenna worth researching in the future.

For the CP Pseudo-ME dipole antenna proposed in Chapter 4, a flat ground plane is employed as the reflector to provide antenna high gain and front-to-back ratio. In the last part of this chapter, a cavity shape reflector has been used to replace the flat ground plane for comparison. However, the comparison only includes the S_{11}, gain, and axial ratio bandwidth due to the time limitation. According to a published research paper [72][73], the cavity shape reflector may significantly increase the 3-dB AR beamwidth significantly, and this potential feature would help satellite communications. Therefore, in future work, more work related to the cavity shape reflector needs to be studied.

In 2030, 6G networks are expected to create a world with everything connected and provide wireless connections with multi-terabytes per second and full-dimensional coverage [82]. Comparing with 5G, 6G reduce communications

196

latency from milliseconds (ms) to microseconds (µs), supporting super-high-definition (SHD) videos and enhance 5G vertical applications, such as the Massive Internet of Things (IoT) and fully autonomous vehicles. To realize the multi-terabytes data transmission, very-large-scale antenna arrays (SM-MIMO) [83] or OAM multiplexing [84] could be applied to increase the system capacity since many parallel data streams could be multiplexing on the same channel. In future work, antennas proposed in this thesis could be used as good basic antennas for implementing in SM-MIMO or OAM multiplexing.

Reference

[1]   S. M. R. Islam, N. Avazov, O. A. Dobre, and S. Member, "Power-Domain Non-Orthogonal Multiple Access (NOMA) in 5G Systems : Potentials and Challenges," *IEEE Commun. Surv. TUTORIALS*, vol. 19, no. 2, pp. 721–742, 2017.

[2]   T. Specification, "TS 138 212 - V15.2.0 - 5G; NR; Multiplexing and channel coding (3GPP TS 38.212 version 15.2.0 Release 15)," vol. 0, 2018.

[3]   J. S. Erik Dahlman, Stefan Parkvall, *5G NR The Next Generation Wireless Access Technology*. .

[4]   "5G Antenna White Paper New 5G, New Antenna."

[5]   J. G. Andrews *et al.*, "What Will 5G Be ?," *IEEE J. Sel. AREAS Commun.*, vol. 32, no. 6, pp. 1065–1082, 2014.

[6]   L. Guevara, "The Role of 5G Technologies : Challenges in Smart Cities and Intelligent Transportation Systems," *Sustainability*, vol. 12, no. 16, p. 6469, 2020.

[7]   T. S. Rappaport *et al.*, "Millimeter Wave Mobile Communications for 5G Cellular : It Will Work !," *IEEE Access*, vol. 1, pp. 335–349, 2013.

[8]   T. S. Rappaport, E. Ben-dor, J. N. Murdock, and Y. Qiao, "38 GHz and 60 GHz Angle-dependent Propagation for Cellular & Peer-to-Peer Wireless Communications," pp. 4568–4573, 2012.

[9]   D. Persson, B. K. Lau, and E. G. Larsson, "Scaling Up MIMO: Opportunities and Challenges with Very Large Arrays," *IEEE Signal Process. Mag.*, no. january 2013, pp. 40–60, 2012.

[10]   Y. J. Sung, T. U. Jang, and Y. Kim, "A Reconfigurable Microstrip Antenna for Switchable Polarization," *IEEE Microw. Wirel. COMPONENTS Lett.*, vol. 14, no. 11, pp. 534–536, 2004.

[11]   S. S. Yang, A. A. Kishk, and K. Lee, "Frequency Reconfigurable U-Slot Microstrip Patch Antenna," *IEEE Antennas Wirel. Propag. Lett.*, vol. 7, pp. 127–129, 2008.

[12]   A. Chlavin, "A New Antenna Feed Having Equal E- and H- Plane Patterns," vol. 93, 1954.

[13]   "IEEE standard definitions of terms for antennas," *IEEE Trans. Antennas Propag.*, vol. 17, no. 3, pp. 262–269, 1969.

[14]   Z. Raida, S. Gona, C. G. Survey, and Z. Skvor, "Electronic Textbook of Electromagnetic Waves," *Radio Eng.*, no. May 2014, 2003.

[15]   J. C. Maxwell, "A_Dynamical_Theory_of_the_Electromagnetic_Field." London, 1864.

[16]   C. a. Balanis, *Antenna Theory: Analysis and Design*, vol. 28, no. 3. 2012.

[17]   J. W. M. Keith R. Carver, "Microstrip Antenna Technology," *IEEE Trans. Commun.*, no. 1, 1981.

[18]   S. R. Saunders and A. A. Zavala, *Antenna and Propagation for Wirless Communication Systems*. .

[19]   L. Ge and K. M. Luk, "A Low-Profile Magneto-Electric Dipole Antenna," *IEEE Trans. Antennas Propagations*, vol. 60, no. 4, pp. 1684–1689, 2012.

[20]   B. G. Duffley, G. A. Morin, M. Mikavica, and Y. M. M. Antar, "A Wide-Band Printed Double-Sided Dipole Array," *IEEE Trans. Antennas Propag.*, vol. 52, no. 2, pp. 628–631, 2004.

[21]   W. X. An, H. Wong, K. L. Lau, S. F. Li, and Q. Xue, "Design of Broadband Dual-Band Dipole for Base Station Antenna," *IEEE Trans. Antennas Propagations*, vol. 60, no. 3, pp. 1592–1595, 2012.

[22]   S. X. Ta, H. Choo, and I. Park, "Broadband Printed-Dipole Antenna and Its Arrays for 5G Applications," *IEEE Antennas Wirel. Propag. Lett.*, vol. 16, pp. 2183–2186, 2017.

[23]   J. D. Kraus, "Antennas." 1988.

[24]   H. Wong, K.-M. Mak, and K.-M. Luk, "Wideband Shorted Bowtie Patch Antenna With Electric Dipole," *IEEE Trans. Antennas Propag.*, vol. 56, no. 7, pp. 2098–2101, 2008.

[25]   K. Luk and H. Wong, "A New Wideband Unidirectional Antenna Element," *Int. J. Microw. Opt. Technol.*, no. 1, pp. 35–44, 2006.

[26]   L. E. I. Ge and K. M. A. N. Luk, "Beamwidth Reconfigurable Magneto-

Electric Dipole Antenna Based on Tunable Strip Grating Reflector," *IEEE Access*, vol. 4, pp. 7039–7045, 2016.

[27] K. He, S. Gong, and F. Gao, "A Wideband Dual-Band Magneto-Electric Dipole," *IEEE Antennas Wirel. Propag. Lett.*, vol. 13, pp. 1729–1732, 2015.

[28] S. Yan, P. J. Soh, and G. A. E. Vandenbosch, "Wearable Dual-Band Magneto-Electric Dipole Antenna for WBAN / WLAN Applications," *IEEE Trans. Antennas Propag.*, vol. 63, no. 9, pp. 4165–4169, 2015.

[29] B. Q. Wu and K. Luk, "A Broadband Dual-Polarized Magneto-Electric Dipole Antenna With Simple Feeds," *IEEE Antennas Wirel. Propag. Lett.*, vol. 8, pp. 60–63, 2009.

[30] Q. Xue, S. W. Liao, and J. H. Xu, "A Differentially-Driven Dual-Polarized Magneto-Electric Dipole Antenna," *IEEE Trans. Antennas Propag.*, vol. 61, no. 1, pp. 425–430, 2013.

[31] Y. Gou, S. Yang, J. Li, and Z. Nie, "A Compact Dual-Polarized Printed Dipole Antenna With High Isolation for Wideband Base Station Applications," *IEEE Trans. Antennas Propag.*, vol. 62, no. 8, pp. 4392–4395, 2014.

[32] A. O. Li and K. Luk, "A Dual Linearly Polarized End-Fire Antenna Array for the 5G Applications," *IEEE Access*, vol. 6, pp. 78276–78285, 2018.

[33] S. J. Yang, Y. M. Pan, S. Member, Y. Zhang, and S. Member, "Low-Profile Dual-Polarized Filtering Magneto-Electric Dipole Antenna for 5G Applications," *IEEE Trans. Antennas Propag.*, vol. 67, no. 10, pp. 6235–6243, 2019.

[34] Y. Li and K. Luk, "A 60-GHz Wideband Circularly Polarized Aperture-Coupled Magneto-ElectricDipole Antenna Array," *IEEE Trans. Antennas Propag.*, vol. 64, no. 4, pp. 1325–1333, 2016.

[35] S. X. Ta and I. Park, "Crossed Dipole Loaded With Magneto-Electric Dipole for Wideband and Wide-Beam Circularly Polarized Radiation," *IEEE Antennas Wirel. Propag. Lett.*, vol. 14, pp. 358–361, 2015.

[36] J. Cao, H. Wang, S. Mou, S. Quan, Z. Ye, and A. Abstract, "W-Band High-Gain Circularly Polarized Aperture-Coupled Magneto-Electric Dipole

Antenna Array With Gap Waveguide Feed Network," *IEEE Antennas Wirel. Propag. Lett.*, vol. 16, pp. 2155–2158, 2017.

[37]   M. Li and K. Luk, "A Wideband Dual-fed Circularly Polarized Antenna," no. 22, pp. 112–114, 2013.

[38]   Y. D. L. and S. N. Tsai, "Coplanar waveguide-fed uniplanar bowtie antenna," *IEEE Trans. Antennas Propag.*, vol. 45, no. 2, pp. 305–306, 1997.

[39]   and K. F. L. A. A. Eldek, A. Z. Elsherbeni, C. E. Smith, "Wide- band slot antenna for radar applications," *in Proc. IEEE Radar Conf.*, Huntsville,AL, pp. 79–84, 2003.

[40]   and E. B. E. A. Soliman, S. Berbels, P. Delmotte, G. A. E. Vandenbosch, "Bowtie slot antenna fed by CPW," *Electron. Lett.*, vol. 35, pp. 514–515, 1999.

[41]   J. F. H. and C. W. Kuo, "CPW-fed bowtie slot antenna," *Microw. Opt. Technol. Lett.*, vol. 19, no. 5, pp. 358–360, 1998.

[42]   and P. S. K. M. Miao, B. L. Ooi, "Broadband CPW-fed wide slot antenna," *Microw. Opt. Technol. Lett.*, vol. 25, no. 3, pp. 206–211, 2000.

[43]   L. Ge and K. M. Luk, "A Magneto-Electric Dipole Antenna With Low-Pro fi le and Simple Structure," *IEEE Antennas Wirel. Propag. Lett.*, vol. 12, pp. 140–142, 2013.

[44]   L. Ge and K. M. Luk, "A Low-Pro fi le Magneto-Electric Dipole Antenna," *IEEE Trans. Antennas Propag.*, vol. 60, no. 4, pp. 1684–1689, 2012.

[45]   K. B. Ng, H. Wong, K. K. So, C. H. Chan, and K. M. Luk, "60 GHz Plated Through Hole Printed Magneto-Electric Dipole Antenna," *IEEE Trans. Antennas Propag.*, vol. 60, no. 7, pp. 3129–3136, 2012.

[46]   S. Liao, Q. Xue, and J. Xu, "A Differentially Fed Magneto-Electric Dipole Antenna with a Simple Structure," *IEEE Antennas Propag. Mag.*, vol. 55, no. 5, 2013.

[47]   L. Cai, H. Wong, and K. Tong, "A Simple Low-Profile Coaxially-Fed Magneto-Electric Dipole Antenna Without Slot-Cavity," *IEEE open J. antennas Propag.*, vol. 1, no. June, pp. 233–238, 2020.

[48]   D. M. Pozar and S. M. Duffy, "A Dual-Band Circularly Polarized

Aperture-Coupled Stacked Microstrip Antenna for Global Positioning Satellite," *IEEE Trans. Antennas Propag.*, vol. 45, no. 11, pp. 1618–1625, 1997.

[49] J. Sze and W. Chen, "Axial-Ratio-Bandwidth Enhancement of a Microstrip-Line-Fed Circularly Polarized Annular-Ring Slot Antenna," *IEEE Trans. Commun.*, vol. 59, no. 7, pp. 2450–2456, 2011.

[50] R. Antennas, K. Tong, and J. Huang, "New Proximity Coupled Feeding Method for Reconfigurable Circularly Polarized Microstrip," *IEEE Trans. Antennas Propag.*, vol. 56, no. 7, pp. 1860–1866, 2008.

[51] W. Encheng and S. Luyao, "An Improved Wideband Dipole Antenna for Global Navigation Satellite System," *IEEE Antennas Wirel. Propag. Lett.*, vol. 13, pp. 1305–1308, 2014.

[52] W. Cao, X. Lv, Q. Wang, Y. Zhao, and X. Yang, "Wideband Circularly Polarized Fabry – Perot Resonator Antenna in Ku-Band," *IEEE Antennas Wirel. Propag. Lett.*, vol. 18, no. 4, pp. 586–590, 2019.

[53] J. Cao, H. Wang, S. Mou, P. Soothar, and J. Zhou, "An Air Cavity-Fed Circularly Polarized Magneto-Electric Dipole Antenna Array With Gap Waveguide Technology for mm-Wave Applications," *IEEE Trans. Antennas Propag.*, vol. 67, no. 9, pp. 6211–6216, 2019.

[54] M. Li and K. Luk, "A Wideband Circularly Polarized Antenna for Microwave and Millimeter-Wave Applications," *IEEE Trans. Commun.*, vol. 62, no. 4, pp. 1872–1879, 2014.

[55] Y. P. Zhang, M. Sun, and L. H. Guo, "On-Chip Antennas for 60-GHz Radios in Silicon Technology," *IEEE Trans. Electron Devices*, vol. 52, no. 7, pp. 1664–1668, 2005.

[56] Y. Miura, S. Member, J. Hirokawa, S. Member, and M. Ando, "Double-Layer Full-Corporate-Feed Hollow- Waveguide Slot Array Antenna in the 60-GHz Band," *IEEE Trans. Antennas Propag.*, vol. 59, no. 8, pp. 2844–2851, 2011.

[57] N. Celik *et al.*, "Implementation and Experimental Verification of a Smart Antenna System Operating at 60 GHz Band," *IEEE Trans. Antennas*

Propag., vol. 56, no. 9, pp. 2790–2800, 2008.

[58] Y. Xing and T. S. Rappaport, "Propagation Measurement System and Approach at 140 GHz – Moving to 6G and Above 100 GHz," 2018.

[59] Z. Zhang, N. Liu, J. Zhao, and G. Fu, "Wideband Circularly Polarized Antenna WIth Gain Imprvoment," *IEEE Antennas Wirel. Propag. Lett.*, vol. 12, pp. 456–459, 2013.

[60] S. Qu, C. H. Chan, Q. Xue, and S. Member, "Wideband and High-Gain Composite Cavity-Backed Crossed Triangular Bowtie Dipoles for Circularly Polarized Radiation," *IEEE Trans. Antennas Propag.*, vol. 58, no. 10, pp. 3157–3164, 2010.

[61] Y. He, S. Member, W. He, H. Wong, and S. Member, "A Wideband Circularly Polarized Cross-Dipole Antenna," *IEEE Antennas Wirel. Propag. Lett.*, vol. 13, pp. 67–70, 2014.

[62] M. Plonus, "Theoretical investigations of scattering from plastic foams," *IEEE Trans. Antennas Propagations*, vol. 13, no. 1, pp. 88–94, 1965.

[63] K. M. L. Kin Fai Tong, KaiFong Lee, "On The Effect of Ground Plane Size to Wideband Shorting-Wall Probe-fed Patch Antennas," vol. 147, no. 6, p. 4577, 2011.

[64] P. R. Orientation and M. Propagation, "Antenna Diversity Performance in Mitigating the Effects of Portable Radiotelephone Orientation and Multipath Propagation," *IEEE Trans. Commun.*, vol. C, no. 5, pp. 620–628, 1983.

[65] C. B. Dietrich, K. Dietze, J. R. Nealy, and W. L. Stutzman, "Spatial , Polarization , and Pattern Diversity for Wireless Handheld Terminals," *IEEE Trans. Antennas Propag.*, vol. 49, no. 9, pp. 1271–1281, 2001.

[66] G. Minatti, S. Maci, P. De Vita, A. Freni, and S. Member, "A Circularly-Polarized Iso fl ux Antenna Based on Anisotropic Metasurface," *IEEE Trans. Antennas Propag.*, vol. 60, no. 11, pp. 4998–5009, 2012.

[67] K. M. Mak and K. M. Luk, "A Circularly Polarized Antenna With Wide Axial Ratio Beamwidth," *IEEE Trans. Antennas Propag.*, vol. 57, no. 10, pp. 3309–3312, 2009.

[68]   L. Wang, H. Yang, and Y. Li, "Design of a New Printed Dipole Antenna Using in High Latitudes for Inmarsat," *IEEE Antennas Wirel. Propag. Lett.*, vol. 10, pp. 358–360, 2011.

[69]   J. Zhang, H. Yang, and D. Yang, "Design of a New High-Gain Circularly Polarized Antenna for Inmarsat Communications," *IEEE Antennas Wirel. Propag. Lett.*, vol. 11, no. c, pp. 350–353, 2012.

[70]   H. Iwasaki, "A Circularly Polarized Small-Size Microstrip Antenna with a Cross Slot," *IEEE Trans. Antennas Propag.*, vol. 44, no. 10, pp. 1399–1401, 1996.

[71]   J. Lee and J. Woo, "Design of a l-type aperture coupled circular polarization patch antenna with a single feed."

[72]   G. P. S. Applications, S. Xuat, T. Jae, J. Han, and I. Park, "Compact Circularly Polarized Composite Cavity-Backed Crossed Dipole for Compact Circularly Polarized Composite Cavity-Backed Crossed Dipole for GPS Applications," *J. Electromagn. Eng. Sci.*, no. August 2014, 2013.

[73]   S. X. Ta, H. Choo, I. Park, and R. W. Ziolkowski, "Multi-Band , Wide-Beam , Circularly Polarized , Crossed , Asymmetrically Barbed Dipole Antennas for GPS Applications," *IEEE Trans. Antennas Propag.*, vol. 61, no. 11, pp. 5771–5775, 2013.

[74]   K. T. Chan, A. Chin, Y. B. Chen, Y. D. Lin, T. S. Duh, and W. J. Lin, "Integrated antennas on Si, proton-implanted Si and Si-on-quartz," *Tech. Dig. - Int. Electron Devices Meet.*, pp. 903–906, 2001.

[75]   T. Zwick, D. Liu, and B. P. Gaucher, "Broadband planar superstrate antenna for integrated millimeterwave transceivers," *IEEE Trans. Antennas Propag.*, vol. 54, no. 10, pp. 2790–2796, 2006.

[76]   K. Mak, S. Member, K. So, and S. Member, "A Magnetoelectric Dipole Leaky-Wave Antenna for Millimeter-Wave Application," *IEEE Trans. Antennas Propag.*, vol. 65, no. 12, pp. 6395–6402, 2017.

[77]   E. Pucci, E. Rajo-iglesias, S. Member, and P. Kildal, "New Microstrip Gap Waveguide on Mushroom-Type EBG for Packaging of Microwave Components," *Ieee Microw. Wirel. components Lett.*, vol. 22, no. 3, pp.

129–131, 2012.

[78] A. Dadgarpour, M. S. Sorkherizi, and A. A. Kishk, "Wideband Low-Loss Magnetoelectric Dipole Antenna for 5G Wireless Network With Gain Enhancement Using Meta Lens and Gap Waveguide Technology Feeding," *IEEE Trans. Antennas Propag.*, vol. 64, no. 12, pp. 5094–5101, 2016.

[79] M. K. A. Rahim, Z. W. Low, P. J. Soh, A. Asrokin, M. H. Jamaluddin, and T. Masri, "Aperture Coupled Microstrip Antenna with Different Feed Sizes and Aperture Positions," in *2006 INTERNATIONAL RF AND MICROWAVE CONFERENCE PROCEEDINGS*, 2006, vol. 00, pp. 31–35.

[80] U. Substrate, R. Coccioli, F. Yang, S. Member, and K. Ma, "Aperture-Coupled Patch Antenna on UC-PBG Substrate," *ieee Trans. Microw. theory thechniques*, vol. 47, no. 11, pp. 2123–2130, 1999.

[81] S. D. Targonski, R. B. Waterhouse, and D. M. Pozar, "Design of Wide-Band Aperture-Stacked Patch Microstrip Antennas," *IEEE Trans. Antennas Propag.*, vol. 46, no. 9, pp. 1245–1251, 1998.

[82] Z. Zhang, Y. Xiao, Z. Ma, M. Xiao, and Z. Ding, "6G Wireless Networks: Vision, Requirements, Architecture, and Key Technologies," *IEEE Veh. Technol. Mag.*, no. July 2019, 2020.

[83] E. Björnson, L. Sanguinetti, H. Wymeersch, J. Hoydis, and T. L. Marzetta, "Massive MIMO is a Reality — What is Next ? Five Promising Research Directions for Antenna Arrays," no. February, 2019.

[84] Y. Ren *et al.*, "Line-of-Sight Millimeter-Wave Communications," *IEEE Trans. Wirel. Commun.*, vol. 16, no. 5, pp. 3151–3161, 2017.